GROOVE LOCATIONS FOR OPTIMUM PERFORMANCE OF TWO-AXIAL GROOVE AND MULTI-LOBE HYDRODYNAMIC BEARINGS

A Thesis

Submitted in partial fulfilment of the

requirements for the degree of

Doctor of Philosophy

By

Lintu Roy

DEPARTMENT OF MECHANICAL ENGINEERING
INDIAN INSTITUTE OF TECHNOLOGY GUWAHATI
December, 2013

CERTIFICATE

It is certified that the work in the thesis entitled **Groove Locations for Optimum Performance of Two-Axial Groove and Multi-Lobe Hydrodynamic Bearings**, by **Lintu Roy**, a student in the Department of Mechanical Engineering, Indian Institute of Technology Guwahati, India, for the award of the degree of Doctor of Philosophy has been carried out under my supervision and that this work has not been submitted elsewhere for a degree.

(S K Kakoty)

Professor

Department of Mechanical Engineering

Indian Institute of Technology Guwahati

December, 2013

Dedicated to my parents

Acknowledgement

First and foremost I want to express my deeply-felt thanks to my thesis supervisor, Professor S K Kakoty, for his warm encouragement and thoughtful guidance. It has been an honour to be his Ph.D student. I appreciate all his contributions of time, ideas, and discussion to make my Ph.D experience productive and stimulating. The joy and enthusiasm he has for research was contagious and motivational for me, even during my tough time in the Ph.D pursuit.

I also thank to the members of my doctoral committee: Professor S K Dwivedy, Professor S Talukdar and Dr. S. Senthilvelan whose helpful suggestions increased both originality and quality of the thesis.

I am happy to acknowledge my debt to Professor Pinakeswar Mahanta, HoD of Mechanical Engineering Department for providing me with necessary arrangements to carry out my research.

I want to express my gratitude to my students at NIT Silchar, Mr. Nithin M Joy and Mr.Chandan Bhagat, not only for their excellent comments, but also for lively discussions about tribology and bearing problems.

Last but not the least; I thank my parents and my family members for their unconditional love, support and encouragement to pursue my interests.

Lintu Roy

IIT Guwahati

Contents

List of Figures

List of Tables

Notation

C	radial clearance (m)
D	diameter of the journal (m)
L	length of the bearing (m)
R	bearing radius (m)
e	eccentricity (m)
ε	eccentricity ratio=e/C
η	coefficient of absolute viscosity of the lubricant (Pa-s)
$\mu, \bar{\mu}$	coefficient of friction, friction variable $= \mu(R/C)$
N	speed of the journal in r.p.s
ϕ	bearing attitude angle
h	film thickness (m) $= C(1+\varepsilon\cos\theta)$ for plain journal bearing and $h = C(1 + \varepsilon\cos(\theta - \varphi))$ for grooved bearing
$\bar{h}$	non-dimensional film thickness $= \frac{h}{C}$
θ_1	position of starting of the first groove
θ_2	position of starting of the second groove
θ_3	position of starting of the third groove

θ_s	position of starting of the fourth groove
U	sliding speed
p	steady state pressure (Pa)
$\bar{p}$	non-dimensional steady state pressure $= \frac{pC^2}{6\eta UR}$.
$\overline{W}_0$	Non dimensional load carrying capacity (N), $\overline{W_0} = \frac{WC^2}{6\eta UR^2 L}$
X	Vertical direction
Z	Horizontal direction
W_X	vertical component (in X direction) of the resultant load
W_Z	vertical component (in Z direction) of the resultant load
P	load per unit bearing area $= \frac{W}{LD}$
S	Sommerfeld number$= \frac{\eta N}{P}\left(\frac{R}{C}\right)^2$
$\bar{q}_z$	non dimensional flow coefficient , $\left(\bar{q}_z = \frac{2Q}{ULC}\right)$
$\bar{p}_1, \bar{p}_2$	perturbed pressures
ε_1, ϕ_1	perturbed eccentricity ratio and attitude angle around the steady state value ε_0, ϕ_0
$K_{XX}, K_{ZZ}, K_{XZ}, K_{ZX}$	stiffness coefficients(N/m)
$\bar{K}_{XX}, \bar{K}_{ZZ}, K_{XZ}, \bar{K}_{ZX}$	non-dimensional stiffness coefficients $= \frac{K_{ij}C}{W}$ where $i = X, Z$ and $j = X, Z$
$D_{XX}, D_{ZZ}, D_{XZ}, D_{ZX}$	damping coefficient (N.s /m)

$\bar{D}_{XX}, \bar{D}_{ZZ}, \bar{D}_{XZ}, \bar{D}_{ZX}$	non-dimensional Damping coefficients $= \frac{C_{ij} C\omega}{W}$ where $i = X, Z$ and $j = X, Z$
t	time (s)
ω, ω_p	journal rotational speed (rad/s), frequency of journal vibration
τ	non-dimensional time, $\tau=\omega_p t$
λ	whirl ratio $= \omega_p / \omega$
$M, \bar{M}$	Rotor mass (kg), mass parameter, $\bar{M} = \frac{MC\omega^2}{W}$
$(\,)_0$	steady state value

Abstract

Rotating machines are one of the most important and widely used machineries in modern engineering world. They are also required to run at high speeds. Plain circular bearing is mostly replaced by some other bearings, as plain bearing does not suit the stability requirements of high speed machines and precision machine tools. In order to improve the stability of a circular bearing, many researchers have tried to change its geometrical configuration. Few examples are pressure-dam bearing, elliptical bearing and multi-lobe bearing. Present day bearings need to operate at ever increasing speeds and loads, which confront the engineer with many new problems. Excessive power losses reduce the efficiency of the engine, high bearing temperature pose a danger to material of the bearing as well as the lubricant and instability, mainly in the form of oil whip, may ruin not only the bearing but the machine itself. New bearing designs are sought to meet the new requirements and these bearings are usually characterized by their non circular cross section. Almost any non circular bearing geometry will enhance shaft stability and under proper conditions this will also reduce power losses and increase oil flow (as compared to circular bearing), thus reducing bearing temperatures.

The grooves provided for lubricant inflow to the clearance area of journal bearings are generally placed in symmetrical locations of the bearings. For example, two axial groove and two-lobe bearings have grooves located horizontally 180^{o} apart, whereas in case of three-lobe and four lobe bearings grooves are placed 120^{o} and 90^{o} apart. However, not much information is available as to whether the bearing performance will be improved or deteriorated if the grooves are placed at other locations.

In view of this, an attempt has been made in the present work to study the effect of groove locations of four different bearing configurations, *viz*, two axial groove, two-lobe, three-lobe and four-lobe bearings by changing the groove locations. It has been found that the bearing performance changes with different configurations, *i.e*., different groove locations. This has led to an exercise of finding out the optimum groove locations which results in the best performance of the bearing in terms of friction variable, non-dimensional load capacity, flow coefficient, mass parameter and combination of all the four individual objectives.

The non-dimensional form of the Reynolds equation has been solved for the steady state non dimensional pressure distribution in a finite difference grid using Gauss-Seidel method with successive over-relaxation (SOR) technique satisfying appropriate boundary conditions. The flow coefficient, friction variable and non-dimensional load capacity are estimated using the pressure distribution. The bearing non-dimensional stiffness and damping coefficients are calculated by perturbing the journal position, and by solving the perturbed Reynolds equations. These coefficients are used to find the rigid rotor stability threshold, mass parameter, a function of speed. An attempt has been made to obtain an optimum configuration of the grooves position around the circumference of the hydrodynamic journal bearing for maximum flow coefficient, minimum friction variable, maximum non-dimensional load capacity, maximum critical speed vis-à-vis mass parameter and minimization of multi-objective function derived combining all the four individual objective functions using Genetic Algorithm.

It has been found that the optimum groove locations are not only different for different objective functions but also different for different eccentricity ratios, *vis-a-vis*, loading conditions. It would definitely not resolve the confusion as to which groove configurations have to be used when loading changes. Therefore, a methodology is proposed to identify the location of the grooves for two axial groove bearing, two-lobe bearings, three-lobe bearings and four-lobe bearings such that the performance characteristics are near to the optimum for any loading condition for a particular objective function. This will be beneficial to the designers as well as manufacturers.

It has been established in the present study that conventional groove locations do not correspond to the optimum bearing performance and there exists particular configurations having other than conventional groove which correspond to the best bearing performance in terms of different objectives for each bearing considered here. Also identification of locations of grooves for two-groove, two lobe, three-lobe and four-lobe bearings obtained such that the performance characteristics are near to the optimum for any loading condition (eccentricity ratio) for different objective functions. However, the presented results need to be validated by experimental study, which is outside the scope of the present work.

CHAPTER 1

Introduction

1.0 State of the Art

Rotating machines are commonly supported on fluid film bearings. In the past, the vast majority of these bearings were plain journal bearings. Industrial turbomachinery, such as steam turbines, gas compressors, pumps and motors, contain a variety of different types of hydrodynamic journal bearings. The types of bearings most commonly found in turbomachinery include:

- plain cylindrical
- axial groove
- pressure dam
- lemon bore
- offset halves
- three-lobe
- four-lobe
- tilting pad

Each of these types of bearings has unique operational characteristics that render it more suitable for one application than another.

The plain journal bearing with two axial groove placed diametrically opposite is the most basic hydrodynamic journal bearing. The eccentric rotating shaft will develop an oil film pressure profile. A hydrodynamic journal bearing is designed to operate normally under hydrodynamic lubrication, where hydrodynamic pressure in the lubricant keeps the sliding surfaces of the bearing and shaft separated from each other. The hydrodynamic pressure is caused by the sliding motion. Many practical situations exist in which direction of loading on a journal bearing varies during its operation. A typical example is a gearbox where the direction of loading changes with rotation. And this will be reflected in a variation of loading direction on the supported bearings.

Plain circular bearing is mostly replaced by some other bearings, as plain bearing does not suit the stability requirements of high-speed machines and precision machine tools. Grooved circular bearings and multi-lobe bearings with two-lobes, three-lobes and four-lobes are

commonly used. The higher the critical speed, the higher is the stability limit. The larger the eccentricity ratio, the more stable is the shaft. In engineering analysis it is essential to know the critical speed at which oil whirl causes instability and avoid it during operation.

In order to satisfy the stability requirements of high-speed machines, researchers replaced the circular bearings with non-circular bearings. Multi-lobe journal bearing is composed of two or more sectors with fixed centre of curvature that does not coincide with the bearing geometrical centre. Multi-lobe bearings are widely used in high speed rotating machinery to suppress instability under lightly loaded conditions.

1.1 Literature Review

1.1.1 Journal bearing and two axial groove bearing

Raimondi and Boyd [1] did extensive numerical studies towards facilitating the analysis and design of journal bearings. Numerical solutions of Reynolds equation were obtained for centrally-loaded bearings having arcs of 360°, 180°, 120° and 60° for L/D values of ∞, 1, 1/2 and 1/4. Assumptions are based on constant viscosity and no film rupture. Performance curves are presented; the ease of application of the charts is shown by two illustrative problems. The effect of changing such design parameters as bearing clearance is illustrated.

Pinkus and Sternlicht [2] in theoretical analysis of Plain Journal bearing and provided various data viz. attitude angle ϕ_o, friction variable, $(R/C)\mu$ and flow coefficient, $\overline{q}_z$ and Sommefeld number, S, for bearings having different L/D ratios values of ∞, 1, 1/2 and 1/4.

Dowson *et. al.* [3] carried out experiments on liquid film journal bearings, by varying the eccentricity ratio, supply pressure and rotational speed, to validate theoretical results of side leakage, film rupture and reformation. Excellent agreement of experimental determination of side leakage with theoretical results is obtained.

Salamone [4] reviewed several different types of hydrodynamic journal bearings which were commonly found in turbomachinery. In this paper emphasis was placed on the key geometric design parameters of each type. This discussion covered plain journal, axial groove, pressure dam, offset split, lemon bore, multi-lobe and tilting pad bearings. He concluded that grooved configuration was more stable than plain journal bearing for some application.

Gethin and Deihi [5] used finite-element model for the incompressible hydrodynamic lubrication of a cylindrical-bore bearing subjected to different loading directions. The model accounted fully for the extent of the lubricant film in both load-carrying and ruptured parts of the bearing. A number of loading directions were considered, and it has been shown that load-

carrying ability, hydrodynamic flow and attitude angle all depend significantly on loading direction.

A computer-aided elastohydrodynamic study of the two-lobe journal bearing was presented by Chandrawat and Sinhasan [6]. Data on the static performance characteristics of a flexible shell two-lobe bearing, operating in laminar and turbulent regimes and using isoviscous-piezoviscous lubricants, were provided in this paper.

The Reynolds Equation, is a partial differential equation governing the pressure distribution of an incompressible and isoviscous fluid was first derived by Osborne Reynolds [7]. The classical Reynolds Equation can be used to describe the pressure distribution in nearly any type of fluid film bearing.

A computer programme was developed by Claro and Miranda [8] that can be used in the analysis of steadily loaded journal bearing. Groove positions that had been considered in the paper were a single groove located at load line and at 90^0 to the load line. The study presented in this paper is one part of broader research project concerning the analysis of hydrodynamic journal bearings fed via axial grooves, which include an experimental progamme for validation of theoretical results. The obtained results of dimensionless side flow and power loss for hydrodynamic journal bearings with a single axial groove at 90^0 to the load line provided by a computer analysis taking full account of the lubricant inlet conditions, had been compared with available experimental measurements. Good correlation was observed. At zero supply pressure, the correlation observed was good for low values of eccentricity ratios and L/D ratios. An increase of these parameters has resulted in increased discrepancies which were for higher values of eccentricity ratios and L/D ratios. For non-zero values of supply pressure and low values of L/D ratios, the correlation of side flow rate was generally not good. At higher supply pressure significant discrepancies have been observed for all values of eccentricity ratios and L/D ratios.

Vijayraghavan and Keith [9] in a numerical study analyzed the performance of oil groove type, groove number and groove location on journal bearing. The analysis involved the use of a cavitation algorithm. The interaction between cavitation phenomena and grooving was determined. Quantitative information was provided for designers to better locate oil feed grooves.

Hirani *et. al.* [10], reported a rapid method for analysis of dynamically loaded journal bearings, wherein analytical pressure expression was proposed to eliminate the need of time-consuming and tedious iterations for pressure calculations.

Cho *et. al*. [11] presented the effects of circumferential groove on the minimum oil film thickness in engine bearings. The fluid film pressures were calculated by using the infinitely short bearing theory for the convenience of analysis. A comparison of minimum oil film thickness of grooved and ungrooved bearing was presented. It was found that circumferential 360^0 groove only reduces the absolute magnitude of the oil film thickness, but 180^0 half groove affects the shape of film thickness curve and position of minimum oil film thickness.

Jang [12] presented an analytical method to investigate the stability of a hydrodynamic Journal bearing with rotating herringbone grooves. The dynamic coefficients of the hydrodynamic journal bearing were calculated using the FEM and the perturbation method. It had been shown that the instability of the hydrodynamic journal bearing with rotating herringbone groove increased with increasing eccentricity and with decreasing groove number, which played the major role in increasing the average and variation of the stiffness coefficients. It also showed that a high rotational speed was another source of instability by increasing the stiffness coefficients without changing the damping coefficients.

Very recently Costa *et. al.* [13] studied the influence of oil supply conditions on the thermo hydrodynamic performance of a single axial groove journal bearing. They showed that oil supply conditions affect bearing performance parameters in different ways. They also found out that the effect of supply pressure on minimum film thickness was dependent on groove location

An experimental study of the influence of oil supply temperature and supply pressure on the performance of a plain journal bearing with two axial grooves located at ±90º to the load line was carried out by Brito *et. al.* [14]. The temperature and pressure fields inside the bearing, oil flow rate, power loss, and the position of shaft center had been presented.

Theoretical prediction of the steady state characteristics of a hydrodynamic short bearing with a circumferential feeding groove was presented by Naimi *et. al.* [15]. Authors derived relationship between the feeding pressure, Sommerfeld number and eccentricity ratio which was used to study the effect of the groove and supply pressure on the oil film and eccentricity.

1.1.2 Multi-lobe bearings

Cylindrical bearings are prone to instability. Therefore, non-cylindrical bearings like two-lobe, three-lobe and four-lobe bearings are widely used in industry in recent times. There are many studies carried out on the performance of such bearings. This section provides a brief account of such studies.

1.1.2.1 Elliptical bearings

A brief survey of literature on elliptical bearings with regard to this research is provided below.

Various literatures are available on elliptical bearings and it has been found that Pinkus [16] was the first to study elliptical bearing. His work was on finite two lobe elliptical bearing with the numerical solution of Reynolds equation. In his work on elliptical bearing the nature of the oil flow, power loss was obtained for various L/D ratios, ellipticity and various operating conditions.

Pinkus [17] investigated the power loss for elliptical and three lobe bearing configuration. Power losses for non cylindrical and cylindrical bearing were plotted with speed and comparison was made with the cylindrical bearing. Expressions were given in both the cases assuming a complete oil film and incomplete oil film. Both his theoretical and experimental results were found to be matching. Power loss was found higher when the shaft operates at some eccentricity ratio.

Pinkus [18] in his experimental work highlighted on resonant whip of a shaft mounted on two multilobe bearings and found that whip occurs at a speed equal to about twice the first natural critical frequency of the shaft. Oil whip characteristics were determined by operating and design variables viz. load, speed, oil viscosity, unbalance excitation and L/D ratio. With the heavier shaft, whipping stopped at a speed equal to the three times the first critical of the shaft. The order of bearing stability is, starting with the most stable bearings, three-lobe, tilting pad, elliptical, three-groove and plain circular

Singh *et. al*. [19] using the variational approach analyzed an elliptical bearing. Various results like load, stiffness were compared with the available data. It was found that beyond an eccentricity ratio of 0.3 there was an increase in load support and stiffness and damping coefficients.

Using the variational solution of Reynolds equation Kumar *et. al*. [20] found out the nature of various parameter viz flow, friction co-efficient with an increase in eccentricity ratio

and stiffness–damping coefficient, temperature rise parameter for two lobe hydrodynamic journal bearing.

A comparative study of various two lobe bearing configuration (elliptical, offset half and another two configuration) had been studied theoretically (both static and dynamic characteristics) by Kumar *et. al*. [21]. It has been shown that, unlike elliptical and offset-halves bearings, which have only limited range of effective dynamic performance, two-lobe configuration can provide consistently good dynamic performance over a wide range of load conditions.

Soni *et. al.* [22] solved Reynolds equation by using Galerkin's technique for both laminar and turbulent flow regimes. Static and dynamic characteristics of two lobe bearing had been studied in terms of load support, oil flow, fluid stiffness and damping co-efficient and critical mass parameter.

Performance characteristics of finite two lobe bearing in fully developed turbulent regimes were studied in terms of load capacity, stiffness-damping co-efficient, and the non-dimensional mass of the journal at various eccentricities for Reynolds number up to 12000 by Soni *et. al*. [23]. It has been found that bearing load capacity, stiffness coefficients ,damping coefficients increases with Reynolds number. But at high eccentricity ratios, the trend is reversed.

Sinhasan and Goyal [24] presented a computer aided study of transient response of two lobe journal bearing with non-Newtonian lubricant. The non linear trajectories obtained indicate that the two lobe journal bearing systems becomes unstable even at values of non-dimensional values of non-dimensinal journal mass less than the critical journal computed using the linearized equations of motion and Routh's criterion.

A methodology for prediction of dynamic coefficients and non-linear simulation of four bearings (two axial groove, elliptical, three lobe, offset bearing) was made by Rao *et al*. [25] in 2003. Dynamic coefficients were obtained using finite perturbation method. Journal centre trajectories for elliptical, three lobe and offset bearings are obtained using the present method for position perturbation and unbalance excitation, and compared with numerical results and the effect of stability of rotor bearing system was studied for both balanced and unbalanced rotor.

Basavaraja *et. al.* [26] studied the performance of a two lobe hole entry hybrid journal bearing system compensated by orifice section. They solved Reynolds equation governing the

flow of lubricant in the clearance space between journal and bearing together with flow through orifice restrictor with has been solved using FEM and Galerkin's method. Numerical results indicated that for two lobe symmetric hole entry hybrid bearing with an offset factor greater than one provides 30 to 50 percent larger direct stiffness and damping coefficients as compared to circular symmetric hole entry hybrid journal bearing system.

1.1.2.2 Three-lobe and four-lobe bearings

Pinkus [27] in an analysis on three lobe bearing presented various characteristics (viz lubricatnt flow, power loss) determined for a wide range of eccentricity ratios. It was shown that three-lobe bearing is superior in quality both in terms of hydrodynamic performance, load capacity and stability.

Falkehagen *et al.* [28] investigated the stability characteristics and transient motion of a finite width three-lobe bearing for a wide range of ellipticity ratio and offset factor. Linearized stiffness and damping coefficient were found out numerically and were used to calculate the threshold of instability for a rigid vertical rotor. Non linear transient orbits were plotted for a balanced rotor and comparisons were made with the linearized stability curve. It was found that the optimum preload factor varied from 0.59 to 0.47 and the corresponding offset factor ranged from 0.8 to 1 for an aspect ratio of 1.

Lund and Thomson [29] gave some design data which included both static and dynamic characteristics for laminar as well as turbulent flow regimes. Theoretical analysis of three lobe bearing based on the solution of Reynolds equation for laminar as well as for turbulent region was presented by Malik *et. al.* [30]. Both static and dynamic characteristics of three-lobe bearing were presented. Load support, frictional power loss, stiffness and damping coefficient, stability margin in terms of critical mass parameter were presented in graphical form.

A comparative study on various configurations of three-lobe bearing (viz unsymmetrical, symmetric upright, unsymmetric inverted, symmetric inverted) was carried out by Sinhasan *et. al.* [31] which was based on static and dynamic performance of three lobe bearings. Reynolds equation for computation of performance characteristics was solved analytically. It was concluded that the static load support of the usual symmetric upright configuration was the best, however, inverted configuration, both symmetrical and unsymmetrical configuration appear more promising from the point of view of the dynamic performance.

An investigation of static & dynamic performance characteristics of three-lobe configuration over a wide range of tilt angle was performed by Malik *et. al.* [32] in terms of stiffness and damping coefficients, mass parameter and whirl ratio. It was found that the tilted configuration exhibited superior dynamic performance than the usual symmetric three-lobe bearing.

Performance of three-lobe bearing with pressure dam by using FEM carried out by Mehta and Rattan [33]. It was found that the stability of threshold could be improved by using pressure dam.

The static characteristics of a three-lobe bearing were studied by Taylor *et al.* [34]. The operating eccentricities within the clearance space, film thickness, and temperature profile were measured at three axial locations. Maximum temperature occurred circumferentially near the point of minimum film thickness. The experimental measurements obtained were verified through analytical data.

The effect of misalignment on the performance characteristic of misaligned three-lobe journal bearing was studied by Arumugam *et. al.* [35]. The various parameters studied were friction, vibration response, minimum film thickness, stiffness and damping coefficients of the fluid film and system natural frequency and damping factor.

Carmen *et.al.* [36] presented results of a nonlinear simulation to assess the effects for one particular bearing test rig previously documented. The nonlinearity had arisen from the finite size orbital motion imposed on the journal or housing during the measurement process to obtain response. The effect of fluid film nonlinearity on the measured data used to calculate the dynamic coefficients had not previously been reported.

The measured static and dynamic characteristics of a highly preloaded three-lobe bearing were presented by Pettinato and Flack [37]. Temperature, eccentricity, attitude angle and circumferential film thickness profile were measured at an operating speed of 900 r.p.m for three load orientations. Dynamic characteristics consisting of eight linearized stiffness and damping co-efficients were presented with respect to Sommerfeld number. Detailed data were provided to facilitate analytical comparison.

The effects of couple stressed fluid, when added to a Newtonian base, were studied by deriving a generalized form of the Reynolds equation by Mehta *et. al.* [38]. A couple stress parameter '*l*' had been used to indicate the length of the long chain molecule being added. Finite

element method had been used to solve the generalized Reynolds equation for each lobe to obtain the respective pressure distributions. Stable equilibrium conditions in terms of eccentricity ratios and the attitude angles had been obtained for the vertical load condition. The journal was perturbed from the equilibrium position to estimate the stiffness and the damping coefficients. It had been observed that slight variation of the couple stress parameter '*l*' had a great influence on the dynamic characteristics, *i.e.,* the stiffness and the damping coefficients. The threshold speed and the critical mass of the journal, obtained as a solution to the linearized equations of motion, were used to demonstrate the increased stability of the journal bearing system.

Batra *et. al.* [39] analyzed the effect of turbulence on the performance of an inverted three-lobe pressure dam bearing which was produced by incorporating a pressure dam in the upper lobe and two relief tracks in the lower two lobes of an ordinary inverted three- lobe bearing. For analysis purpose different values (0, 1500, 3000, and 6000) of Reynolds number were considered to study the effect of turbulence. The results showed that for an inverted three lobe bearing supporting rigid or flexible rotors, the zone of infinite stability as well as minimum threshold speed increased with increase in turbulence, thus indicating better stability at higher turbulence level.

Sometimes the line of action of the load does not pass through the axis of a bearing and is shifted on either side by a few degrees. Load orientation is one of the factors that affect the stability of a three-lobe bearing. The effect of load orientation on the stability of a three-lobe had been discussed by Bhushan [40]. The results showed that stability of a three-lobe bearing supporting either rigid or flexible rotor was increased for the positive values of load orientation, *i.e*., when the load line is shifted in the opposite direction of rotation.

Flack *et. al.* [41] in an experimental and theoretical investigation measured the pressure profile along the centre line of the four-lobe bearing and compared with the theoretical results. Both half Sommerfield and Reynolds boundary conditions were used in the theoretical prediction and it was found that experimental data correlate most with half Sommerfeld condition.

In an experimental testing of preloaded four-lobe bearing with flexible rotor obtained the unbalance response and instability of threshold at various running speed by Leader *et. al.* [42]. Ten different orientations of the bearing were used. The rotor system exhibited an instability in the form oil whip at a speed twice the critical speed of the rotor.

Bhushan *et. al.* [43] studied the effect of pressure dams and relief track on the performance of an ordinary four lobe bearing. Finite element method was used to analyse the bearing with and without pressure dams. The pressure dam bearing was found to be more stable than bearings without pressure dam.

Bhushan *et. al.* [44] analyzed the effect of pressure dam and relief track on the performance of an ordinary four-lobe bearing by using FEM. It was found that by incorporating pressure dam high pressure were generated at the steps or dams which ensured higher stability of the bearing. The analysis showed that four-lobe pressure dam bearing was superior to ordinary four lobe bearing.

Bhusan et al. [45] analyzed static and dynamic characteristics of a four-lobe pressure dam bearing which supported a rigid and flexible rotor to determine its performance when L/D ratio change from 0.75 to 1.5. Stability of four-lobe pressure dam bearing increased with the decrease in L/D ratio.

Mehta *et. al.* [46] analyzed the performance of a four-lobe pressure dam bearing which was produced by incorporating two pressure dams on the upper two lobes and two relief-tracks on the lower two lobes of an ordinary four-lobe bearing. The results show that the performance of a four-lobe bearing with pressure dams is superior to that of an ordinary four-lobe bearing.

A non-linear transient method was used by Pai and Majumdar [47] to predict the journal centre trajectory for a submerged four-lobe oil journal bearing under (i) unidirectional instant load, (ii) unidirectional periodic load, and (iii) variable rotating load. The Reynolds equation was integrated using the Jakobsson-Floberg-Olsson cavitation zone model, and oil film prehistory effects were taken into account. The journal centre trajectories obtained were compared with those obtained for submerged plain cylindrical bearings under similar loading conditions. It was observed that the excursions of the journal centre were subdued, unlike for the plain cylindrical bearings, where the journal centre had a large excursion before it became stable or ended in a limit cycle. Interesting trajectories were observed for the periodic load.

The static and dynamic performance characteristics of four-lobe bearing operating with couple stress lubricant were studied by Chetti [48]. The effects of the couple stress parameter on the key performance of a four-lobe journal bearing such as the load carrying capacity, the friction force, side leakage, the stiffness and damping, the critical mass and whirl ratio were determined. The computed results showed that the presence of couple stresses improved the

performance characteristics of a four-lobe bearing compared to that lubricated with Newtonian fluids

1.1.3 Optimization of Journal bearing

The art of journal bearing design has progressed considerably since the advent of high speed digital computers. Analytical solutions of Reynolds equation have been replaced by the computerised numerical solutions for the finite length journal bearing, thus replacing the conventional long hand-graphical procedure. It is a rather lengthy exercise to obtain a suitable design of bearing using hand techniques and to achieve something approaching an optimum design takes considerably longer time.

Seireg and Ezzat [49] presented an automated system for the selection of the length, clearance, and lubricant viscosity which optimized the performance of a hydrodynamic journal bearing, under specified values or ranges of load and speed. The study illustrated the feasibility of applying optimal programming techniques for the development of bearing design systems.

Bosma and Moes [50] provided a new type of design chart for pivoted-pad thrust bearings. The dimensionless groups of parameters representing minimum film thickness and bearing traction for one single pad, respectively, had been plotted in a new design chart. Some illustrative examples for optimization of pivoted-pad thrust bearings had also been included. Some attention was paid to the stiffness of the film of lubricant. A design chart for film stiffness was added for this purpose.

Rowe *et .al*. [51] discussed selection of suitable values for hybrid hydrostatic bearing design variables with a view to minimizing power dissipation and reducing the temperature rise. It was suggested that there was an optimum sill width ratio for any bearing and that the optimization process was most conveniently carried out with reference to dimensionless optimization parameter. It was found that hydrodynamic lift was always small in comparison to hydrostatic load support irrespective of speed at optimum conditions.

Dowson and Ashton [52] presented operating characteristics evaluated from the computed solution of Reynolds equation graphically. The optimum design objectives were stated explicitly in terms of operating characteristics and were minimized within both design and operating constrains. Optimum design was provided for a set of running conditions for minimum power loss. A comparison was made of the optimum design obtained for three different design objectives. Results from the computerised design technique were compared with the solution given by long-hand design procedure.

Rowe and Koshal [53] reported a new technique for optimizing hybrid journal bearings. The method involved the comparison of the bearings to be optimized with a reference bearing on the basis of load/ total power, load/ pumping power and load/ flow.

Determination of the shape of a steadily loaded journal bearing, operating with an incompressible iso-viscous lubricant, which had the greatest load capacity for a given minimum film thickness was the main work performed by Mcallister *and* Rodhe [54]

A mathematical technique was described by Kumar [55] to determine the optimum set of tolerances on the journal and bearing bore which guarantee the correct operating performance of plain journal bearings at a minimum manufacturing cost. The method of solution was based on the Lagrange multiplier technique of calculus wherein the cost, expressed as an analytical function of tolerance, was minimized subject to the mathematical constraint condition. The constraint condition was that the maximum permissible tolerance on diametral clearance must not be exceeded. A numerical example to illustrate the use of the technique was included.

Herbinyt et.al. [56] formulated an optimization problem with a view to maximizing the load-carrying capacity of hydrostatic journal bearings. Equations governing the performance of multi-recess hydrostatic journal bearings were summarized. Practical design limits and operational constraints were also defined. The optimization process was based on Rosenbrock method. Results illustrating the effect of area ratio, axial land width and circumferential land width on load capacity, flow rate and power ratio had been reported. Precision bearings with small clearances and low pressure ratios were recommended for applications involving low supply pressures, while bearings with large clearances and pressure ratios close to 0.5 were recommended for applications involving high supply pressures.

Matsumoto and Hashimoto [58] optimized the design procedure of high-speed, short journal bearings under laminar and turbulent flow conditions using Successive Quadratic Programming, Genetic Algorithm and Direct Search method. Simplified closed form design formulae incorporating short bearing assumption to the modified turbulent Reynolds equation were obtained for eccentricity ratio, friction force, film temperature rise, supply lubricant quantity and whirl onset velocity as a function of design variables such as radial clearance, slenderness ratio and average viscosity of lubricants.

Yang *et. al*. [59] presented an enhanced artificial life algorithm for optimum design of short journal bearing. As artificial life organisms have a sensing system, they can find the resource they want and metabolize it. The characteristics of artificial life are emergence and dynamic interaction with the environment. In other words, the micro-interaction with each other in the artificial life's group results in emergent colonization in the whole system. In this paper, artificial life algorithm by using the above characteristics was applied to the optimum design of short journal bearing. The optimized results were compared with those of Genetic Algorithm and Successive Quadratic Programming and identified the optimizing ability.

Boedo and Eshkabilov [60] implemented a Genetic Algorithm scheme suitable to the optimal shape design of finite-width, iso-viscous, fluid film journal bearings under steady load and steady journal rotation. Optimal bearing geometry was found to offer a small improvement in load carrying capacity and a substantial improvement in oil flow over purely cylindrical designs.

Hirani [61] formulated an optimization model based on a hybrid solution scheme for journal bearings with multi-objective optimization (minimization of temperature rise, minimization of oil feed flow, minimization of power loss) and discrete design variables (lubricant viscosity, radial clearance, length–diameter ratio) related to the design of a journal bearing. The objective of bearing optimization was to minimize a linear combination (weighted sum) of power loss and oil flow. Constraints were imposed on the maximum fluid film pressure, minimum film thickness, maximum temperature rise and critical speed. Genetic Algorithm was used as the optimization tool with a penalty to those solutions that violate constraints. The paper attempts to remove the difficulty of selecting the weighting factor in multi-objective journal bearing optimization problems.

A survey of current continuous nonlinear multi-objective optimization (MOO) concepts and methods was presented by Marler and Arora [62]. It consolidated seemingly different terminology and methods. The methods were divided into three major categories: methods with a priori articulation of preferences, methods with a posterior articulation of preferences, and methods with no articulation of preferences. Genetic Algorithms were surveyed as well. Commentary had been provided on three fronts, concerning the advantages and pitfalls of individual methods, the different classes of methods, and the field of MOO as a whole. The Characteristics of the most significant methods were summarized. Conclusions were drawn to reflect often-neglected ideas and applicability to engineering problems. It was found that no

single approach was superior. Rather, the selection of a specific method depended on the type of information that was provided in the problem, the user's preferences, the solution requirements, and the availability of software.

John McCall [63] presented Genetic algorithms (GAs), a heuristic search and optimization technique inspired by natural evolution. The algorithms had been successfully applied to a wide range of real-world problems of significant complexity.

An optimum design of high-speed short journal bearing using an enhanced artificial life algorithm (EALA) to compute the solutions of optimization problem was proposed by Song et.al. [64]. The artificial life optimization algorithm is a stochastic searching algorithm using the feature of artificial life. The feature of R-tabu method, which prevents converging to the local minimum, was combined with the ALA. One of the features of the R-tabu method was to divide any given searching region into several sub-steps. As the result of the combination of the two methods, the EALA not only converged faster than the ALA, but also led to a more accurate solution. In addition, this algorithm could also find all global optimum solutions.

An optimal design of hydrodynamic journal bearing using mass conserving thermal analysis and Genetic Algorithms was presented by Hirani [65]. Simultaneous minimization of power loss and oil flow, subjected to constraints on film thickness, film pressure, and temperature rise between the bearing surfaces, was the objective of this study. The radial clearance, L/D ratio, oil groove location, feed pressure, and the oil viscosity were the design variables. The rank-based genetic algorithm was used to deal with the discrete variables and multimodal objective functions and to capture Pareto optimal points.

Hirani and Suh [66] described the optimum design methodology for improving operating characteristics of fluid-film steadily loaded journal bearings. This methodology consisted of (i) a simplified closed form solution to accelerate the computation, (ii) finite difference mass conserving algorithm for accurate prediction of lubricant flow and power loss, (iii) Pareto optimal concept to avoid subjective decision on priority of objective functions, (iv) a Genetic Algorithm to deal with multimodal nature of hydrodynamic-bearing and develop a Pareto optimal front, (v) fitness sharing to maintain genetic diversity of the population used in genetic algorithm, and (vi) axiomatic design to provide inside of objective functions and design variables. In the optimum design of journal bearings, the design variables such as radial clearance, length to diameter ratio, groove geometry, oil viscosity and supply pressure were used to simultaneously minimize oil flow and power loss. A step-by-step procedure, results in form of

graphs and tables were presented to demonstrate the concept and effectiveness of suggested design methodology.

A brief review on optimum design provided by Chetan *et.al.* [67] revealed that numbers of researchers have been working on various aspects of performance of the journal bearing, ranging from temperature rise, geometry of grooves, instability, clearance etc. The parametric optimization had been performed by many researchers since there had been lot of developments in computer hardware and software technologies.

Mathew *et.al.* [68] covered the basic concepts, advantages of the canonical or traditional Genetic Algorithm. Few illustrations were given in detail. A variety of applications were also mentioned. The transition scheme of the Genetic Algorithm was probabilistic, whereas traditional methods used gradient information. Because of these features of Genetic Algorithm, they were used as general purpose optimization algorithm. The most striking difference between GAs and many traditional optimization methods was that GAs work with a population of points instead of a single point and the expected GA solution might be a global solution. Another advantage with a population-based search algorithm was that the multiple optimal solutions could be captured in the population easily, thereby reducing the effort to use the same algorithm many times.

Bean [69] in his paper presented a general Genetic Algorithm to address a wide variety of sequencing and optimization problems including multiple machine scheduling, resource allocation, and the quadratic assignment problem. When addressing such problems, Genetic Algorithms typically had difficulty maintaining feasibility from parent to offspring. This was overcome with a robust representation technique called *random keys*. Computational results were shown for multiple machine scheduling, resource allocation, and quadratic assignment problems.

Fonseca and Fleming [70] discussed contemporary multi-objective evolutionary approaches, ranging from the conventional analytical aggregation of the different objectives into a single function to a number of population- based approaches and the more recent ranking schemes based on the definition of Pareto-optimality. The sensitivity of different methods to objective scaling and/ or possible concavities in the trade-off surface was considered, and related to the (static) fitness landscapes such methods induced on the search space. From the discussion, directions for future research in multi-objective fitness assignment and search strategies were

identified, including the incorporation of decision making in the selection procedure, fitness sharing, and adaptive representations.

Tamaki *et. al.* [71] reviewed several Genetic Algorithm (GA) approaches to multi-objective optimization problems (MOPs). The key point of GAs to MOPs was designing efficient selection/ reproduction operators so that a variety of Pareto optimal solutions were generated. From this viewpoint, the paper reviewed several devices proposed for multi-objective optimization by GAs such as the parallel selection method, the Pareto based ranking, and the fitness sharing. Characteristics of these approaches had been confirmed through computational experiments with a simple example. Moreover, two practical applications of the GA approaches to MOPs were introduced briefly.

According to a review by David and Lamont [72] multi-objective evolutionary algorithms (MOEAs) continued to have substantial success across a variety of multi-objective optimization problem (MOP) applications, from pedagogical multifunction optimization to real-world engineering design. The variety of MOEAs as well as their numerous applications suggested a classification framework be developed. Evolutionary algorithms (EAs) were initially extended and applied during the mid-eighties in an attempt to stochastically solve problems of this generic class. During the past decade, a variety of multi-objective EA (MOEA) techniques have been proposed and applied to many scientific and engineering applications. Current multi-objective EA (MOEA) theoretical developments were evaluated; specific topics addressed include fitness functions, Pareto ranking, niching, fitness sharing, mating restriction, and secondary populations. Analysis resulted in validated MOEA design recommendations for new applications and was hoped to stimulate new theoretical approaches. An integral aspect of this paper was the "points to ponder" when redesigning current MOEAs and EAs for solving multi-objective optimization problem (MOPs).

Marler and Arora [73] presented a survey of predominant, continuous, and nonlinear multi-objective optimization methods. Fundamental concepts were discussed in the context of the criterion space and the design space. Seemingly different methods and terminology were consolidated and related with commentary on their strengths and weaknesses. The Characteristics of the most significant methods were summarized. Conclusions drawn reflected often-neglected ideas and applicability to engineering problems. Genetic Algorithms required one to set several heuristic parameters and this process was not necessarily straightforward. However, some codes allowed this process to be invisible to the user making Genetic multi-objective algorithms relatively easy to use. It was found that no single approach was superior.

Rather, the selection of a specific method depends on the type of information that is provided in the problem, the user's preferences, the solution requirements, and the availability of software.

Kao and Zahara [74] suggested that heuristic optimization provided a robust and efficient approach for solving complex real-world problems. The focus of this research was on a hybrid method combining two heuristic optimization techniques, Genetic Algorithms (GA) and particle swarm optimization (PSO) for the global optimization of multimodal functions. Denoted as GA-PSO, this hybrid technique incorporated concepts from GA and PSO and created individuals in a new generation not only by crossover and mutation operations as found in GA but also by mechanisms of PSO.

The difference between GAs and many traditional optimization methods is that GAs work with a population of points instead of a single point as pointed out by Mathew *et.al.* [68]. Because there are more than one string being processed simultaneously, it is very likely that the expected GA solution may be a global solution. Another advantage with a population-based search algorithm is that multiple optimal solutions can be captured in the population easily, thereby reducing the effort to use the same algorithm many times. Genetic algorithms perform a multiple directional search by maintaining a population of potential solutions. The population-to-population approach attempts to make the search escape from local optima. John McCall [63] presented Genetic algorithms (GAs), a heuristic search and optimization technique inspired by natural evolution. The algorithms had been successfully applied to a wide range of real-world problems of significant complexity. The use of Genetic Algorithm to deal with hydrodynamic-bearing problem is supported by Hirani and Suh [66] , Kao and Zahara [74] as well as many literatures.

Majumdar [75] in his book discusses the basic principles and equations governing Hydrodynamic Lubrication. The author has made an effort to explain the theory and present an exposition of the fundamentals of fluid film bearings. The major portion of the book is devoted to hydrodynamic theory and its application to bearings design.

1.3 Scope of the present work

It has been observed that various works that have been carried out include Numerical solution of Reynolds equation, steady state and dynamic characteristics of lobe bearings, stability analysis, comparison of the different characteristics of multi-lobe bearings etc.. It has been observed that no attempt has been made to find out the effect of different configurations on the performances of two axial groove, two lobe, three-lobe and four-lobe bearings by varying groove and lobe

angles. In view of this, it is required to study the effect of different groove location on various design parameters like friction variable, flow rate, load carrying capacity and mass parameter. Further, it is also necessary to optimize the groove location of two-groove, two, three and four lobe bearings with single and multi objective functions. In view of this it has been decided to carry out the following:

(i) To estimate the steady state and dynamic characteristics for various eccentricity ratios of two grooves bearings, two-lobe bearings, three-lobe bearings and four- lobe bearing by changing the groove angle and the locations of grooves.

(ii) To determine the stability characteristics of two-groove bearing, two-lobe bearings, three-lobe bearings and four-lobe bearings for different configurations of the bearing. The linear perturbation method would be used to estimate the Stability margins.

(iii) To search for groove locations for optimum performance of the four types of bearings on the basis of the maximization of flow coefficients, the maximization of non dimensional load capacity, the maximization of mass parameter and the minimization of friction variable.

(iv) To search for optimum groove locations for optimum performance of the four types of bearings on the basis of a multi-objective function formulated by combining the maximization of flow coefficients, the maximization non dimensional load capacity, the maximization of mass parameter and the minimization of friction variable.

(v) To analyze different optimum configurations for different objective functions and loading condition and to find out the most suitable configuration for all loading condition.

1.4 Organization of the Thesis

The present work deals the effect of different groove location on various design parameters like friction variable, flow rate, load carrying capacity and mass parameter. The different bearings configurations studied are two axial groove, two-lobe, three-lobe and four-lobe. The present thesis is broadly divided into seven chapter. Chapter 1 deals with the state of the art and literature review of previous works. The scope of the present work has been drawn on the literature review in this chapter.

The basic equation, which is used frequently in the hydrodynamic theory of lubrication are provided in chapter 2. The geometry of two axial groove bearings, two-lobe bearings, three-lobe and four-lobe bearings are also discussed in chapter 2. The non-dimensional load, flow

coefficient, friction variable expressions are written in dimensionless form. The expressions for bearing non-dimensional stiffness coefficients and the rigid rotor stability threshold parameter, non dimensional mass parameter are also given in chapter 2. The theory behind the Optimization Techniques used in finding out optimum groove locations is also discussed in chapter 2. Chapter 3 deals with analysis and identification of Groove locations of two axial groove bearings for optimum performance. Also identification of locations of grooves for two-groove bearing has been obtained in this chapter such that the performance characteristics are near to the optimum for any loading condition (eccentricity ratio) for different objective functions. Chapter 4 deals with analysis and identification of Groove locations of two-lobe bearings for optimum performance. A Comparison of optimum non-dimensional load capacity, optimum flow coefficient, friction variable and optimum Mass parameter with groove position placed along the horizontal direction 180^0 apart is made in this chapter. Also identification of locations of grooves for two-lobe bearing has been obtained in this chapter such that the performance characteristics are near to the optimum for any loading condition (eccentricity ratio) for different objective functions. Chapter 5 deals with analysis and identification of Groove locations of three-lobe bearings for optimum performance. A Comparison of optimum non-dimensional load capacity, optimum flow coefficient, friction variable and optimum Mass parameter with groove position placed symmetrically placed 120^0 apart is made in this chapter, also identification of locations of grooves for three-lobe bearing has been obtained in this chapter such that the performance characteristics are near to the optimum for any loading condition (eccentricity ratio) for different objective functions. Chapter 6 deals with analysis and identification of Groove locations of four-bearings for optimum performance. A Comparison of optimum non-dimensional load capacity, optimum flow coefficient, friction variable and optimum Mass parameter with groove position placed symmetrically placed 90^0 apart is made in this chapter and also identification of locations of grooves for four-lobe bearing has been obtained in this chapter such that the performance characteristics are near to the optimum for any loading condition (eccentricity ratio) for different objective functions. Finally, the major inferences drawn from the work carried out in this thesis are produced in chapter 7.

CHAPTER 2

Basic Equations, geometry of Lobe Bearings and optimization technique

2.0 Introduction

The basic equations which are used frequently in the hydrodynamic theory of lubrication are provided in this chapter. Geometry of two-lobe, three-lobe and four-lobe bearings are also included in this chapter. Besides the optimization Technique used in the present work has been briefly discussed. Since multi-objective optimization also will be carried out, therefore the formulation of multi-objective functions has been incorporated in this chapter.

2.1 Reynolds equation in the hydrodynamic theory

The governing equation is the Reynolds equation in two dimensions. It can be written for an incompressible isoviscous fluid [7] as follows:

$$\frac{\partial}{\partial x}\left(\frac{\rho h^3}{\eta}\frac{\partial p}{\partial x}\right)+\frac{\partial}{\partial z}\left(\frac{\rho h^3}{\eta}\frac{\partial p}{\partial z}\right)=6U\frac{\partial}{\partial x}(\rho h)+12\frac{\partial}{\partial t}(\rho h) \qquad (2.1)$$

The geometry and co-ordinate system of the plain journal bearing has been shown in Fig. 2.1

Film thickness, $h = C + eCos\theta$ (2.2)

Equation (2.1) can be written in non dimensionless form as in Eqn (2.3) [75] :

$$\frac{\partial}{\partial\theta}\left(\bar{h}^{\,3}\frac{\partial p}{\partial\theta}\right)+\left(\frac{D}{L}\right)^2\frac{\partial}{\partial\bar{z}}\left(\bar{h}^{\,3}\frac{\partial p}{\partial\bar{z}}\right)=\frac{\partial\bar{h}}{\partial\theta}+2\lambda\frac{\partial\bar{h}}{\partial\tau} \qquad (2.3)$$

Where, $\theta=\frac{x}{R},\bar{z}=\frac{z}{L/2},\bar{h}=\frac{h}{C},\bar{p}=\frac{pC^2}{6\eta UR},\tau=\omega_p t,\lambda=\frac{\omega_p}{\omega}$

2.2 Linear Perturbation Method

Let ε_0,ϕ_0 are the steady state eccentricity ratio and attitude angle respectively. Now assuming that the Journal whirls about the mean steady state position and considering only the first order perturbation, pressure and film thickness are expressed in Eqns 2.4 and 2.5 as follows:

$$\bar{p} = \bar{p}_0 + \varepsilon_1 e^{i\lambda\tau}\bar{p}_1 + \varepsilon_0\phi_1 e^{i\lambda\tau}\bar{p}_2 \tag{2.4}$$

$$\bar{h} = \bar{h}_0 + \varepsilon_1 e^{i\lambda\tau}\cos\theta + \varepsilon_0\phi_1 e^{i\lambda\tau}\sin\theta \tag{2.5}$$

Where, $\bar{p}_0$ is the steady state pressure component, and $\bar{p}_1, \bar{p}_2$ are the dynamics pressure components.

Substituting $\bar{p}$ and $\bar{h}$ in the Reynolds equation and equating the coefficients of $\varepsilon_0, \varepsilon_1 e^{i\lambda\tau}$ and $\varepsilon_0\phi_1 e^{i\lambda\tau}$ the following set of three equations (Eqns 2.6 to 2.8)are obtained when higher order terms are neglected.

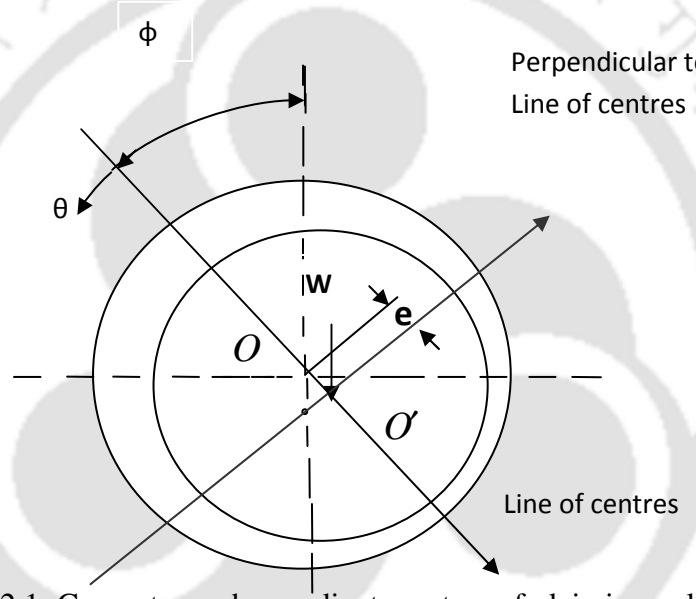

Figure 2.1: Geometry and co-ordinate system of plain journal bearing

$$\frac{\partial}{\partial\theta}\left(\bar{h}_0^{\,3}\frac{\partial\bar{p}_0}{\partial\theta}\right) + \left(\frac{D}{L}\right)^2\frac{\partial}{\partial\bar{z}}\left(\bar{h}_0^{\,3}\frac{\partial\bar{p}_0}{\partial\bar{z}}\right) = \frac{\partial\bar{h}_0}{\partial\theta} \tag{2.6}$$

$$\frac{\partial}{\partial\theta}\left(\bar{h}_0^{\,3}\frac{\partial\bar{p}_1}{\partial\theta}\right) + \left(\frac{D}{L}\right)^2\frac{\partial}{\partial\bar{z}}\left(\bar{h}_0^{\,3}\frac{\partial\bar{p}_1}{\partial\bar{z}}\right) + 3\frac{\partial}{\partial\theta}\left(\bar{h}_0^{\,2}\frac{\partial\bar{p}_0}{\partial\theta}\cos\theta\right) + \left(\frac{D}{L}\right)^2\frac{\partial}{\partial\bar{z}}\left(\bar{h}_0^{\,2}\frac{\partial\bar{p}_0}{\partial\bar{z}}\cos\theta\right) = \sin\theta + i2\lambda\cos\theta \tag{2.7}$$

$$\frac{\partial}{\partial\theta}\left(\bar{h}_0^{\,3}\frac{\partial\bar{p}_2}{\partial\theta}\right) + \left(\frac{D}{L}\right)^2\frac{\partial}{\partial\bar{z}}\left(\bar{h}_0^{\,3}\frac{\partial\bar{p}_2}{\partial\bar{z}}\right) + 3\frac{\partial}{\partial\theta}\left(\bar{h}_0^{\,2}\frac{\partial\bar{p}_0}{\partial\theta}\sin\theta\right) + \left(\frac{D}{L}\right)^2\frac{\partial}{\partial\bar{z}}\left(\bar{h}_0^{\,2}\frac{\partial\bar{p}_0}{\partial\bar{z}}\sin\theta\right) = -\cos\theta + i2\lambda\sin\theta \tag{2.8}$$

2.3 Boundary conditions

Boundary conditions used for the steady state pressure and dynamic pressure distribution are as follows:

$$\frac{\partial \overline{p}_i}{\partial \theta} = 0 \text{ and } \overline{p}_i = 0 \text{ at } \theta = \theta_r$$

$$\overline{p}_i(\theta, \overline{z}) = 0 \text{ when } \theta_s \le \theta \le \theta_e$$

where, $\overline{p}_i = \overline{p}_0, \overline{p}_1, \overline{p}_2$

and

$\theta s =$ starting angle of the groove w. r. t vertical axis

$\theta e =$ angle at which the groove ends w. r. t vertical axis

$\theta r =$ angle at which the film cavitates w. r. t vertical axis

There are other boundary conditions used particularly for analysis of dynamic characteristics, like Kicinski, JFO etc., however, the present analysis uses Reynolds boundary conditions for two reasons. The first being this set of boundary conditions can be easily implemented in iterative schemes and second being the present methodology is validated by comparing results based on Reynolds boundary conditions [2, 29].

2.4 Non-Dimensional load Capacity

The non-dimensional steady state load components are given by

$$\overline{W}_{X_0} = \int_{\theta_1}^{\theta_2} \int_0^1 \overline{p}_0 \cos\theta \, d\theta \, d\overline{z} \tag{2.9}$$

$$\overline{W}_{Z_0} = \int_{\theta_1}^{\theta_2} \int_0^1 \overline{p}_0 \sin\theta \, d\theta \, d\overline{z} \tag{2.10}$$

$$\overline{W}_0 = \sqrt{\overline{W}_{X_0}{}^2 + \overline{W}_{Z_0}{}^2} \tag{2.11}$$

Non dimensional load carrying capacity $\overline{W}_0 = \mathrm{WC}^2 / 6\eta \mathrm{UR}^2 \mathrm{L}$

2.5 Solution Scheme

Equation (2.6) is solved for the steady state pressure distribution $(\bar{p}_0)$, discretizing in a finite difference grid and using Gauss-Seidel method with successive over-relaxation (SOR) technique satisfying the boundary conditions. The convergence criterion adopted for pressure calculation is $\left|1-\frac{\Sigma\bar{p}_{old}}{\Sigma\bar{p}_{new}}\right| \leq 10^{-5}$. With chosen bearing eccentricity and arbitrary attitude angle picked at random results in magnitude of forces generated due to pressure wedge in the bearing. The attitude angle is changed till the horizontal force component $\left(\bar{W}_{Z_0}\right)$ in the pressure wedge becomes zero. This eventually locates the attitude angle. For this equilibrium position the vertical force $(\bar{W}_{X_0})$ gives the load capacity $\bar{W}_0$. The Sommerfeld number is given by S= $\frac{1}{\pi\bar{W}_0}$.

Mesh convergence was found with a Mesh size of 88 x14 and therefore, the results were generated using this mesh size. The mesh size is the same for the clearance zone including the lobe locations.

2.6 Design Parameters

The flow coefficient in the dimensionless form is given in Eqn 2.12 [2] :

$$\bar{q}_Z = \frac{1}{2}\left(\frac{D}{L}\right)^2 \int_0^{2\pi} \bar{h}_0^{\,3} \frac{\partial\bar{p}_0}{\partial\bar{z}} d\theta \qquad (2.12)$$

The friction variable, $\bar{\mu} = (R/C)\mu = \frac{\bar{F}}{\bar{W}_0}$, is given in Eqn 2.13 [75] :

$$\bar{\mu} = \mu(R/C) = \frac{\int_0^{2\pi} (3\bar{h}\frac{\partial\bar{p}_0}{\partial\theta} + \frac{1}{\bar{h}}) d\theta}{6\bar{W}} \qquad (2.13)$$

2.7 Dynamic Coefficients

The equations (2.7) and (2.8) for $\bar{p}_1$ and $\bar{p}_2$ are solved satisfying the boundary conditions and known values of $\bar{p}_0$ using the same procedure used for calculating steady state pressure. Dynamic loads due to $\bar{p}_1$ and $\bar{p}_2$ are given by in Eqns 2.14 and 2.15 :

$$\overline{W}_{X1} = \int_{\theta_E}^{\theta_S}\int_{0}^{1} \overline{p}_1 \cos\theta d\theta d\overline{z} \qquad \overline{W}_{Z1} = \int_{\theta_E}^{\theta_S}\int_{0}^{1} \overline{p}_1 \sin\theta d\theta d\overline{z} \tag{2.14}$$

and $$\overline{W}_{X2} = \int_{\theta_E}^{\theta_S}\int_{0}^{1} \overline{p}_2 \cos\theta d\theta d\overline{z} \qquad \overline{W}_{X2} = \int_{\theta_E}^{\theta_S}\int_{0}^{1} \overline{p}_2 \sin\theta d\theta d\overline{z} \tag{2.15}$$

Dynamic forces of each half lobe are added vectorially and total horizontal and vertical components are determined.

It is found that the fluid film, which supports the bearing, is equivalent to a spring mass damping system. Since the journal executes small harmonic oscillations about its steady state position; the dynamic load carrying capacity are expressed as a spring and a viscous damping force. The stiffness and damping coefficients presented in Eqns 2.16 and 2.17

$$\overline{K}_{XX} = -\mathrm{Re}(\overline{W}_{X1}) ; \overline{K}_{ZX} = -\mathrm{Re}(W_{Zt1}) ; \overline{K}_{XZ} = -\mathrm{Re}(\overline{W}_{Xt2}) ; \overline{K}_{ZZ} = -\mathrm{Re}(\overline{W}_{Zt2}) \tag{2.16}$$

$$\overline{C}_{XX} = -\mathrm{Im}(\overline{W}_{Xt1}) ; \overline{C}_{ZX} = -\mathrm{Im}(\overline{W}_{Zt1}) ; \overline{C}_{XZ} = -\mathrm{Im}(\overline{W}_{Xt2}) ; \overline{C}_{ZZ} = -\mathrm{Im}(\overline{W}_{Zt2}) \tag{2.17}$$

where $\overline{W}_{Xt1}$ and $\overline{W}_{Xt2}$ are total vertical load due to perturbation of steady state position .Similarly $\overline{W}_{Zt1}$ and $\overline{W}_{Zt2}$ are total horizontal load.

2.8 Stability Analysis

Self excited vibration of the rotor due to fluid film force is known as oil whirl, the frequency of this vibration is about $\frac{\omega}{2}$, where ω is the rotational speed of the rotor. Considering a rotor of mass 2m supported by two bearings. The non dimensional lineralised equations of Journal motion can be written as follows.

$$\overline{\mathrm{M}}\Delta\ddot{\overline{\mathrm{x}}} + \overline{\mathrm{K}}_{\mathrm{XX}}\Delta\overline{\mathrm{x}} + \overline{\mathrm{K}}_{\mathrm{XZ}}\Delta\overline{\mathrm{z}} + \overline{\mathrm{C}}_{\mathrm{XX}}\Delta\dot{\overline{\mathrm{x}}} + + \overline{\mathrm{C}}_{\mathrm{XX}}\Delta\dot{\overline{\mathrm{z}}} = 0 \tag{2.18}$$

$$\overline{\mathrm{M}}\Delta\ddot{\overline{\mathrm{z}}} + \overline{\mathrm{K}}_{\mathrm{ZX}}\Delta\overline{\mathrm{x}} + \overline{\mathrm{K}}_{\mathrm{ZZ}}\Delta\overline{\mathrm{z}} + \overline{\mathrm{C}}_{\mathrm{ZX}}\Delta\dot{\overline{\mathrm{x}}} + + \overline{\mathrm{C}}_{\mathrm{ZZ}}\Delta\dot{\overline{\mathrm{z}}} = 0 \tag{2.19}$$

where $\overline{M} = \frac{mC\omega^2}{W}$, a non dimensional mass parameter.

The steady state equilibrium position of the journal is x_0, z_0 and Δx and Δz are the perturbed amount from the steady state position at time 't'. Therefore, the following expressions are arrived at.

$$\left.\begin{aligned} &\bar{x} = \bar{x}_0 e^{i\lambda\tau},\ \bar{z} = \bar{z}_0 e^{i\lambda\tau} \\ &\dot{\bar{x}} = i\lambda\bar{x}_0 e^{i\lambda\tau},\ \dot{\bar{z}} = i\lambda\bar{z}_0 e^{i\lambda\tau} \\ &\ddot{\bar{x}} = -\lambda^2\bar{x}_0 e^{i\lambda\tau},\ \ddot{\bar{z}} = -\lambda^2\bar{z}_0 e^{i\lambda\tau} \end{aligned}\right\} \qquad (2.20)$$

Substituting the expressions of Eqn.2.20, the equations of motion (Eqns.2.18 and 2.19), a characteristic equation is formed as show in Eqn 2.21:

$$\begin{bmatrix} -\lambda^2\bar{M} + i\lambda\bar{C}_{XX} + K_{XX} & \bar{K}_{XZ} + i\lambda\bar{C}_{XZ} \\ \bar{K}_{ZX} + i\lambda\bar{C}_{ZX} & -\lambda^2 M + i\lambda\bar{C}_{ZZ} + \bar{K}_{ZZ} \end{bmatrix} \begin{Bmatrix} \bar{x}_0 \\ \bar{z}_0 \end{Bmatrix} e^{i\lambda\tau} = \begin{Bmatrix} 0 \\ 0 \end{Bmatrix} \qquad (2.21)$$

Solving the characteristic equation, the following expressions for the mass parameter, $\bar{M}$,and the whirl ratio, λ, are arrived at:

$$\lambda^2\bar{M} = \frac{\bar{K}_{XX}\bar{C}_{ZZ} + \bar{K}_{ZZ}\bar{C}_{XX} - (\bar{K}_{XZ}\bar{C}_{ZX} + \bar{K}_{ZX}\bar{C}_{XZ})}{\bar{C}_{XX} + \bar{C}_{ZZ}} = k_0 \qquad (2.22)$$

$$\text{So, } \lambda^2 = \frac{(\bar{K}_{XX} - k_0)(\bar{K}_{ZZ} - k_0) - \bar{K}_{XZ}\bar{K}_{ZX}}{\bar{C}_{XX}\bar{C}_{ZZ} - \bar{C}_{XZ}\bar{C}_{ZX}} \text{ and } \bar{M} = \frac{k_0}{\lambda^2} \qquad (2.23)$$

For a chosen static equilibrium position, the values of dynamic coefficients are determined. These values are used to calculate the value of $\bar{M}$ and λ . When the mass parameter of a rotor bearing system exceeds the value calculated by the above method, the instability occurs in the system. The value of mass parameter at the threshold of instability is known as the critical mass parameter $(\bar{M}_{crit})$ and corresponding whirl ratio is known as critical whirl ratio (λ_{crit}).

2.9 Geometry of bearings

2.9.1. Geometry of two-groove bearing

Two grooves of 10^0 circumferential extension and two 170^0 arcs with coinciding centres of the arcs and the bearing has been shown in Fig. 2.2. θ is measured from the vertical axis X and the

attitude angle, ϕ, is the angle between the load line and the centre to centre line. The bearing is the same as a plain journal bearing except the two grooves provided 180^0 apart in the horizontal direction, Z

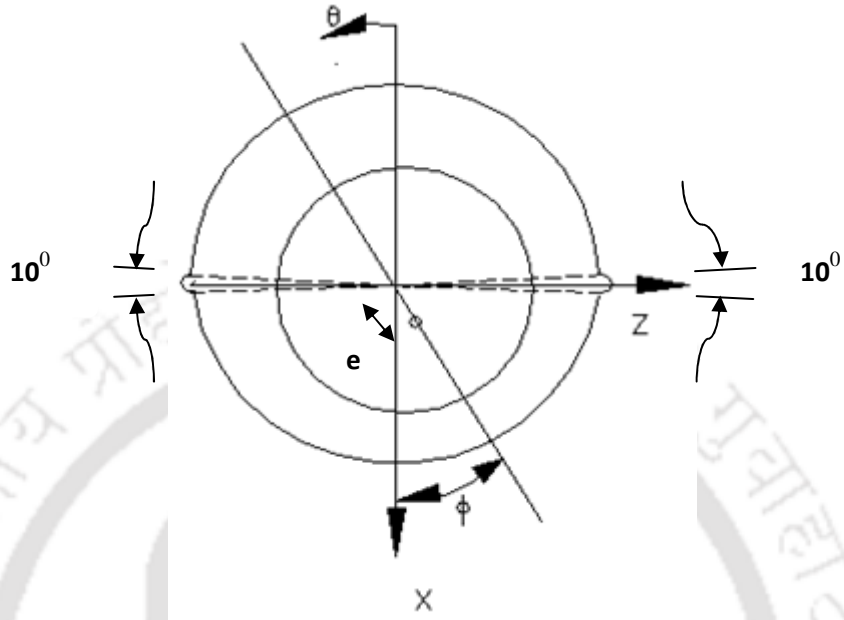

Figure 2.2: Geometry and co-ordinate system of two axial groove bearing

2.9.2. Geometry of two-lobe bearing

Geometry and co-ordinate system for two-lobe bearing are shown in Fig. 2.3 and Fig. 2.4. Lobes are separated by axial grooves of 10^0 circumferential extensions for the provision of oil inlet in the journal bearing clearance area.

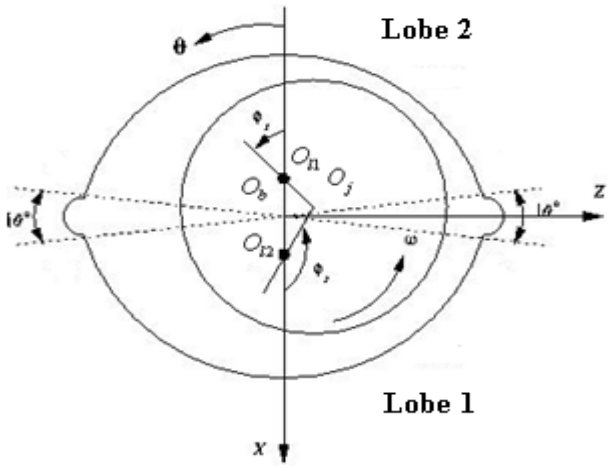

Figure 2.3: Geometry and co-ordinate system of 2 lobe bearing

Two-lobe bearing is made up of two circular arcs each with its own centre of curvature o_l displaced a distance'd' from the geometric centre of the bearing. Fig.2.2 shows two lobes of 170^0 arc separated by two axial oil grooves of 10^0 extensions in horizontal direction. In Fig. 2.3, geometry and co-ordinate system used for the analysis of two-lobe bearing is presented. For any given shaft position, lobe eccentricity ratios $(\varepsilon_1, \varepsilon_2)$ and attitude angles (ϕ_1, ϕ_2) can be related with bearing eccentricity ratio (ε), attitude angle (ϕ) and ellipticity ratio (δ) by simple trigonometric relations obtained from Fig. 2.4.

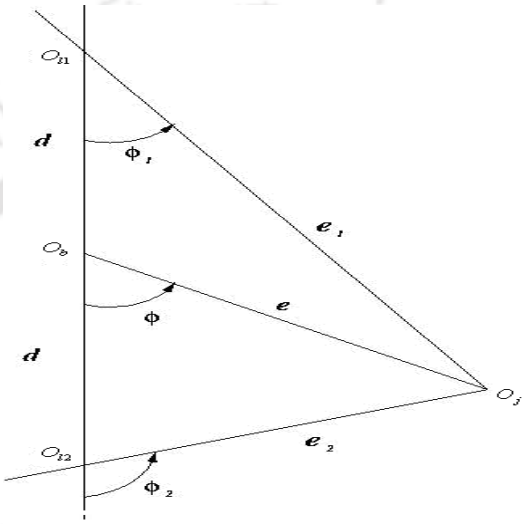

Figure 2.4: Lobe eccentricities and attitude angles of a 2-lobe bearing

The journal centre, bearing geometric centre, centre of the lobe 1 and centre of the lobe 2 are represented by o_j, o_b, o_{l1} and o_{l2} respectively. From simple trigonometry, following relationships for Eqns 2.24 through 2.30 are obtained:

For lobe 1

$$e_1^{\,2} = e^2 + d^2 - 2ed\cos(\pi - \phi) \tag{2.24}$$

Dividing both sides by c^2, one gets,

$$\varepsilon_1^{\,2} = \varepsilon^2 + \delta^2 + 2\varepsilon\delta\cos(\phi) \tag{2.25}$$

$$\varepsilon_1 = \sqrt{\varepsilon^2 + \delta^2 + 2\varepsilon\delta\cos\phi} \tag{2.26}$$

where $\delta = \frac{d}{c}$ is the bearing ellipticity ratio and $\varepsilon_1 = \frac{e_1}{c}$ is the eccentricity ratio of lobe 1.

Also $$\tan\phi_1 = \frac{e\sin\phi}{d + e\cos\phi} \tag{2.27}$$

$$\phi_1 = \tan^{-1}\frac{e\sin\phi}{d + e\cos\phi}$$

For lobe 2

$$e_2^{\,2} = e^2 + d^2 - 2ed\cos\phi \tag{2.28}$$

$$\varepsilon_2 = \sqrt{\varepsilon^2 + \delta^2 - 2\varepsilon\delta\cos\phi}$$

(2.29)

Where $\varepsilon_2 = \frac{e_2}{c}$ is the eccentricity ratio of lobe 2.

Also $$\phi_2 = \pi - \tan^{-1}\frac{\varepsilon\sin\phi}{\delta - \varepsilon\cos\phi} \tag{2.30}$$

2.9.3. Geometry of three-lobe bearing

The bearing as shown in Fig. 2.5, consists of three lobes, the centre of each lobe displaced an equal distance called ellipticity, from the centre of the bearing. The maximum span of lobe is 120^0. The lobes, however, are separated by axial grooves for admitting oil and in this work 10^0 grooves are allotted. So the net span of each lobe is 110^0.The individual lobe eccentricities $(\varepsilon_1, \varepsilon_2, \varepsilon_3)$ and attitude angles (ϕ_1, ϕ_2, ϕ_3) are related to the bearing eccentricity and attitude angle. These relationships are presented in Eqns 2.31 through 2.36 are obtained from Fig. 2.6 by following the similar procedure used for two-lobe bearing.

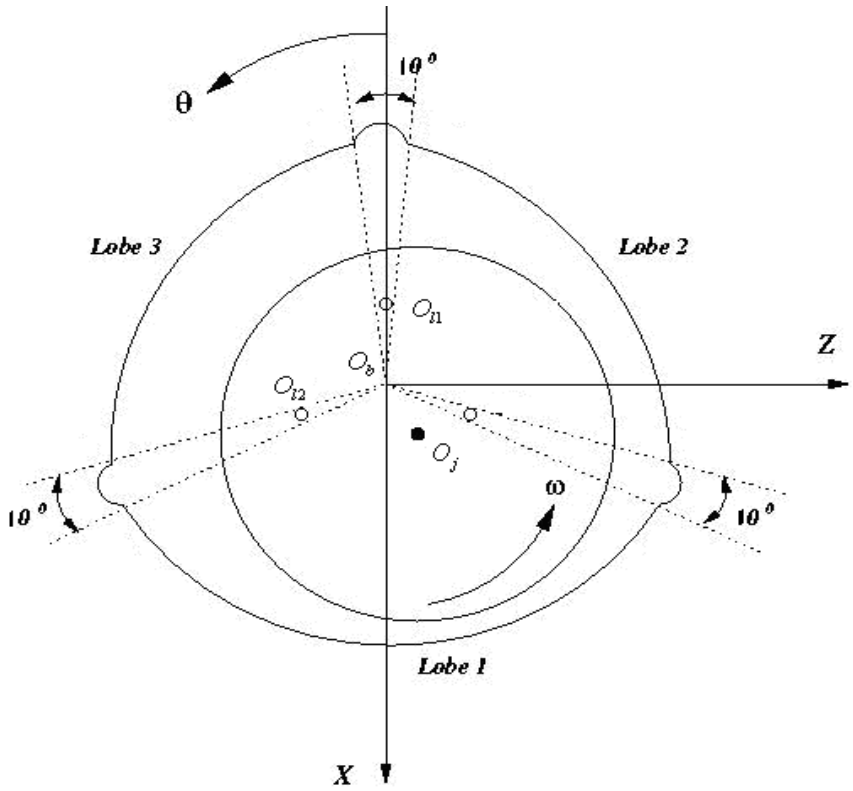

Figure 2.5: Geometry and co-ordinate system of 3 lobe bearing

For lobe 1

$$\varepsilon_1 = \sqrt{\varepsilon^2 + \delta^2 + 2\varepsilon\delta\cos\phi} \tag{2.31}$$

$$\phi_1 = \tan^{-1}\frac{e\sin\phi}{d + e\cos\phi} \tag{2.32}$$

For lobe 2

$$\varepsilon_2 = \sqrt{\varepsilon^2 + \delta^2 - 2\varepsilon\delta\cos(\frac{\pi}{3} + \phi)} \tag{2.33}$$

$$\phi_2 = \frac{2\pi}{3} - \tan^{-1}\frac{\varepsilon\sin\left(\frac{\pi}{3} + \phi\right)}{\delta - \varepsilon\cos\left(\frac{\pi}{3} + \phi\right)} \tag{2.34}$$

For lobe 3

$$\varepsilon_3 = \sqrt{\varepsilon^2 + \delta^2 - 2\varepsilon\delta\cos\left(\frac{\pi}{3} - \phi\right)} \tag{2.35}$$

$$\phi_3 = \frac{2\pi}{3} \tan^{-1} \frac{\varepsilon \sin\left(\frac{\pi}{3} - \phi\right)}{\delta - \varepsilon \cos\left(\frac{\pi}{3} - \phi\right)} \tag{2.36}$$

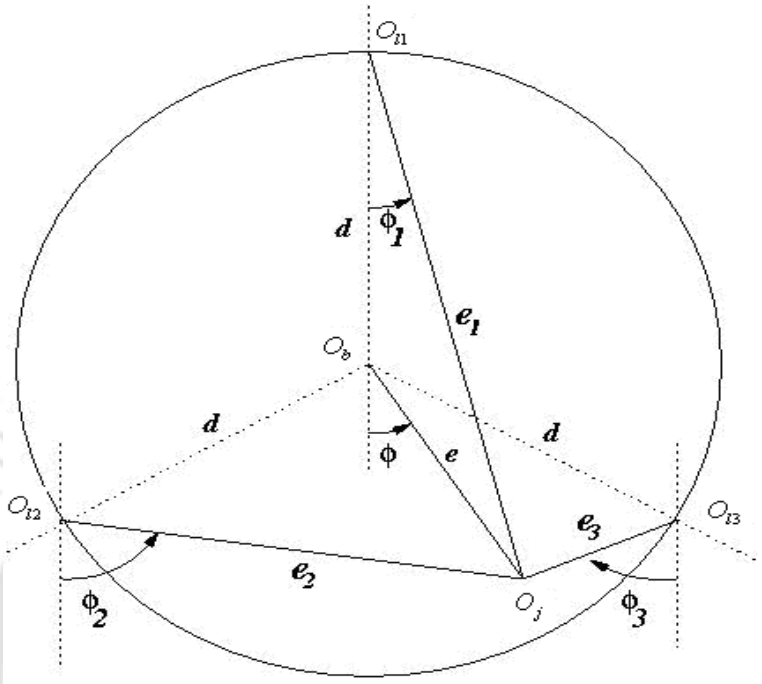

Figure 2.6: Lobe eccentricities and attitude angles of 3 lobe bearing

2.9.4. Geometry of four-lobe bearing

The bearing as shown in Fig. 2.7, consists of four lobes, the centre of each lobe displaced an equal distance, called ellipticity, from the centre of the bearing. The maximum span of a lobe is 90^0. The lobes however are separated by axial grooves for admitting oil and in this work 10^0 grooves are considered. So the net span of each lobe is 80^0. The individual lobe eccentricities $(\varepsilon_1, \varepsilon_2, \varepsilon_3, \varepsilon_4)$ and attitude angles $(\phi_1, \phi_2, \phi_3, \phi_4)$ are related to the bearing eccentricity and attitude angle. These relations are presented in Eqns 2.37 through 2.44 are obtained from Fig. 2.8 by following the similar procedure used for two-lobe and three-lobe bearings.

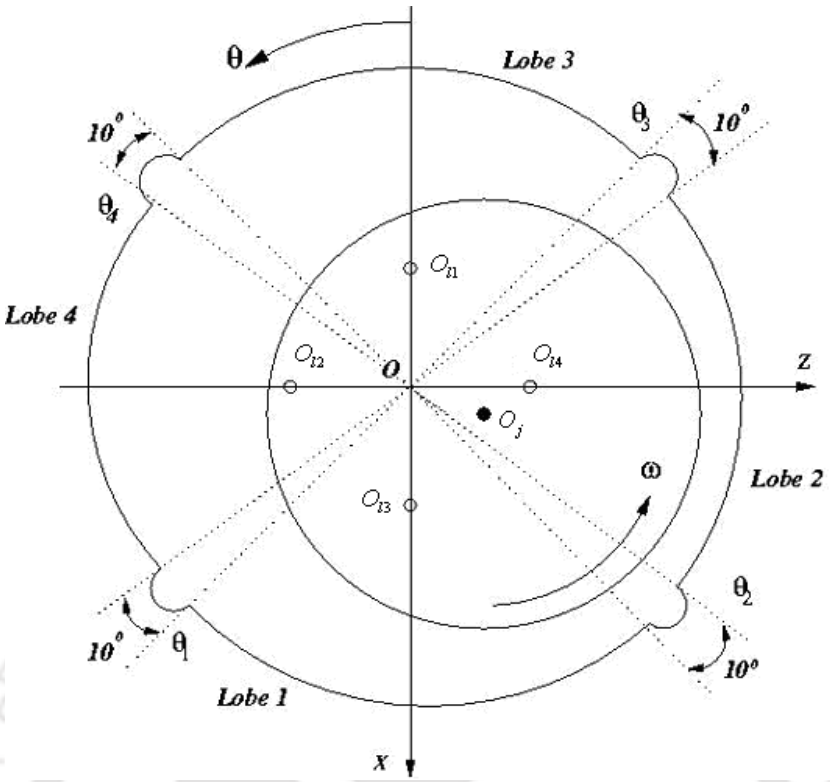

Figure 2.7: Geometry and co-ordinate system of 4-lobe bearing

For lobe 1

$$\varepsilon_1 = \sqrt{\varepsilon^2 + \delta^2 + 2\varepsilon\delta\cos\phi} \tag{2.37}$$

$$\phi_1 = \tan^{-1}\frac{\varepsilon\sin\phi}{\delta + \varepsilon\cos\phi} \tag{2.38}$$

For lobe 2 $$\varepsilon_2 = \sqrt{\varepsilon^2 + \delta^2 - 2\varepsilon\delta\cos\left(\frac{\pi}{2} + \phi\right)} \tag{2.39}$$

$$\phi_2 = \frac{\pi}{2} - \tan^{-1}\frac{\varepsilon\sin\left(\frac{\pi}{2} + \phi\right)}{\delta - \varepsilon\cos\left(\frac{\pi}{2} + \phi\right)} \tag{2.40}$$

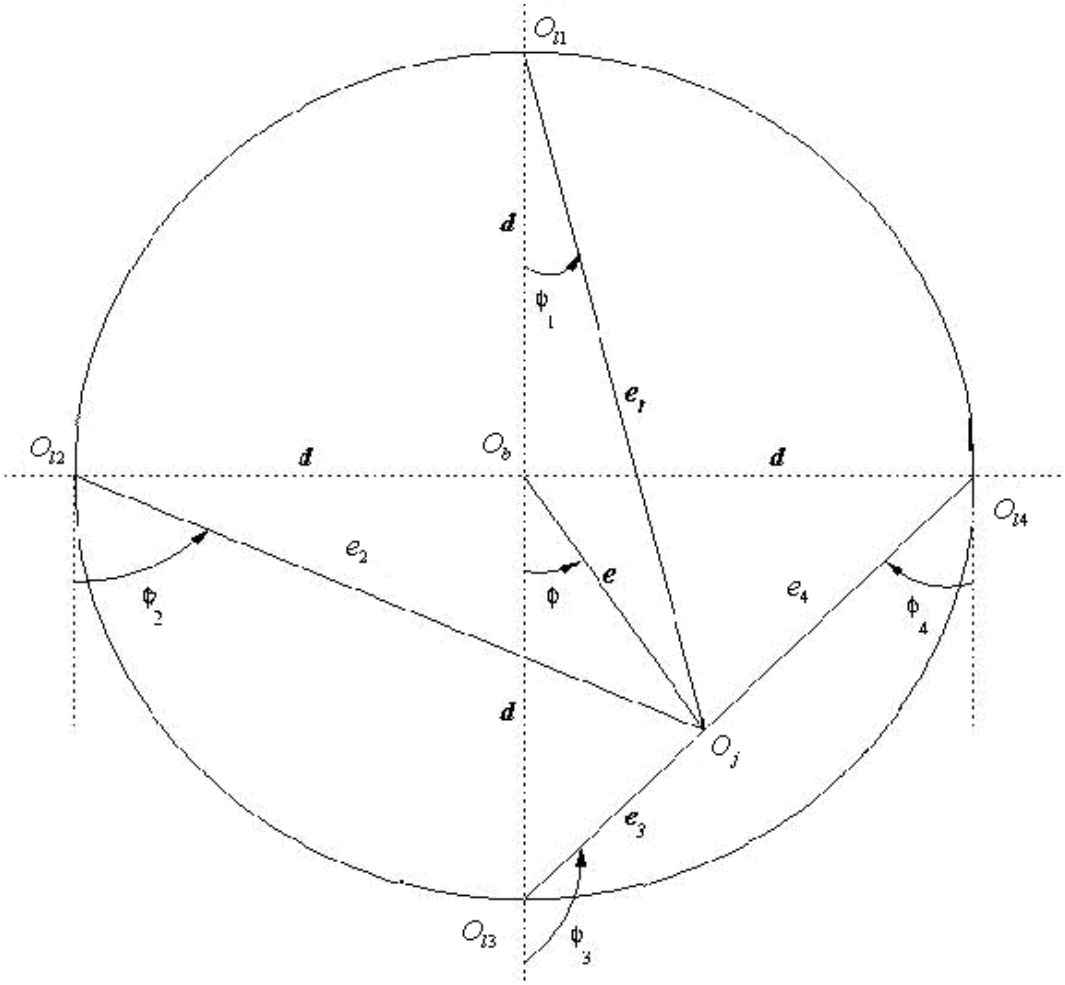

Figure 2.8: Lobe eccentricities and attitude angles of 4 lobe bearing

For lobe 3 $$\varepsilon_3 = \sqrt{\varepsilon^2 + \delta^2 - 2\varepsilon\delta\cos\phi} \quad (2.41)$$

$$\phi_3 = \pi - \tan^{-1}\frac{\varepsilon\sin\phi}{\delta - \varepsilon\cos\phi} \quad (2.42)$$

For lobe 4 $$\varepsilon_4 = \sqrt{\varepsilon^2 + \delta^2 - -2\varepsilon\delta\cos\left(\frac{\pi}{2} - \phi\right)} \quad (2.43)$$

$$\phi_4 = \frac{\pi}{2} - \tan^{-1}\frac{\varepsilon\cos\phi}{\delta - \varepsilon\sin\phi} \quad (2.44)$$

2.10 Optimization Techniques

2.10.1 Real coded Genetic algorithm Computational procedure

In finding out optimum results using Genetic Algorithm (GA), variables called genes will form chromosome. A set of chromosome is called population. With uniform probability distribution all chromosomes in the population are initialized. The population of each generation will have feasible design variables (Chromosome) in terms of their allowable ranges but may be infeasible otherwise. The main steps involved in the genetic algorithm are discussed below and shown in a flow chart (Fig. 2.9). The generic algorithm convergence rate to true optima depends on the probability of crossover and mutation on one hand, and the maximum generation, on the other hand. In order to preserve a few very good strings, and rejecting low-fitness strings, a high crossover probability is preferred. The mutation operator helps to retain the diversity in the population, but disrupts the progress towards a converged population and interferes with beneficial action of the selection and crossover. Therefore, a low probability, 0.001–0.1, is preferred. The genetic algorithm updates its population on every generation, with a guarantee of better or equivalent fitness strings. For well-behaved functions, 30–40 generations are sufficient. For steep and irregular functions, 50–100 generations are preferred [68]. Considering these factors, a population size of 50, mutation probability of 0.1 and a cross over probability of 0.8 have been selected. The difference between GAs and many traditional optimization methods is that GAs work with a population of points instead of a single point. On the other hand, since GAs require only function values at various discrete points, a discrete or discontinuous function can be handled with no extra burden. This allows GAs to be applied to a wide variety of problems. Another advantage with a population-based search algorithm is that multiple optimal solutions can be captured in the population easily, thereby reducing the effort to use the same algorithm many times. Genetic algorithms perform a multiple directional search by maintaining a population of potential solutions. The population-to-population approach attempts to make the search escape from local optima [68]. GAs are very helpful when the developer does not have precise domain expertise, because GAs possess the ability to explore and learn from their domain.

GA has been used in this work as GA, being a heuristic search and optimization technique inspired by natural evolution, has been successfully applied to a wide range of real-world problems of significant complexity [67]. It has been suggested that heuristic optimization provides a robust and efficient approach for solving complex real-world problems [67].

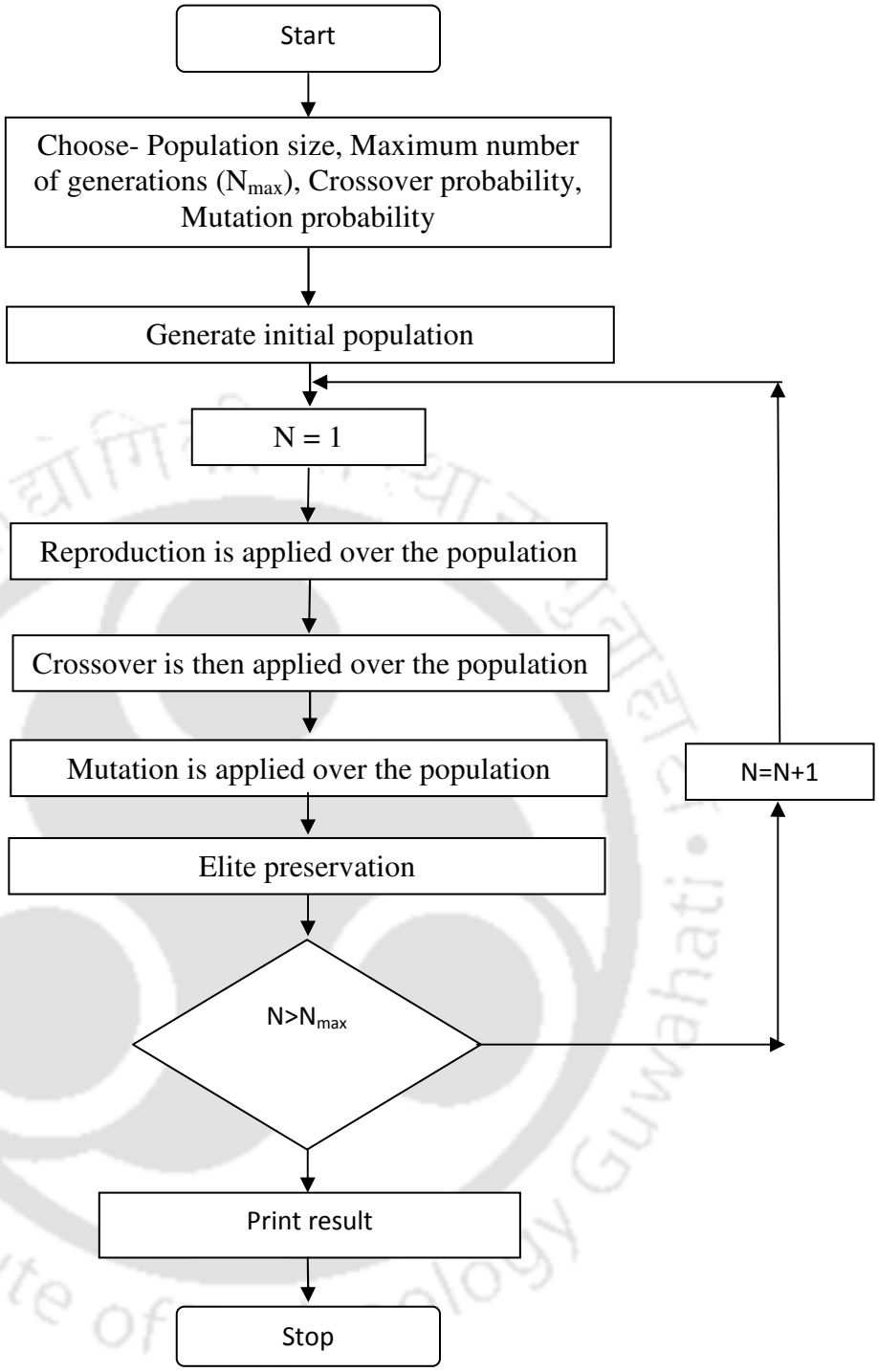

Figure 2.9: Flow chart for real coded Genetic Algorithm

The optimization problem can be mathematically represented as

Optimize (minimize or maximize) $F_j(x, p)$ $j = 1,2,3.....,J$ with variable bounds as

$x_i^{\min} < x_i < x_i^{\max}$ with $j = 1,2,3....., n$, p is a vector of design parameters, subjected to constrains:

$g_k(x) \geq 0$ where, $k = 1,2,3....., k$. $F_j(x, p)$ are the objective functions for the design problem. (2.45)

2.11 Formulation of Multi-Objective function

The weighted sum strategy is often [58,61] used to convert the multi-objective problem of minimizing the objective vector into a scalar problem by constructing a weighted sum of all objectives. In the present work, the multi-objective function formulated as given in Eqn 2.46

$$\text{Minimize} \quad f = w_1\left[\bar{\mu}\Big/\left(\bar{\mu}_{\max}-\bar{\mu}_{\min}\right)\right]+w_2\left[1-\bar{q}_z\Big/\left(\bar{q}_{z\max}-\bar{q}_{z\min}\right)\right] +w_3\left[1-\bar{w}\Big/\left(\bar{w}_{\max}-\bar{w}_{\min}\right)\right]+w_4\left[1-\bar{M}\Big/\left(\bar{M}_{\max}-\bar{M}_{\min}\right)\right] \tag{2.46}$$

Where, $\bar{\mu}=\mu(\frac{R}{C})$=friction variable, $\bar{q}_z$ =flow coefficient, $\bar{w}$ =non-dimensional load capacity and $\bar{M}=\dfrac{MC\omega^2}{W}$ = mass parameter, w_1, w_2, w_3, and w_4, are the associated weight. $\bar{\mu}_{\max}$, $\bar{\mu}_{\min}$ are the corresponding maximum and minimum value and so on.

2.12 Summary:

The Reynolds equation which is the governing equation in hydrodynamic lubrication has been included in this chapter. The linear perturbation method is explained to find out the dynamic coefficients and then to find out the stability parameter. Geometries of two axial groove, two-lobe, three-lobe and four-lobe bearings are also included in this chapter. Further a brief outline of the optimization technique used in this work has been presented. Finally the formulation of multi-objective function has been incorporated. The equations, solution schemes, geometry, optimization technique and multi-objective functions are used in the following four chapters for different bearings.

CHAPTER 3

Analysis of two axial groove bearings

3.0 Introduction

Axial groove bearings are very common in many type of commercial machinery including turbines, generators, motors, pumps and compressors, and have slightly better dynamic properties than the plain journal bearings. It is similar to plain journal bearings, but two axial grooves are provided for oil supply. There is no preload and has a high tendency of instability in two-groove bearings same as in the plain journal bearing. An axial groove is particularly useful for distributing oil over the entire length of the bearing to control its temperature. An alternative location for an axial groove is 90^0 to the load line. In some instances, two axial grooves running parallel at $\pm 90^0$ to the load line are used in industry applications, with the axial grooves formed at the split between the halves of a cylindrical bearing. If the bearing is steadily loaded, either the supply hole or an axial groove can do the job as long as it is placed in the unloaded portion of the bearing. Clearly, pressure generation is interrupted if a groove or a supply hole is placed in the active region where hydrodynamic pressure is generated.

3.1 Estimation of Steady state and dynamic characteristics

A journal bearing fed by two axial grooves has a wide practical application due to its good load carrying capacity and ability to operate when reversal of shaft rotation occurs. These bearing usually have the grooves positioned orthogonal to the predominant load direction. Among the previous works on two axial groove oil journal bearings; Lund and Thomson [29] obtained dynamic coefficients of plain circular bearing with two 20^0 axial grooves. Before starting the analysis of two axial groove bearing, a comparison of present set of results of steady state values of attitude angle ϕ_o, friction variable, $(R/C)\mu$ and flow coefficient, $\overline{q}_z$ and Sommefeld number, S, has been made with published results of Pinkus and Sternlicht [2] for plain journal bearing for L/D=1 and shown in Table 3.1. The results are found to be in good agreement.

Similarly a comparison of steady state and dynamic characteristics is also made with the published results of Lund and Thomson [29] for two axial groove bearings for L/D=1 with two 20^0 axial groove and presented in Table 3.2. In this case too, the results are found to be in good agreement.

Table 3.1: Comparison of the results for Plain Journal bearing with those obtained by Pinkus [2]

ε	ϕ		S		Friction variable, $\bar{\mu}$		Flow co efficient $\bar{q}_z$	
0.1	79	[79]	1.32	[1.35]	28.26	[*]	0.15	[0.16]
0.2	73	[74]	0.631	[0.632]	12.8	[12.9]	0.306	[0.361]
0.3	68	[68]	0.388	[0.382]	8.18	[8.04]		[*]
0.4	62	[62]	0.260	[0.261]	5.78	[5.80]	0.604	[0.607]
0.5	56	[56]	0.178	[0.179]	4.28	[4.31]		[*]
0.6	50	[50]	0.120	[0.120]	3.22	[3.21]	0.896	[0.938]
0.7	43	[43]	0.0771	[0.0765]	2.40	[2.36]	0.896	[*]
0.8	36	[36]	0.0448	[0.0448]	1.70	[1.71]	1.18	[1.24]

Table 3.2: Comparison of present results with [29] for L/D=1 and 20^0 axial groove placed horizontally 180^o apart

ε	S	ϕ	$\bar{K}_{XX}$	$\bar{K}_{XZ}$	$\bar{K}_{ZX}$	$\bar{K}_{ZZ}$	$\bar{C}_{XX}$	$\bar{C}_{XZ} = \bar{C}_{ZX}$	$\bar{C}_{ZZ}$
0.103	1.453 [1.470]	75.862 [75.99]	1.487 [1.53]	10.219 [10.14]	-3.254 [-3.01]	1.5605 [1.50]	20.508 [20.34]	1.596 [1.53]	6.623 [6.15]
0.150	0.980 [0.991]	70.462 [70.58]	1.511 [1.56]	7.345 [7.29]	-2.34 [-2.16]	1.579 [1.52]	14.792 [14.66]	1.657 [1.58]	4.866 [4.49]
0.224	0.629 [0.635]	63.459 [63.54]	1.562 [1.62]	5.381 [5.33]	-1.743 [-1.56]	1.622 [1.56]	10. 915 [10.80]	1.794 [1.70]	3.738 [3.410]
0.352	0.352 [0.358]	56.100 [55.41]	1.727 [1.95]	4.042 [3.94]	-1.243 [-0.97]	1.684 [1.48]	8.238 [8.02]	2.037 [1.63]	2.977 [2.37]
0.460	0.232 [0.235]	49.925 [49.27]	2.134 [2.19]	3.574 [3.57]	-0.855 [-0.80]	1.598 [1.48]	7.348 [7.36]	1.959 [1.89]	2.336 [2.19]
0.559	0.157 [0.159]	45.107 [44.33]	2.677 [2.73]	3.369 [3.36]	-0.506 [-0.48]	1.529 [1.48]	6.899 [6.94]	1.841 [1.78]	1.838 [1.74]
0.650	0.106 [0.108]	40.120 [39.72]	3.427 [3.45]	3.353 [3.34]	-0.226 [-0.23]	1.475 [1.44]	6.855 [6.89]	1.742 [1.72]	1.474 [1.43]
0.734	0.070 [0. 071]	35.58 [35.16]	4.449 [4.49]	3.522 [3.50]	0.038 [0.03]	1.478 [1.44]	7.138 [7.15]	1.750 [1.70]	1.254 [1.20]
0.773	0.056 [0.056]	35.58 [32.86]	5.170 [5.23]	3.684 [3.65]	0.174 [0.18]	1.487 [1.45]	7.444 [7.42]	1.767 [1.71]	1.161 [1.10]
0.811	0.0437 [0.044]	35.58 [30.687]	6.147 [6.22]	3.916 [3.88]	0.339 [0.35]	1.504 [1.46]	7.863 [7.81]	1.793 [1.72]	1.071 [1.01]
0.883	0.023 [0.024]	25.117 [25.02]	9.933 [9.77]	4.657 [4.69]	0.938 [0.83]	1.521 [1.53]	8.867 [9.17]	1.651 [1.78]	0.780 [0.83]

3.2 Analysis of steady state and dynamic characteristics

3.2.1 Groove size for better performance

To ascertain the size of the groove for better performance, a comparison of non-dimensional load is made for different groove angles as shown in Table 3.3. It has been observed from the tabulated results that the load carrying capacity is slightly higher with 10^o groove angles in comparison to 20^o and 30^o groove angles in case of two axial groove bearings. Therefore, 10^o groove angles are considered throughout the analysis.

Table 3.3: Comparison of non-dimensional load values using 10^o, 20^o and 30^o groove angles

	$\bar{W}$		
ε	10^o groove	20^o groove	30^o groove
0.2	0.077	0.074	0.071
0.4	0.186	0.181	0.175
0.6	0.406	0.399	0.389
0.8	1.135	1.123	1.107

3.2.2 Bearing Performance with different Groove locations

The current practice is that the grooves are placed horizontally 180^o apart for two-axial groove bearings. An attempt has been made in this section to find out if the bearing performances are the same or different when groove locations are different from the current practice. In view of this many different configurations are studied and performance characteristics have been estimated. However, results showing the differences in performance characteristics of only one configuration (UP-UP 70^o) have been shown here to save space. UP-UP-70^0configuration means that both grooves are 70^0 above the horizontal. The groove angle considered is 10^o. The results are presented in Figs. 3.1 through 3.4. It has been observed that with change in groove locations, the various steady state and dynamic characteristics also change. Therefore, it is obvious that there has to be a certain configuration which corresponds to the optimum performance.

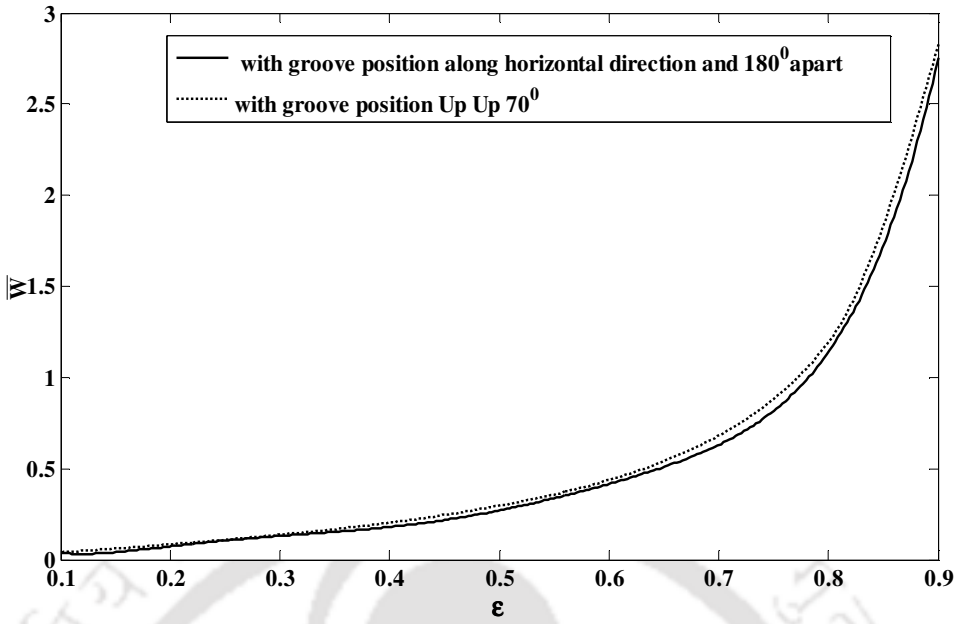

Figure 3.1: Variation of non-dimensional load capacity ratio with ε

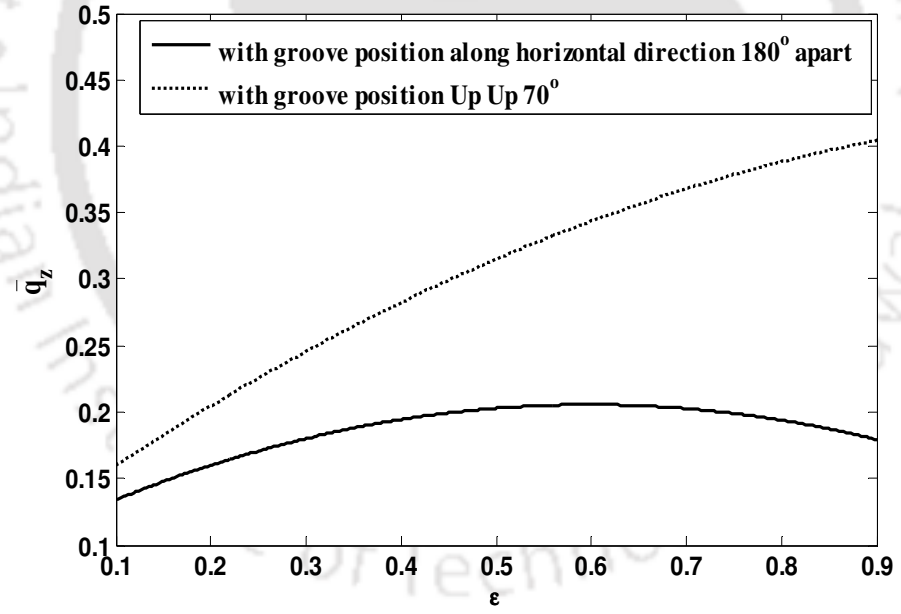

Figure 3.2: Variation of flow coefifcient with ε

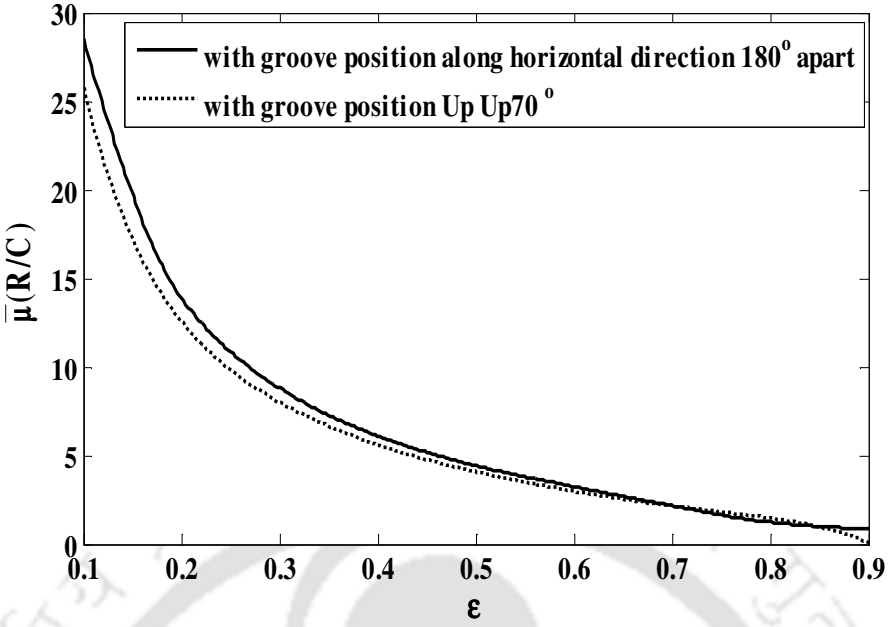

Figure 3.3: Variation of friction variable with ε

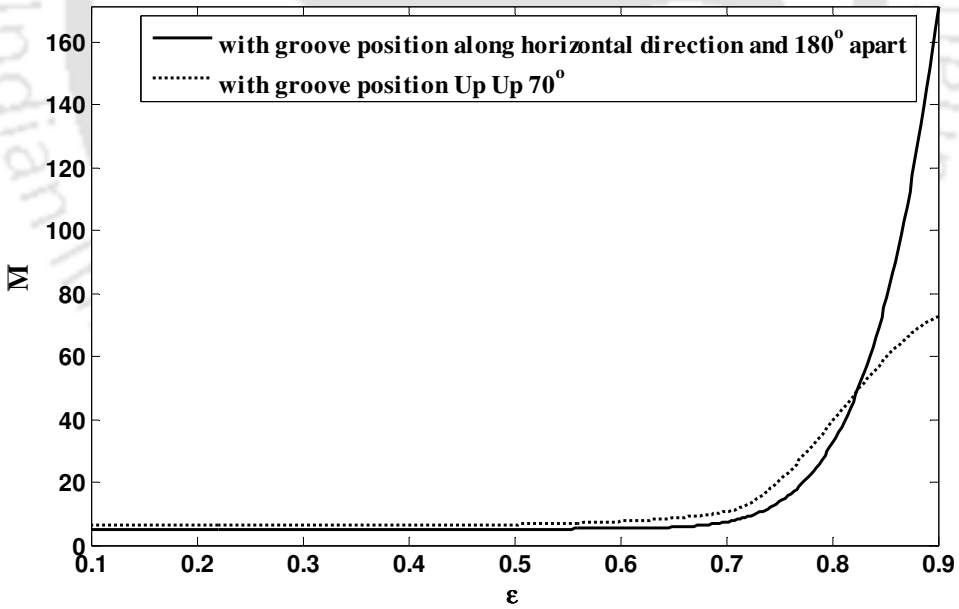

Figure 3.4: Variation of mass parameter with ε

3.2.3 Determination of optimum location of groove

It has been shown in the previous section that the locations of grooves have influence in flow coefficient ($\bar{q}_z$), frictional variable ($\bar{\mu}$), non-dimensional load capacity ($\bar{W}$) and mass

parameter ($\overline{M}$) of two axial groove bearing. In view of this, an attempt has been made to locate the groove locations of two axial groove bearing which correspond to optimum performances in terms of the four parameters mentioned above.

Genetic Algorithm (GA) has been used to find the optimum solution as outlined in Chapter 2. The problem is framed with four objectives. The variables used in the problem are in starting angle of first groove (θ_1), starting angle of second groove (θ_2) Case –I. The optimum configurations have been obtained for eccentricity ratio ranging from 0.1 to 0.9 in this case. In Case –II, the eccentricity ratio (ε), starting angle of first groove (θ_1), starting angle of second groove (θ_2) are variables and act as Chromosome. The objectives are minimization of friction variable, $\bar{\mu}$ (Eqn. 2.22), maximization of non-dimensional load capacity, $\overline{W}$ (Eqn. 2.20), flow coefficient $\overline{q}_z$ (Eqn 2.21), maximization of mass parameter, $\overline{M}$ (Eqn. 2.31). Objective function framing is the same for both the cases and variable bounds are shown in Table 3.4.

Table 3.4: Variable bounds for the bearing problem

Case	Variable	Lower Bound	Upper Bound
I	Starting angle of first	15°	180°
	Starting angle of second	170°	345°
II	ε	0.1	0.9
	Starting angle of first	15°	180°
	Starting angle of second	170°	345°

An optimum groove location has been obtained for the objective functions outlined above with the help of Genetic Algorithm (GA) toolbox of MatLab. The obtained results from GA have been compared with the results obtained using Sequential Quadratic Programming (SQP). The optimum value of fitness function obtained corresponding to minimization of friction variable has been tabulated for both GA and SQP in Table 3.5.

SQP method represents the state of the art in nonlinear programming methods. Schittkowski [57] for example, has implemented and tested a version that outperforms every other tested method in terms of efficiency, accuracy, and percentage of successful solutions, over a large number of test problems.

It has been observed that the results obtained using both the methods are exactly the same. Similarly, maximum non-dimensional load capacity, maximum flow coefficient, maximum mass parameter values are also found to match for both the methods. However, GA

has been used in this work as GA, being a heuristic search and optimization technique inspired by natural evolution, has been successfully applied to a wide range of real-world problems of significant complexity [64].

Table 3.5: Comparison of GA and SQP results

ε	Objective function value (Minimum Friction Variable)	
	GA results	SQP results
0.1	25.844	25.844
0.2	12.572	12.572
0.3	7.988	7.988
0.4	5.587	5.587
0.5	4.064	2.981
0.6	2.993	2.993
0.7	2.156	2.156
0.8	1.119	1.462
0.9	0.848	0.848

Initially a single objective function has been taken up. The generic algorithm convergence rate to true optima depends on the probability of crossover and mutation on one hand, and the maximum generation, on the other hand. In order to preserve a few very good strings, and rejecting low-fitness strings, a high crossover probability is preferred. The mutation operator helps to retain the diversity in the population, but disrupts the progress towards a converged population and interferes with beneficial action of the selection and crossover. Therefore, a low probability, 0.001–0.1, is preferred. The genetic algorithm updates its population on every generation, with a guarantee of better or equivalent fitness strings. For well-behaved functions, 30–40 generations are sufficient. For steep and irregular functions, 50–100 generations are preferred [68]. Considering these factors, a population size of 50, mutation probability of 0.1 and a cross over probability of 0.8 have been selected.

The optimum groove locations for minimum friction variable, non-dimensional load capacity, flow coefficient, mass parameter and multiobjective function (section 2.11) at different

ε are shown in Figures 3.5 through 3.9. θ_1 and θ_2 are the starting angles of the first and the second groove respectively in degrees.

From the results presented here, it can be inferred that the second groove locations are sensitive to the type of objective function whereas the first groove is more or less the same. The practice and the notion of convenience of keeping groove locations horizontally 180^o apart need to be thoroughly looked into as the present results show that optimum groove locations are not horizontally 180^o apart for the objective functions considered in the present work.

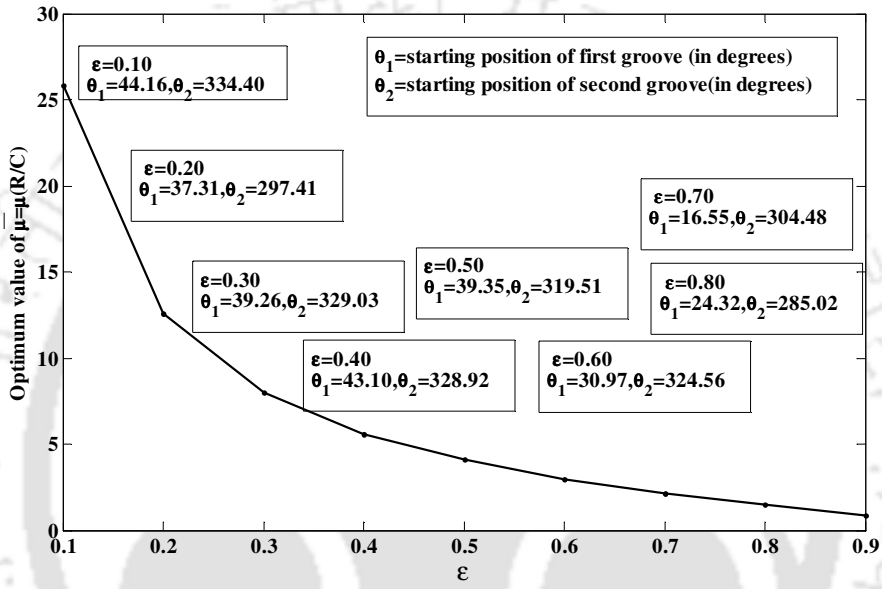

Figure 3.5: Variation of friction variable at optimum grooving location for different ε

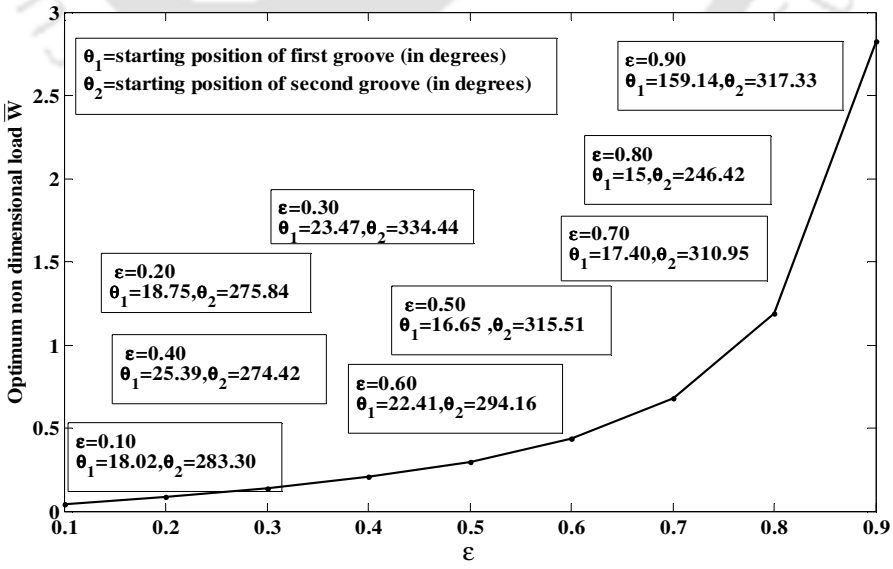

Figure 3.6: Variation of $\overline{W}$ at optimum grooving location for different ε

Optimum parameters are compared with those with groove locations along horizontal direction and 180^0 apart as shown in Tables 3.6 and Table 3.7. Corresponding groove locations for optimum parameters are also shown in the Tables. It is evident from this comparison that there is a significant improvement in the performance characteristics, e.g., friction variable, flow coefficient, load and mass parameter.

The three variables, *viz*, eccentricity ratio (ε), starting angles of the first groove (θ_1) and the second groove (θ_2) are taken as chromosome in the Case II. The variable bounds are presented in Table 3.4.

In genetic algorithm, in each generation the fitness values of the objective function of the individuals is determined. These values express the fitness of the solutions of the new generations, one cycle of genetic algorithm called a generation. In each generation if the solution is improved, it is stored as the best solution. This is repeated till convergence.

The optimum results obtained for friction variable, flow coefficient, non-dimensional load capacity and mass parameter are shown in Figures 3.10 through 3.14.

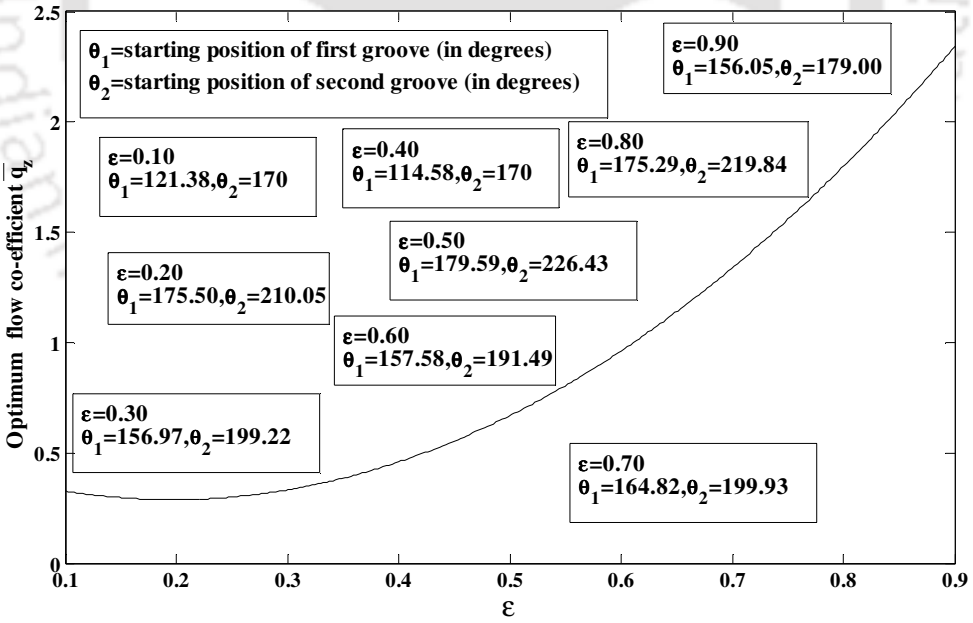

Figure 3.7: Variation of flow coefficient at optimum grooving location for different ε

The optimum configurations obtained for all the objective functions are shown in Table 3.8. It has been observed that the optimum configurations correspond to higher eccentricity ratio except for the multi-objective function. From the results presented here, it can be inferred that

the second groove locations are sensitive to the type of objective function, whereas the first groove is more or less the same.

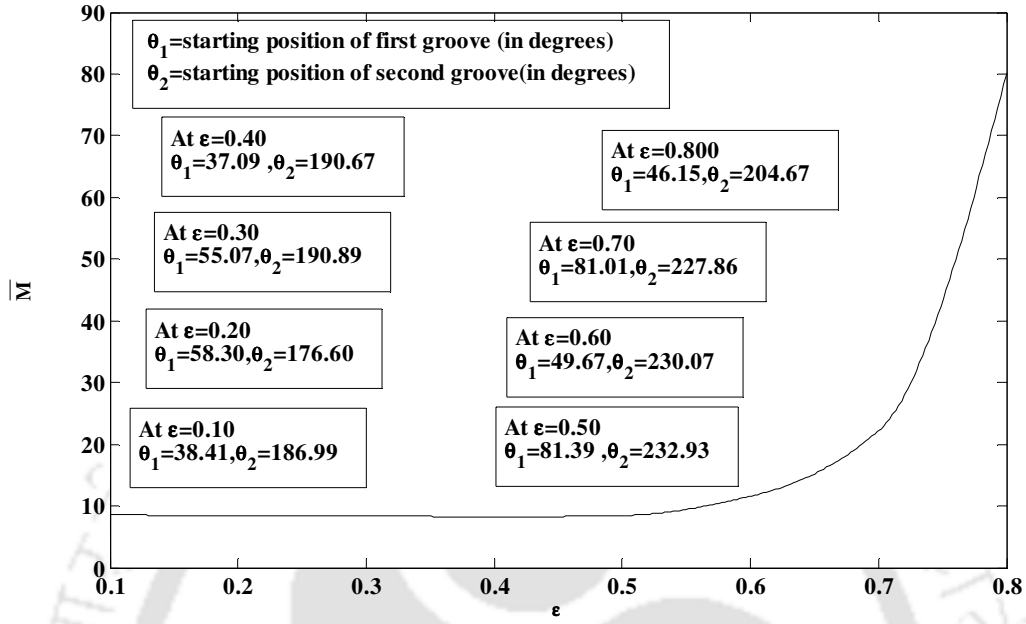

Figure 3.8: Variation of mass-parameter at optimum grooving location for different ε

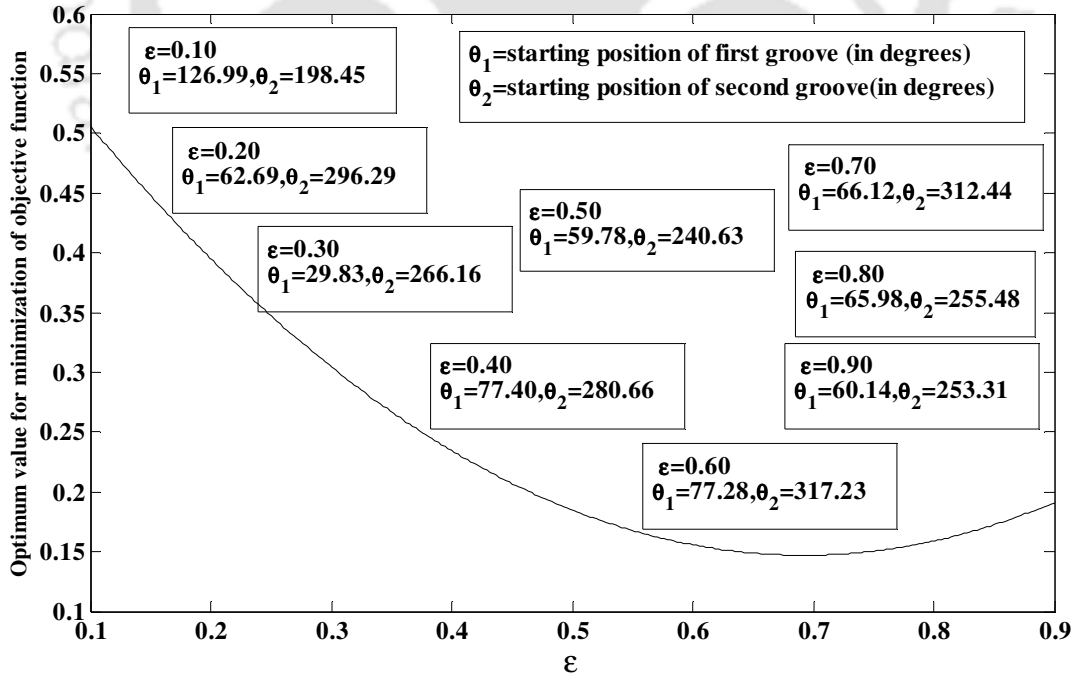

Figure 3.9: Optimum value obtained by minimization of a multiobjective function for different ε

To find out if the bearing performances are the same or different when groove locations are different from the current practice, performance parameters (friction variable, flow coefficient, non dimensional load and mass parameter values) at optimum position are compared with the groove position along horizontal direction and 180^0 apart.

Table 3.6: Comparison of optimum friction variable and optimum flow coefficient with friction variable and flow coefficient with groove position along horizontal direction and 180^0 apart

ε	Minimization of $\mu(R/C)$	Optimum	Maximization of $\bar{q}_z$	Optimum configuration
	Horizontal Grooves (Optimum Configuration)		Horizontal Grooves (Optimum configuration)	
0.1	28.57(25.844)	$\theta_1 = 44.16$	0.1429(0.160)	$\theta_1 = 18.02$
		$\theta_2 = 334.407$		$\theta_2 = 283.305$
0.2	13.875(12.572)	$\theta_1 = 37.138$	0.173(0.266)	$\theta_1 = 18.758$
		$\theta_2 = 297.416$		$\theta_2 = 275.848$
0.3	8.8024(7.988)	$\theta_1 = 39.268$	0.202(0.513)	$\theta_1 = 23.472$
		$\theta_2 = 329.033$		$\theta_2 = 334.44$
0.4	6.1002(5.5876)	$\theta_1 = 43.106$	0.210 (0.640)	$\theta_1 = 25.399$
		$\theta_2 = 328.928$		$\theta_2 = 274.428$
0.5	4.4136(4.064)	$\theta_1 = 39.357$	0.205 (0.753)	$\theta_1 = 16.651$
		$\theta_2 = 319.51$		$\theta_2 = 315.517$
0.6	3.237(2.9811)	$\theta_1 = 30.971$	0.192 (0.972)	$\theta_1 = 22.416$
		$\theta_2 = 324.569$		$\theta_2 = 294.16$
0.7	2.1582(2.1568)	$\theta_1 = 16.553$	0.179(1.12)	$\theta_1 = 17.409$
		$\theta_2 = 304.483$		$\theta_2 = 310.956$
0.8	1.2303(1.1198)	$\theta_1 = 33.348$	0.176(1.23)	$\theta_1 = 15$
		$\theta_2 = 283.355$		$\theta_2 = 246.425$
0.9	0.862(0.8480)	$\theta_1 = 36.188$	0.208(2.834)	$\theta_1 = 159.145$
		$\theta_2 = 312.891$		$\theta_2 = 317.331$

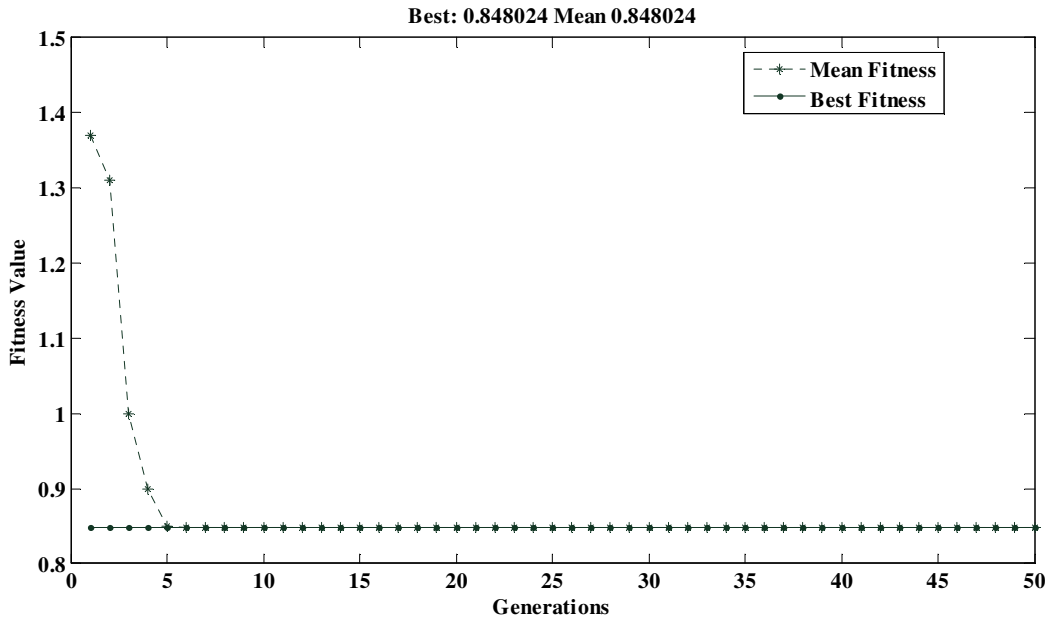

Figure 3.10:Fitness value considering friction variable as objective function

Table 3.7: Comparison of optimum non-dimensional load and optimum Mass parameter with non-dimensional load and Mass parameter groove position along horizontal direction and 180^0 apart

ε	Maximization of $\overline{W}$	Optimum configuration	Maximization of $\overline{M}$	Optimum configuration
	Horizontal Grooves (Optimum Configuration)		Horizontal Grooves (Optimum configuration)	
0.1	0.0368(0.0408)	$\theta_1 = 121.386$ $\theta_2 = 170$	4.832(8.584)	$\theta_1 = 38.411$ $\theta_2 = 186.998$
0.2	0.077(0.0819)	$\theta_1 = 175.502$ $\theta_2 = 210.059$	4.865(8.432)	$\theta_1 = 58.309$ $\theta_2 = 176.604$
0.3	0.124(0.1372)	$\theta_1 = 156.972$ $\theta_2 = 199.222$	4.853(8.403)	$\theta_1 = 55.0701$ $\theta_2 = 190.894$
0.4	0.186(0.2039)	$\theta_1 = 114.583$ $\theta_2 = 170$	4.802(8.177)	$\theta_1 = 37.098$ $\theta_2 = 190.677$
0.5	0.2731(0.2965)	$\theta_1 = 179.597$ $\theta_2 = 226.430$	4.943(19.461)	$\theta_1 = 81.3940$ $\theta_2 = 232.931$
0.6	0.4067(0.4371)	$\theta_1 = 157.584$ $\theta_2 = 191.492$	5.339(19.589)	$\theta_1 = 49.674$ $\theta_2 = 230.075$
0.7	0.639(0.6799)	$\theta_1 = 164.828$ $\theta_2 = 199.933$	7.336(22.144)	$\theta_1 = 81.0131$ $\theta_2 = 227.8693$
0.8	1.1384(1.195)	$\theta_1 = 175.297$ $\theta_2 = 219.844$	32.94(80.225)	$\theta_1 = 46.150$ $\theta_2 = 204.679$
0.9	2.7514(2.831)	$\theta_1 = 31.094$ $\theta_2 = 288.778$	39.341(181.260)	$\theta_1 = 116.528$ $\theta_2 = 201.846$

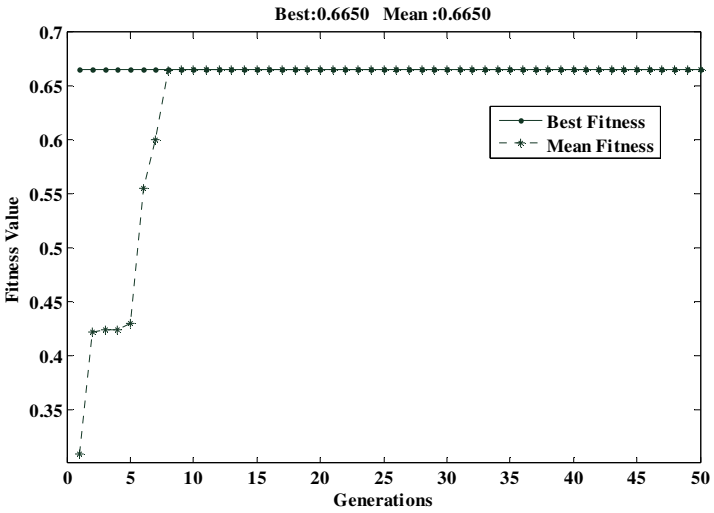

Figure 3.11: Fitness value considering flow coefficient as objective function

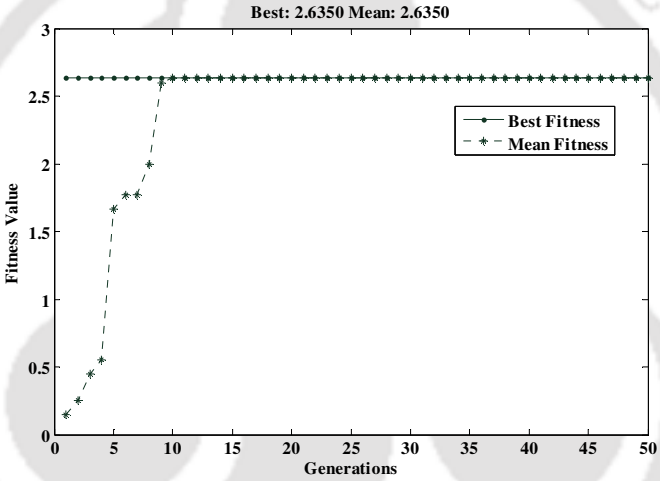

Figure 3.12: Fitness value considering non-dimensional load capacity as objective function

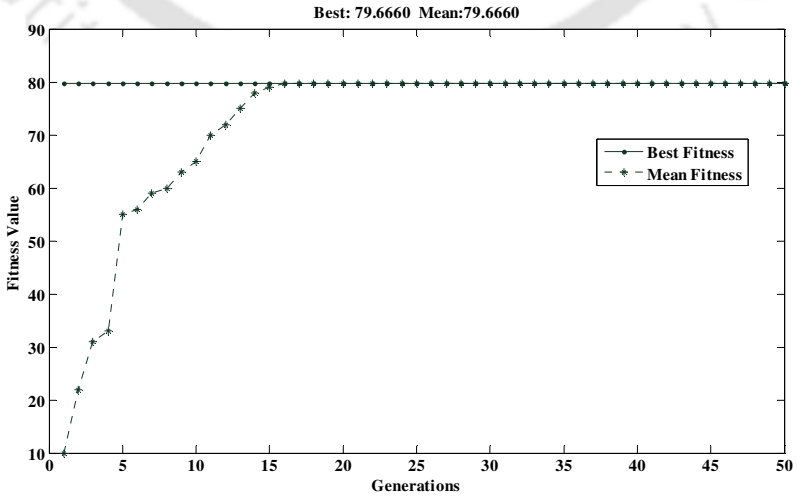

Figure 3.13: Fitness value considering mass parameter as objective function

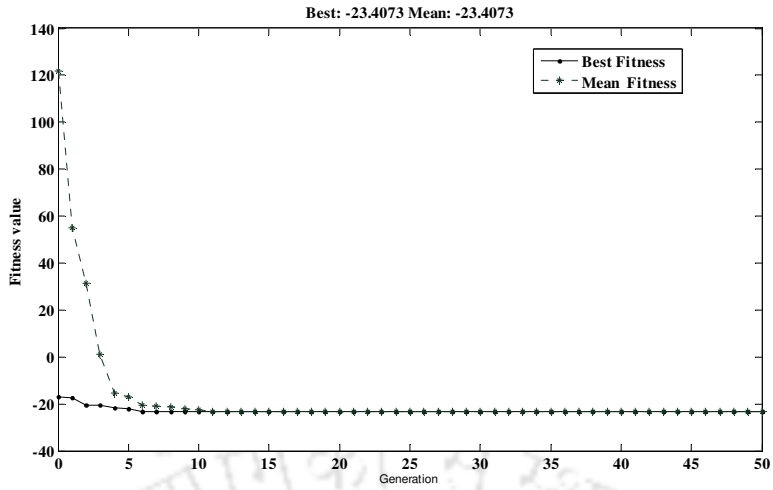

Figure 3.14 : Fitness value for multi-objective function

Table 3.8: Optimum groove location with different objectives as in case -II

Objective function	ε	θ_1	θ_2
Minimum Friction variable	0.889	36.178	312.991
Maximum flow coefficient	0.411	25.389	274.428
Maximum load	0.975	163.375	283.619
Maximum mass parameter	0.799	46.150	204.679
Optimization the multi-objective function	0.470	26.96	178.879

3.2.4 Determination of near to the optimum location of groove

It has been observed from the foregoing analysis that the groove locations are different for different eccentricity ratios as well as for different objective functions for two axial groove bearings. This would be confusing for the manufacturers as well as the users as to which bearing configuration would be appropriate for a particular application. It would be more confusing when the load varies since the optimum configurations are different for different loading conditions, vis-a-vis, eccentricity ratios. Therefore, there is a need to identify the locations of grooves such that the performance characteristics are near to the optimum for any loading condition (eccentricity ratio) for a particular objective function. The manufacturers and designers will be immensely benefitted if such groove locations can be determined by some method. This issue is taken up in this section. The groove locations are rounded off to the nearest number eliminating the decimal places. The step by step procedure for finding out the near to optimum locations has been described below:

Procedure: The optimum configurations are different for different eccentricity ratios. Therefore, one such optimum configuration for a particular eccentricity ratio is applied for all

other eccentricity ratios. The differences of objective function values for the optimum and the new configurations for all the eccentricity ratios are estimated and summed up. The other configurations are also tried in a similar manner. Finally the configuration which provides minimum differences of the summations is selected as the one 'near to optimum configuration. An example for the objective function of minimum friction variable has been presented in Tables 3.9a, 3.9b, 3.9c and 3.9d for better understanding of the procedure.

Table 3.9a: Obtaining near to the optimum configuration from the optimum configuration when objective function is friction variable.

ε	Optimum configuration		$\mu(\frac{R}{C})$	Fixed configuration(1)		$\mu(\frac{R}{C})$	Difference
	θ_1	θ_2	(1)	θ_1	θ_2	(2)	(1-2)
0.1	44.16	334.407	25.8	44.16	334.407	25.8	0
0.2	37.138	297.416	12.57272			12.61	-0.038
0.3	39.268	329.033	7.98882			8.0103	-0.0123
0.4	43.106	328.928	5.587606			5.6602	-0.072
0.5	39.357	319.51	4.064312			4.068	-0.004
0.6	30.971	324.569	2.981166			3.0028	-0.0217
0.7	16.553	304.483	2.156866			2.1468	-0.01
0.8	24.327	285.026	1.1198			1.6593	-0.1395
0.9	36.188	312.891	0.848024			0.854473	- 0.0064
	Summation						-0.2605

Table 3.9b: Obtaining near to the optimum configuration from the optimum configuration when objective function is friction variable.

Fixed configuration(2)		$\mu(\frac{R}{C})$	Difference	Fixed configuration(3)		$\mu(\frac{R}{C})$	Difference
θ_1	θ_2	(3)	(1-3)	θ_1	θ_2	(4)	(1-4)
37.138	297.416	25.9907	-0.1467	39.268	329.033	25.990	-0.146
		12.57272	-0.0007			12.617	-0.045
		7.998	0			8.036	0
		5.623	-0.0354			5.623	-0.0354
		4.08	-0.016			4.09	-0.026
		3.03	-0.0489			2.993	-0.0119
		2.158	-0.0012			2.159	-0.0022
		1.561	-0.4412			1.557	-0.437
		0.9119	-0.0639			0.212	-0.072
Summation			-0.7540				-0.7757

Table 3.9c: Obtaining near to the optimum configuration from the optimum configuration when objective function is friction variable.

Fixed configuration(4)		$\mu(\frac{R}{C})$	Difference	Fixed configuration(5)		$\mu(\frac{R}{C})$	Difference
θ_1	θ_2	(5)	(1-5)	θ_1	θ_2	(6)	(1-6)
43.106	328.92	25.9907	-0.1467	39.357	319.5	25.9907	-0.146
		12.6218	-0.0498			12.6189	-0.0469
		8.0088	-0.0108			8.0104	-0.0214
		5.58760	0			5.6634	-0.0758
		4.0678	-0.0038			4.06431	0
		2.9965	-0.0154			2.99	-0.0089
		2.17	-0.0132			2.17	-0.0132
		1.7592	-0.639			1.7592	-0.6394
		0.86352	-0.0155			0.898	-0.05
Summation			-0.8946				-0.9936

Table 3.9d: Obtaining near to the optimum configuration from the optimum configuration when objective function is friction variable.

Fixed configuration (6)		$\mu(\frac{R}{C})$	Difference	Fixed configuration (7)		$\mu(\frac{R}{C})$	Difference	Fixed configuration (8)		$\mu(\frac{R}{C})$	Difference
θ_1	θ_2	(6)	(1-6)	θ_1	θ_2	(7)	(1-7)	θ_1	θ_2	(8)	(1-8)
30.9	324.5	25.99	-0.146	16.55	304.4	25.	-0.146	33.34	283	26.05	-0.209
		12.61	-0.038			12.	-0.038			12.62	-0.04
		8.00	-0.002			8.0	-0.032			8.03	-0.035
		5.62	-0.032			5.6	-0.032			5.62	-0.040
		4.05	-0.006			4.0	-0.004			4.07	-0.013
		2.98	0			3.0	-0.048			2.99	-0.018
		2.16	-0.004			2.1	0			2.16	-0.004
		1.71	-0.590			1.6	-0.482			1.11	0
		0.98	-0.132			0.9	-0.142			0.99	-0.150
Summation			-0.948				-0.908				-0.518

Since the summation of differences is minimum for the configuration 1, therefore, configuration 1 is considered as the 'near to the optimum configuration'.

A similar procedure has been followed for other objective functions as well to arrive at the 'near to the optimum configurations'. The various near to the optimum configurations obtained are presented in Table 3.10 and also in Figs. 3.15 through 3.18.

Table 3.10: Near to the optimum configuration for different objectives

Objective function	θ_1	θ_2
Minimization of friction variable	44	334
Maximization of flow coefficient	23	334
Maximization of load	124	187
Maximization of mass parameter	46	206
Minimization of multi-objective function	62	276

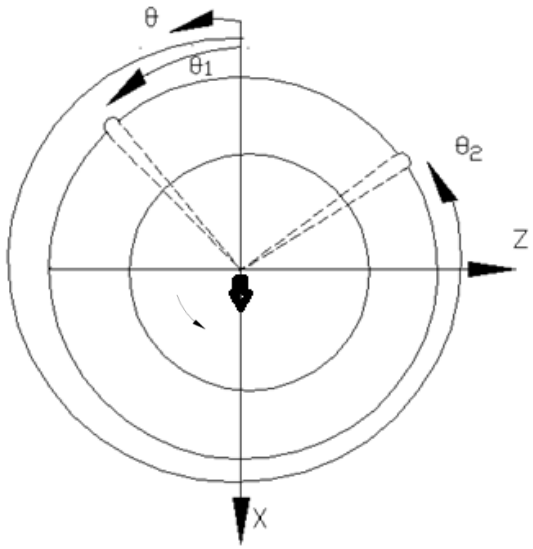

Figure 3.15 : Near optimum configuration for minimization of friction variable

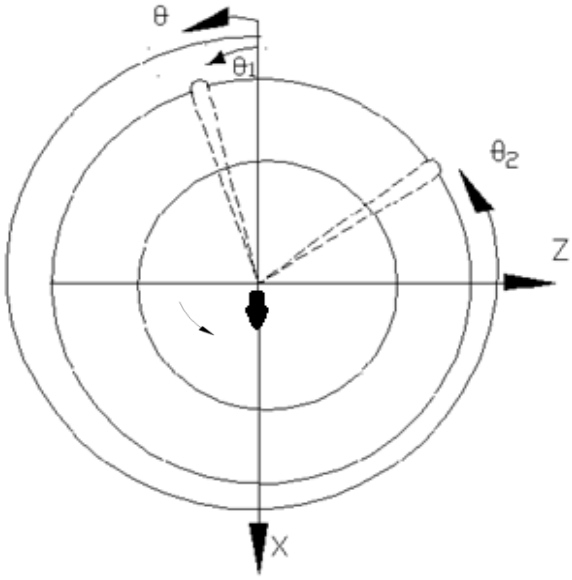

Figure 3.16 : Near optimum configuration for maximization of flow coefficient

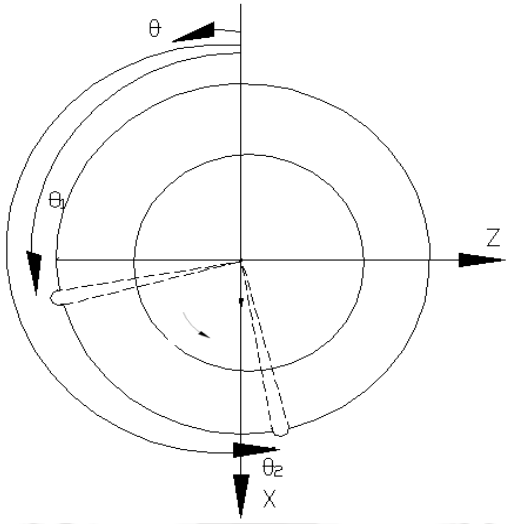

Figure 3.17 : Near optimum configuration for maximization non dimensional load capacity

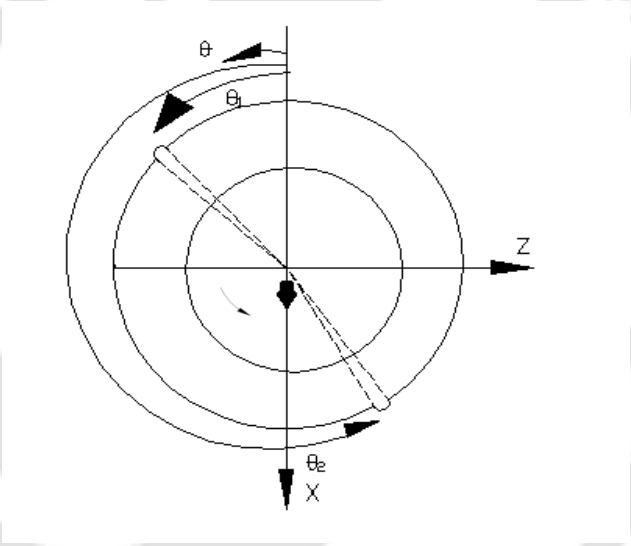

Figure 3.18 : Near optimum configuration for maximization of mass parameter

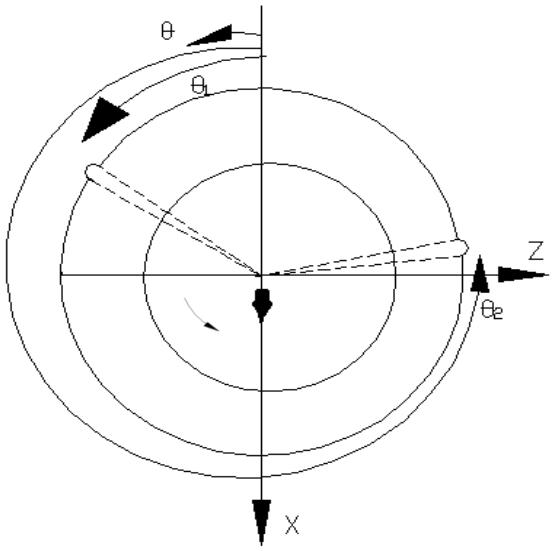

Figure 3.19 : Near optimum configuration for minimization of a multi-objective function

3.3 Summary

In the present chapter, analysis (both steady state and dynamic) of two axial groove bearings is performed. The optimum groove locations for different objective functions, viz., maximization of non-dimensional load capacity, flow coefficient and mass parameter and minimization of friction variable have been obtained with the help of Genetic Algorithm (GA) toolbox of MatLab. It is observed that the optimum groove locations for two axial groove bearing correspond to significant performance enhancement of two axial groove bearing. It has been found that the optimum groove locations are not only different for different objective functions but also different for different eccentricity ratios, *vis-a-vis*, loading conditions. Therefore, the identification of locations of grooves for two-groove bearing has been obtained such that the performance characteristics are near to the optimum for any loading condition (eccentricity ratio) for different objective functions.

CHAPTER 4

Analysis of two-lobe bearings

4.0 Introduction

It has been seen in Chapter 3 that there exists optimum groove locations which enhances the two axial groove bearing performance significantly. In view of this the study of optimum groove locations has been extended to two-lobe bearings. It was indicated earlier that the hydrodynamic bearings operating at high speed are often confronted with problems of instability, known as oil whirl leading to whip. Instability may cause catastrophic failure of the rotor-bearing systems. Satisfactory dynamic characteristics are an essential requirement of a good bearing design and bearing of non circular cross section hold good promise for applications where bearing stiffness and stability are major considerations. In general non circular bearing geometry enhances shaft stability, besides resulting in reduction/ increase of power loss and increase in oil flow compared to circular bearing, thus reduction in temperature rise at some operating condtions. Two-lobe journal bearings are used in supporting the heavy rotors of turbo generators. The use of two-lobe bearings, considered to be more stable than ordinary plain cylindrical bearings as indicated by Kumar et.al. [20].

4.1 Estimation of Steady state and dynamic characteristics

Before starting the analysis of two-lobe bearing, a comparison of non-dimensional values of steady state and dynamic characteristics has been made with the published results of Lund and Thomson [29] for L/D=1 with two 20^0 axial groove , $\delta = 0.5$ and presented in Table 4.1. The present results are found to be in good agreement with those of Lund and Thomson. [29].

Table 4.1: Steady state and dynamic characteristics of two-lobe journal bearing for $\frac{L}{D} = 1,\ \delta = 0.5$ with two 20^0 axial grooves

ε	Results	S	ϕ	$\bar{K}_{XX}$	$\bar{K}_{XZ}$	$\bar{K}_{ZX}$	$\bar{K}_{ZZ}$	$\bar{C}_{XX}$	$\bar{C}_{XZ} = \bar{C}_{ZX}$	$\bar{C}_{ZZ}$
0.050	Present	1.450	93.91	38.47	22.75	-22.12	-1.24	79.21	-28.09	18.60
	[29]	1.442	93.91	38.58	22.65	-22.14	-1.29	79.05	-28.14	18.60
0.100	Present	0.690	93.12	18.79	11.21	-10.73	-0.20	38.54	-12.86	9.360
	[29]	0.698	93.12	18.93	11.25	-10.79	-0.24	38.73	-12.97	9.400
0.150	Present	0.440	91.97	12.18	7.46	-6.83	0.26	24.97	-7.45	6.342
	[29]	0.442	91.97	12.28	7.45	-6.87	0.26	25.00	-7.500	6.360
0.200	Present	0.300	90.37	8.85	5.54	-4.76	0.58	17.86	-4.480	4.800
	[29]	0.308	90.37	8.93	5.58	-4.79	0.58	17.99	-4.500	4.820
0.239	Present	0.230	88.80	7.24	4.66	-3.67	0.77	14.42	-2.910	4.020
	[29]	0.240	88.80	7.31	4.70	-3.70	0.77	14.54	-2.930	4.040
0.250	Present	0.220	88.28	6.95	4.51	-3.43	0.82	13.74	-2.550	3.860
	[29]	0.224	88.28	6.87	4.49	-3.41	0.82	13.68	-2.510	3.850
0.260	Present	0.210	87.79	6.57	4.32	-3.18	0.88	12.99	-2.170	3.680
	[29]	0.213	87.79	6.65	4.36	-3.21	0.86	13.09	-2.230	3.700
0.304	Present	0.170	87.79	5.83	3.98	-2.61	1.08	11.32	-1.240	3.440
	[29]	0.161	83.29	5.63	3.84	-2.32	1.01	10.75	-1.020	3.070
0.350	Present	0.120	81.80	4.94	3.52	-1.51	1.14	9.02	-0.010	2.490
	[29]	0.120	81.80	4.99	3.54	-1.52	1.14	9.04	-0.010	2.490
0.381	Present	0.090	78.65	4.76	3.44	-1.010	1.220	8.23	0.580	2.110
	[29]	0.097	78.65	4.82	3.46	-1.010	1.210	8.26	0.560	2.100
0.451	Present	0.040	63.70	6.16	3.81	0.171	1.400	7.89	1.580	1.170
	[29]	0.045	63.70	6.25	3.83	0.190	1.400	7.88	1.560	1.160

4.2 Analysis of steady state and dynamic characteristics

4.2.1 Groove size for better performance

To ascertain the size of the groove for better performance, a comparison of non-dimensional load capacity is made for different groove angles as shown in Table 4.2. It has been observed from the presented results that the non-dimensional load capacity is slightly higher with 10^o groove angles in comparison to 20^o and 30^o groove angles in case of two-lobe bearings except

for an eccentricity ratio of 0.451. Therefore, 10º groove angles are considered throughout the analysis.

Table 4.2: Comparison of non-dimensional load capacity values using 10^{o}, 20^{o} and 30^{o} groove angles

	$\bar{W}$		
ε	10^{o} groove	20^{o} groove	30^{o} groove
0.050	0.037	0.036	0.035
0.203	0.182	0.172	0.158
0.304	0.346	0.329	0.312
0.451	1.165	1.134	1.234

4.2.2 Bearing Performance with different Groove locations

The current practice is that the grooves are placed horizontally 180^{o} apart for two-lobe bearings. An attempt has been made in this section to find out if the bearing performances are the same or different when groove locations are different from the current practice. In view of this many different configurations are studied and performance characteristics have been estimated. However, results showing the differences in performance characteristics of only one configuration (UP-UP 45^{o}) have been shown here to save space in Figs. 4.1 through 4.4. Here UP-UP 45^{0} configuration means that both grooves are 45^{0} above the horizontal position. The groove angle considered is 10^{o}. It has been observed that with the change in groove locations, the various steady state and dynamic characteristics also change. Therefore, it is obvious that there has to be a certain configuration which corresponds to the optimum performance of two-lobe bearing.

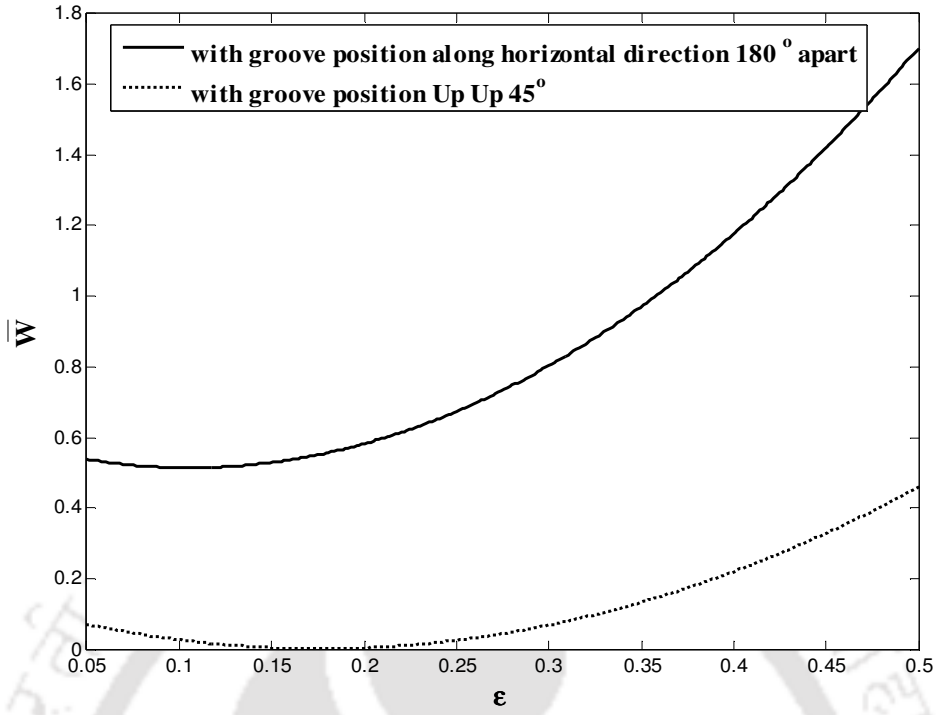

Figure 4.1: Variation of non-dimensional load capacity with ε

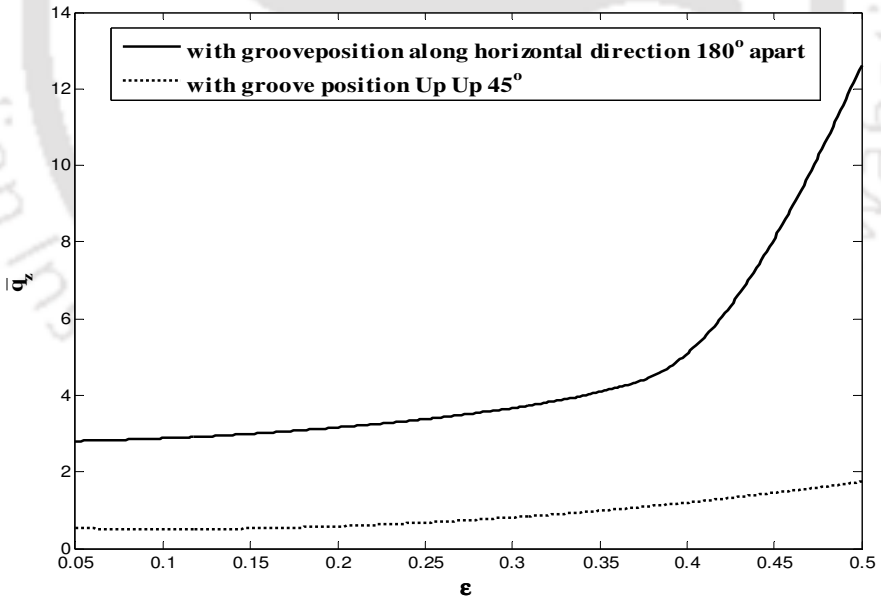

Figure 4.2: Variation of non-dimensional flow coefficient with ε

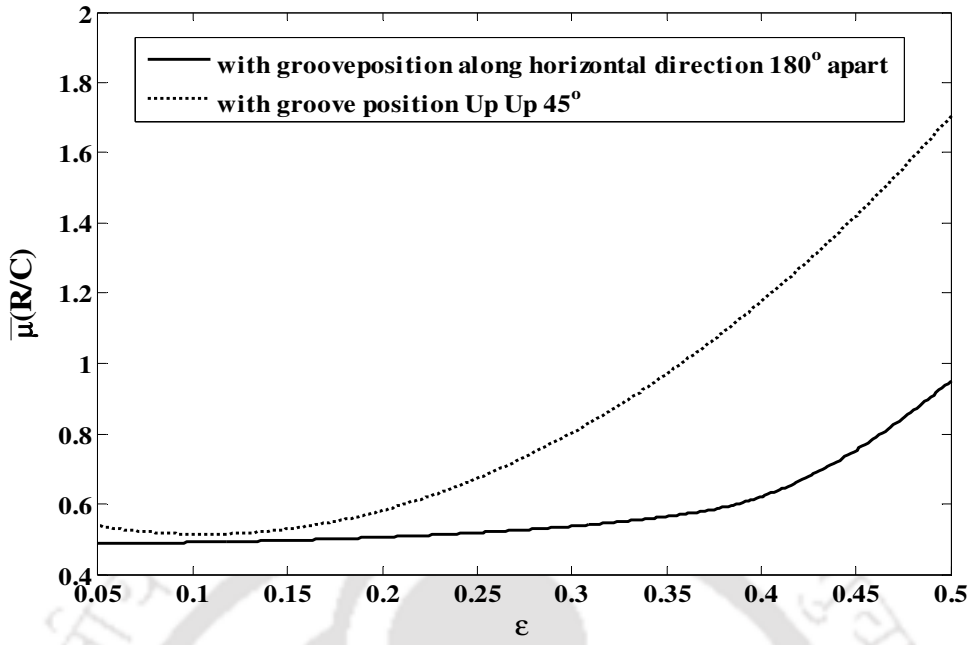

Figure 4.3: Variation of non-dimensional friction variable with ε

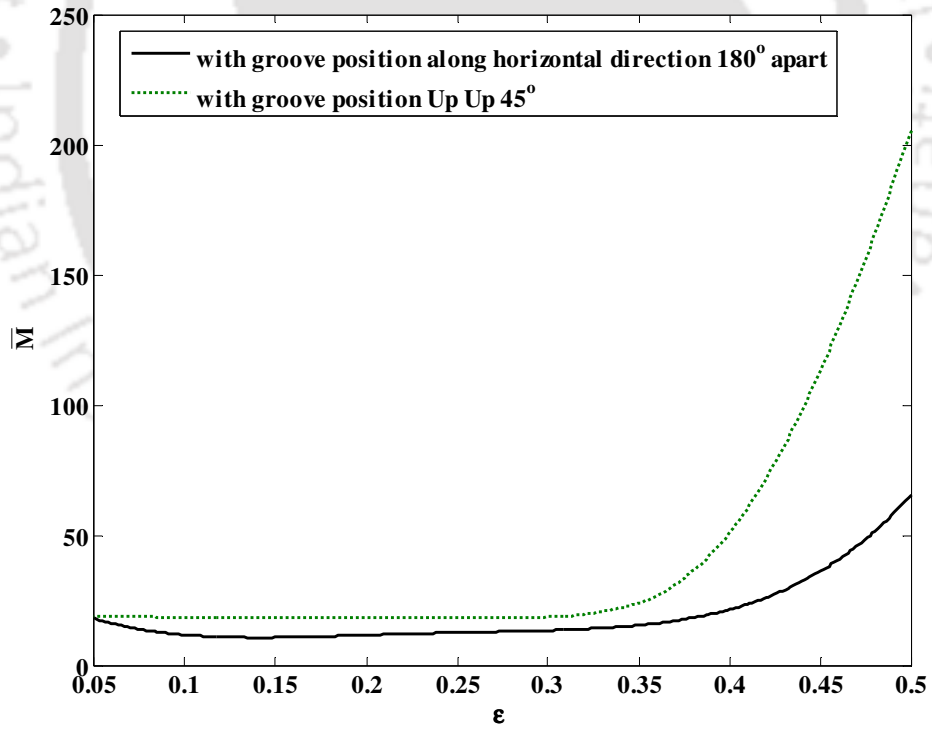

Figure 4.4: Variation of non-dimensional mass parameter with ε

4.2.3 Determination of optimum location of groove

It has been shown in the previous section that the location of the groove have influence in flow ($\bar{q}_z$), frictional variable ($\bar{\mu}$), non-dimensional load capacity ($\bar{W}$) and mass parameter ($\bar{M}$). In view of this, an attempt has been made to locate the groove locations which correspond to optimum performances in terms of the four parameters mentioned above.

The objective functions and optimization technique are the same as for two-axial groove bearing. Genetic Algorithm (GA) has been used to find the optimum solution as outlined in Chapter 2.

From the results presented here, it can be inferred that the groove locations are sensitive to the type of objective function. The practice and the notion of convenience of keeping groove locations horizontal 180^o apart need to be thoroughly looked into as the present results show that optimum groove locations are not horizontally 180^o apart for the objective function considered in the present work. A Comparison of Optimum non-dimensional friction variable, flow coefficient, non-dimensional load capacity and mass parameter with groove location horizontally 180^0 apart has been made as shown in Tables 4.5 and 4.6. It is very much clear from the comparison that there is a significant improvement in the optimum value of friction variable, flow coefficient, non-dimensional load capacity and mass parameter value than that of two-lobe bearing with grooves location along horizontal direction and 180^0 apart(Fig 2.3). The problem is framed with four objectives. The variables used in the problem are starting angle of first groove (θ_1), starting angle of second groove (θ_2) in Case –I. The optimum configurations have been obtained for eccentricity ratio ranging from 0.05 to 0.451 in this case. In Case –II, the eccentricity ratio (ε), starting angle of first groove (θ_1), starting angle of second groove (θ_2) are variables and act as Chromosome. The objectives are minimization of friction variable, $\bar{\mu}$ (Eqn. 2.22), maximization of non-dimensional load capacity, $\bar{W}$ (Eqn. 2.20), maximization of flow coefficient $\bar{q}_z$ (Eqn 2.21), maximization of mass parameter, $\bar{M}$ (Eqn. 2.31). Objective function framing is the same for both the cases and variable bounds are shown in Table 4.3.

Table 4.3: Variable bounds for the bearing problem

Case	Variable	Lower Bound	Upper Bound
I	Starting angle of first groove	15°	180°
	Starting angle of second	170°	345°
II	ε	0.05	0.451
	Starting angle of first groove	15°	180°
	Starting angle of second	170°	345°

Optimum groove locations for two-lobe bearings have been obtained using Genetic Algorithm (GA) toolbox of MatLab as it was done for two axial groove bearings in Chapter 3. The obtained results from GA have been compared with the results obtained using Sequential quadratic programming (SQP). The optimum value of fitness function obtained corresponding to maximization of flow coefficient has been tabulated for both GA and SQP in Table 4.4.
It has been observed that the results obtained using both the methods are exactly the same. Similarly maximum non-dimensional load capacity, minimum friction variable, maximum mass parameter values are also found to match for both the methods. However, GA has been used in this work for the same reason as stated in Chapter 3.

Initially a single objective function has been taken up. Here in case of two-lobe bearing a population size of 50, mutation probability of 0.1 and a cross over probability of 0.8 have been selected as discussed in case of two axial groove bearing in the previous chapter. The optimum groove locations for minimum friction variable, non-dimensional load capacity, flow coefficient , and mass parameter at different ε are shown in Figs. 4.5 through 4.8. θ_1 and θ_2 are the starting locations of the first and the second groove respectively in degrees.

It has been observed that the first groove location remain in the range (51^o to 170.69^0), (70.72^o to 131.48^o), (99.94^o to 179.96^0) and (15^o to 163.26^0) respectively when objective functions are friction variable, non-dimensional load capacity, flow coefficient, and mass parameter. However, the second groove location varies in the range of (184.32^o to 338.19^o), (193.11^o to 229.70^o), (212.98^o to 336.84^o) and (170^o to 241.82^o) respectively when objective functions are friction variable, non-dimensional load capacity, flow coefficient and mass parameter. The optimum groove locations for the multi-objective function (section 2.11) have been presented in Fig. 4.9. It has been observed that the first groove location varies in the range (15 to 120.98^0) , the second groove location varies in the range (199.85^o to 212.98^o) in this case.

The three variables, *viz*, eccentricity ratio(ε), starting angles of the first groove (θ_1) and the second groove (θ_2) are taken as chromosome in the Case II. The variable bounds are

presented in Table 4.3. The optimum results obtained for friction variable, flow coefficient, non-dimensional load capacity and mass parameter are shown in Figures 4.10 through 4.14.

Table 4.4: Comparison of GA and SQP results

ε	Objective function value (Maximum flow coefficient)	
	GA results	SQP results
0.05	7.047	7.047
0.1	7.967	7.967
0.15	6.414	6.414
0.2	5.992	5.992
0.239	5.569	5.569
0.25	5.686	5.686
0.260	6.398	6.398
0.304	6.853	6.853
0.350	12.506	12.506
0.381	18.010	18.010
0.451	49.101	49.101

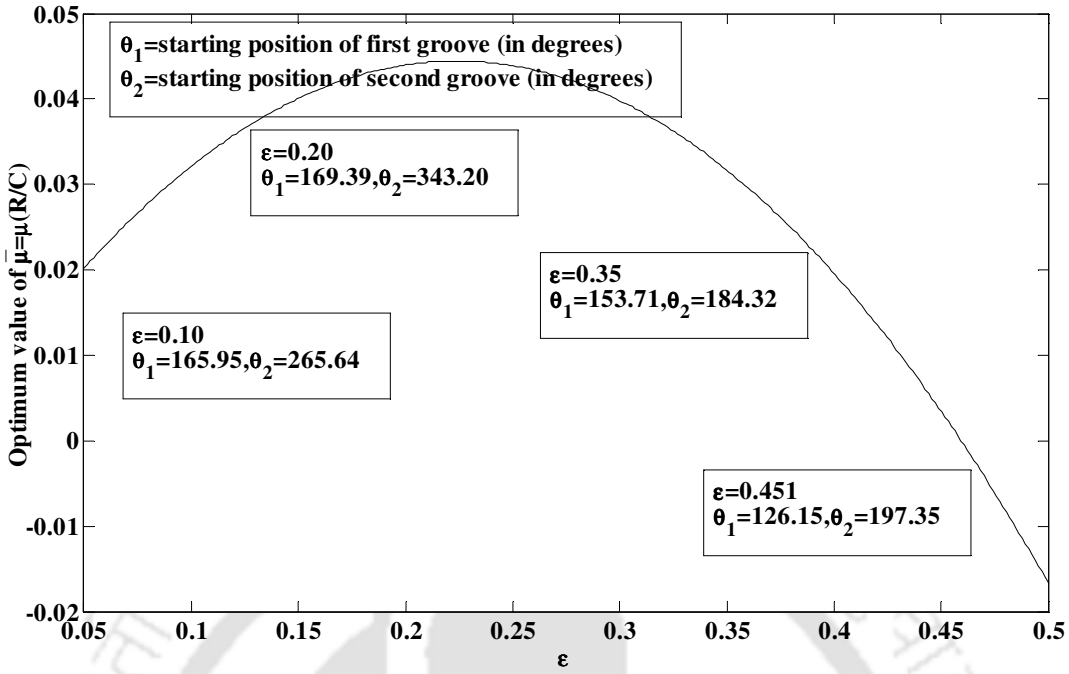

Figure 4.5: Variation of friction variable at optimum groove location for different ε

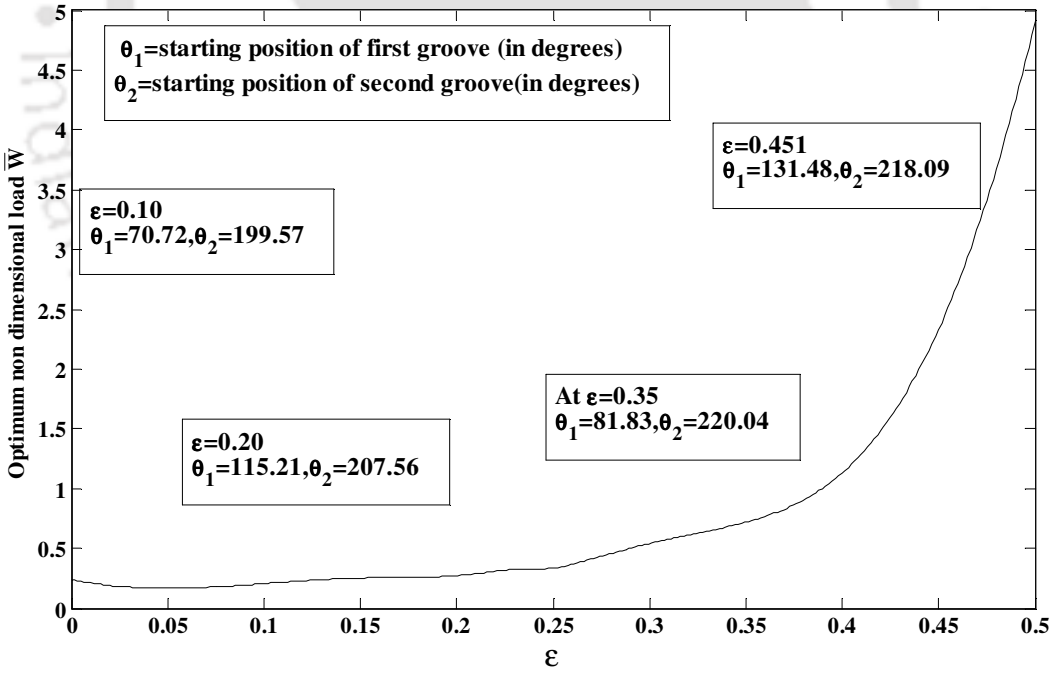

Figure 4.6: Variation of $\overline{W}$ at optimum groove location for different ε

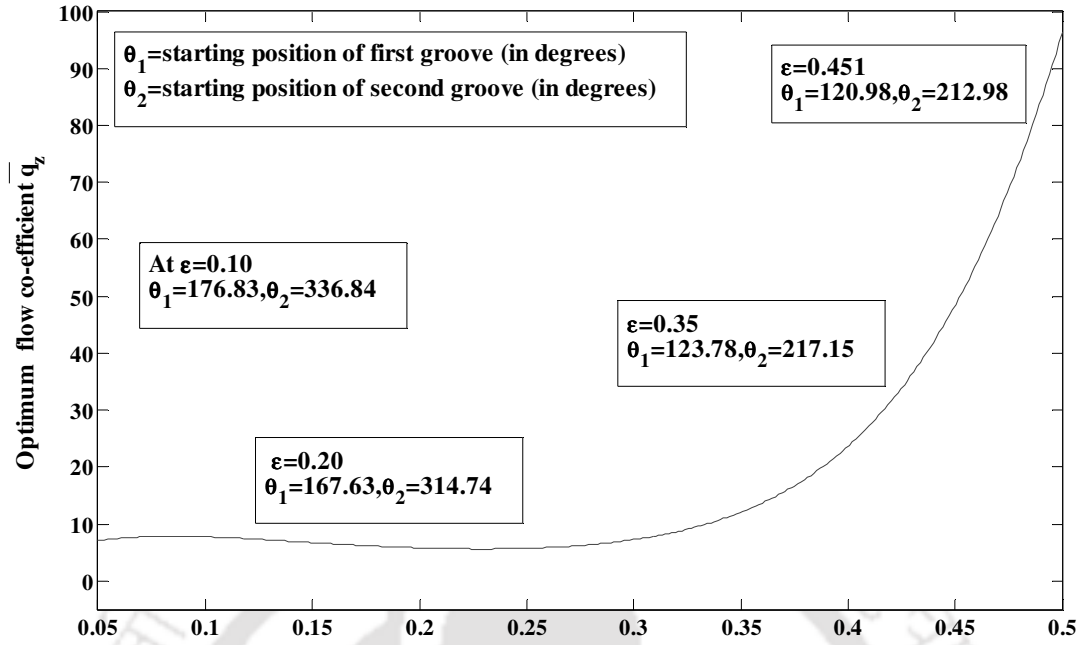

Figure 4.7: Variation of flow at optimum groove location for different ε

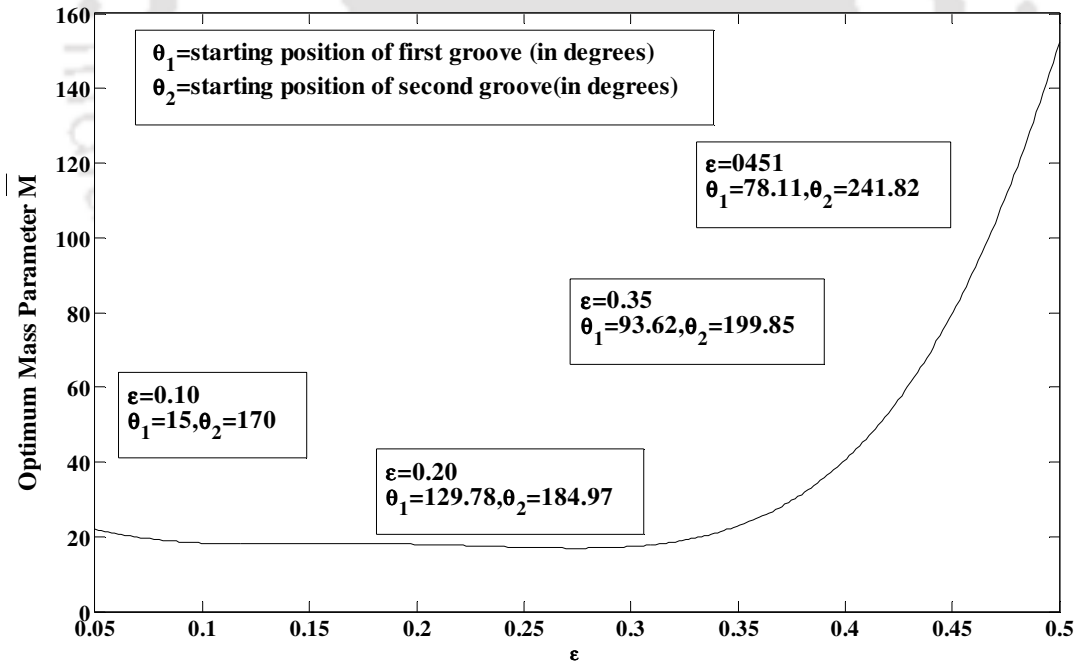

Figure 4.8: Variation of non dimensional mass parameter at optimum groove location for different ε

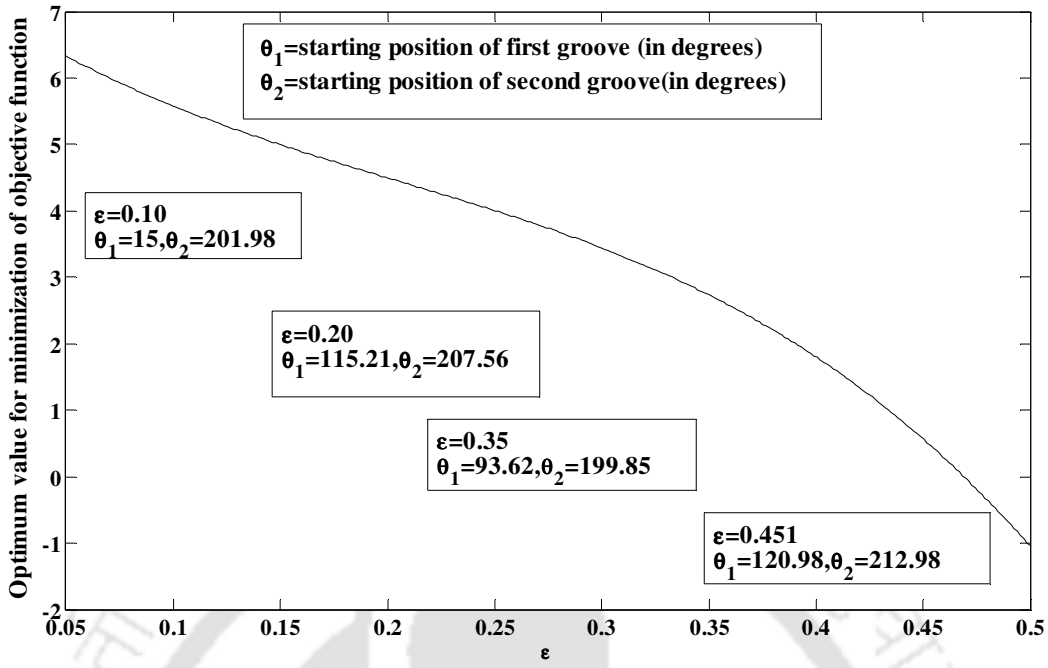

Figure 4.9: Optimum value obtained by minimization of a multi-objective function for different ε

In genetic algorithm, in each generation the fitness values of the objective function of the individuals is determined. These values express the fitness of the solutions of the new generations, one cycle of genetic algorithm called a generation. In each generation if the solution is improved, it is stored as the best solution. This is repeated till convergence.

It has been observed from the results presented in Table 4.7 that the first groove location varies from (99.1423^{o} to 179.425^{o}) whereas the second groove location varies from (190.045^{o} to 292.105^{o}) for all the objectives. However, all the configurations are found to be different from the current practice of horizontally 180^{o} apart configuration. It has also been seen that optimum eccentricity ratios are different for different objective functions.

When eccentricity ratio (ε), starting angle of first groove (θ_1), starting angle of second groove (θ_2) are variables and acts as Chromosome as in Case –II, the optimum configuration for the same is presented in Table 4.7 and also in Figures 4.15 through 4.19

Table 4.5: Comparison of Optimum friction variable and flow coefficient results with groove location along horizontal direction and 180^0 apart

ε	μ(R/C) Hz-Hz (optimum values)	Optimum configuration	$\bar{q}_z$ Hz-Hz (optimum values)	Optimum configuration
0.050	0.963(0.031)	θ_1= 170.69,θ_2= 330.29	4.420 (7.0472)	θ_1= 179.83,θ_2= 277.68
0.100	0.399(0.036)	θ_1= 165.95,θ_2=265.641	4.569 (7.9675)	θ_1= 176.85,θ_2= 336.84
0.150	0.396(0.032)	θ_1= 155.76,θ_2=322.64	4.811 (6.4145)	θ_1= 179.96,θ_2= 258.40
0.200	0.393(0.039)	θ_1= 169.398,θ_2=343.20	5.136 (5.9923)	θ_1= 167.63,θ_2= 314.74
0.239	0.390(0.039)	θ_1= 159.519,θ_2=338.19	5.439 (5.569)	θ_1= 112.30,θ_2= 227.660
0.250	0.390(0.032)	θ_1= 149.734,θ_2=188.623	5.531 (5.686)	θ_1= 111.12,θ_2= 219.78
0.260	0.389(0.039)	θ_1= 160.92,θ_2=222.69	5.617 (6.3981)	θ_1= 111.12,θ_2= 219.78
0.304	0.387(0.038)	θ_1= 155.31,θ_2=239.06	6.012 (6.853)	θ_1= 99.948,θ_2= 242.389
0.350	0.388(0.0394)	θ_1= 153.71,θ_2=184.32	6.437 (12.506)	θ_1= 123.78,θ_2= 217.158
0.381	0.393(0.0391)	θ_1= 51.46,θ_2=235.34	6.704(18.010)	θ_1= 130.78,θ_2= 213.023
0.451	0.457(0.0055)	θ_1= 126.15,θ_2=197.35	6.986 (49.101)	θ_1= 120.98,θ_2= 212.984

Table 4.6: Comparison of non-dimensional load capacity and mass parameter results with groove location along horizontal direction and 180^0 apart

ε	$\bar{W}$ Hz-Hz (optimum values)	Optimum configuration	$\bar{M}$ Hz-Hz (optimum values)	Optimum configuration
0.050	0.037 (0.1671)	θ_1= 84.59,θ_2= 199.957	18.002 (19.400)	θ_1= 15,θ_2= 170
0.100	0.075(0.205)	θ_1= 70.72,θ_2=199.57	11.591 (20.400)	θ_1= 15,θ_2= 170
0.150	0.127 (0.252)	θ_1= 89.876,θ_2=217.09	10.870 (20.543)	θ_1= 113.77,θ_2= 190.57
0.200	0.182 (0.273)	θ_1= 115.21,θ_2=207.56	11.530 (20.700)	θ_1= 129.78,θ_2= 184.97
0.239	0.233(0.329)	θ_1= 84.941,θ_2=218.326	12.293 (20.998)	θ_1= 163.26,θ_2= 191.59
0.250	0.249 (0.334)	θ_1= 80.425,θ_2=193.11	12.590 (21.098)	θ_1= 102.72,θ_2= 191.59
0.260	0.265 (0.368)	θ_1= 84.736,θ_2=200.626	12.658 (21.630)	θ_1= 152.09,θ_2= 189.40
0.304	0.345 (0.556)	θ_1= 102.094,θ_2=224.06	13.686 (22.450)	θ_1= 40.168,θ_2= 191.45
0.350	0.458 (0.7190)	θ_1= 81.83,θ_2=220.040	15.410(26.345)	θ_1= 93.623,θ_2= 199.859
0.381	0.565 (0.9151)	θ_1= 117.223,θ_2=229.70	18.279 (28.425)	θ_1= 156.87,θ_2= 199.11
0.451	1.137 (2.370)	θ_1= 131.48,θ_2=218.091	36.470 (81.260)	θ_1= 78.114,θ_2= 241.822

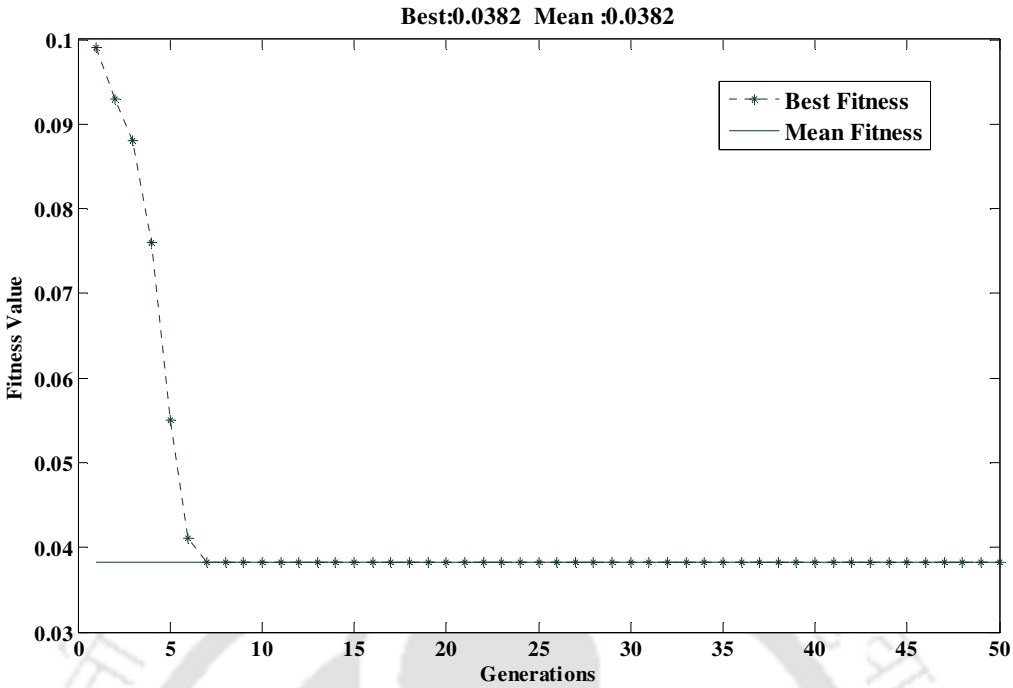

Figure 4.10:Fitness value considering friction variable as objective function

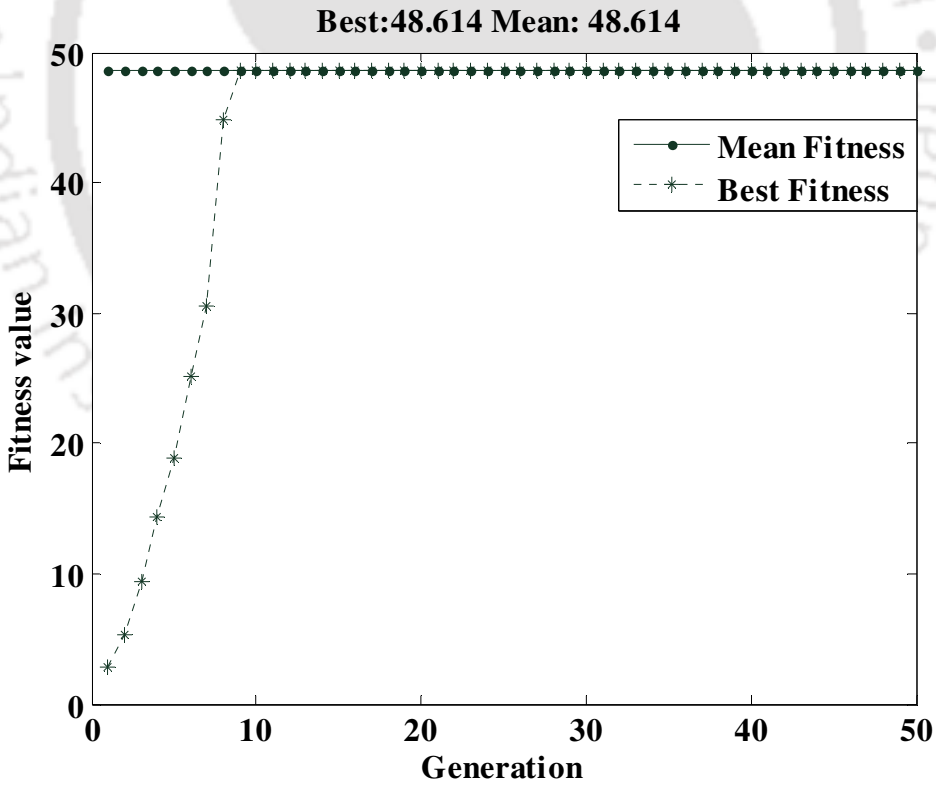

Figure 4.11: Fitness value considering flow coefficient as objective function

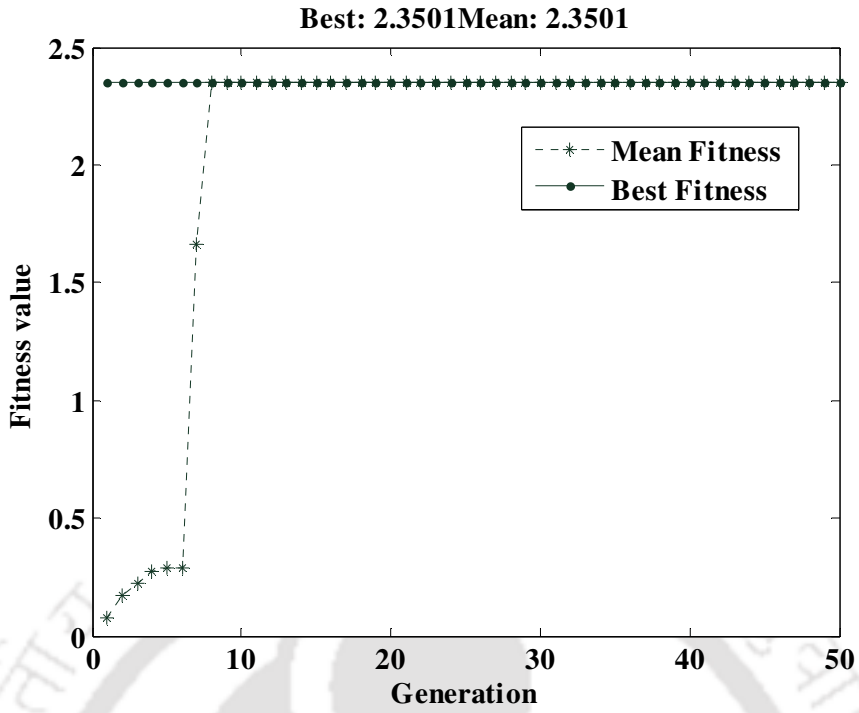

Figure 4.12: Fitness value considering non-dimensional load capacity as objective function

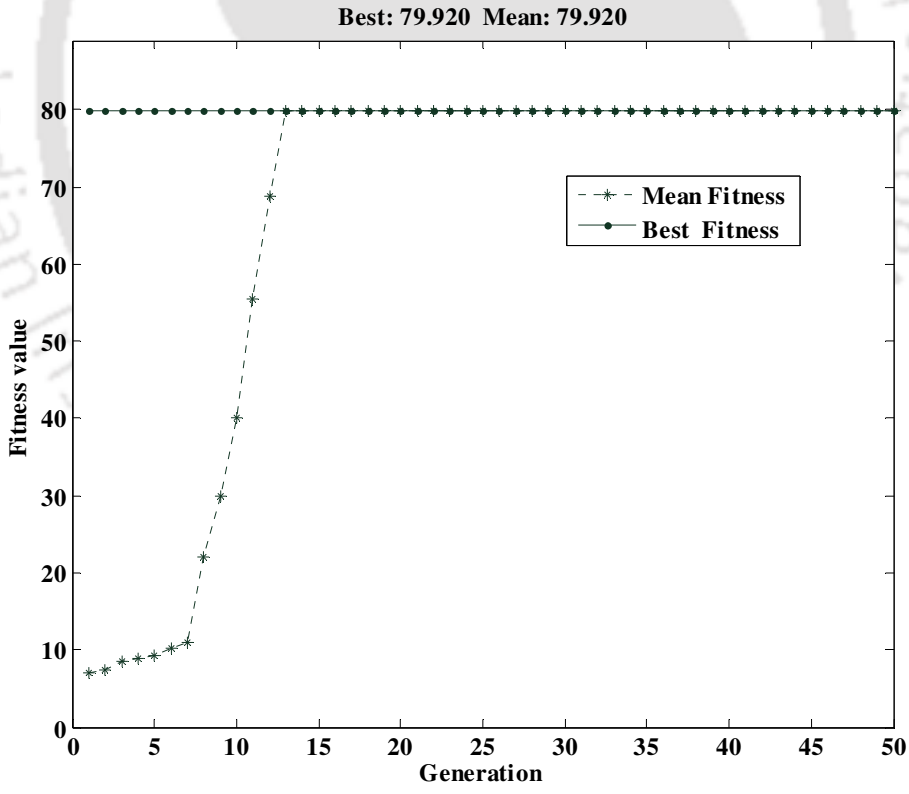

Figure 4.13: Fitness value considering mass parameter as objective function

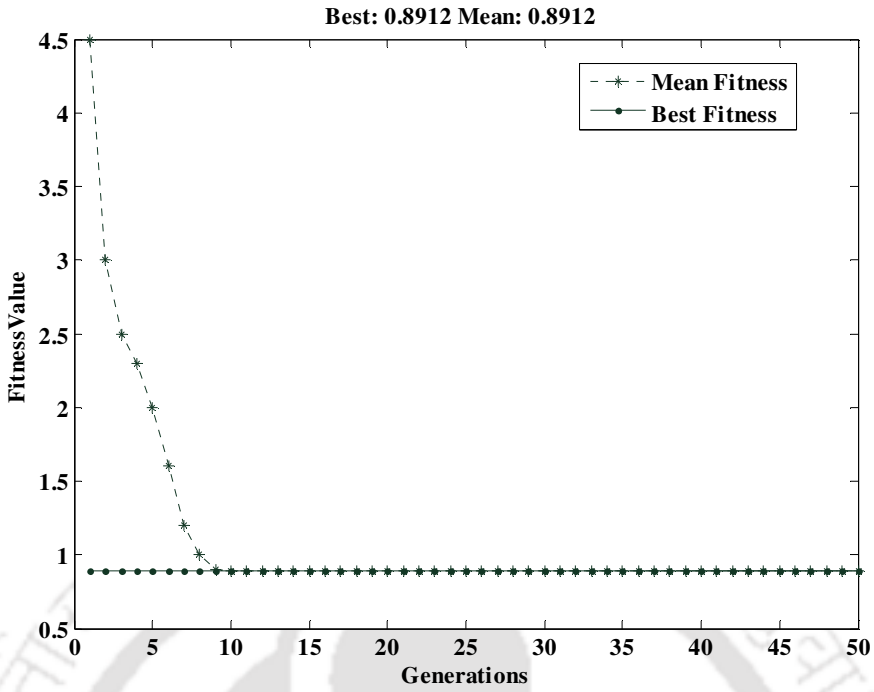

Figure 4.14: Fitness value for multi-objective function

Table 4.7: Optimum groove location with different objectives as in case -II

Objective function	ε	θ_1	θ_2
Minimization of friction variable	0.2324	148.11	190.045
Maximization of flow coefficient	0.4409	136.684	246.070
Maximization of non-dimensional load capacity	0.446	179.425	292.105
Maximization of mass parameter	0.373	99.1423	225.869
Optimization of all the combined objectives	0.450	100	245

4.2.4 Determination of near to the optimum location of groove

It has been observed that the optimum groove locations are different for different loading condition (eccentricity ratio) as well as for different objective functions in case of two-lobe bearing. The same was observed for two-axial groove bearings and therefore, 'near to the optimum configurations' were identified. Therefore, it has been decided to identify 'near to the optimum configurations' for two-lobe bearings for different objective functions following the same procedure outlined in Chapter 2. The results are presented in Table 4.8

Table 4.8: Near to the optimum configuration for different objectives

Objective function	θ_1	θ_2
Minimization of friction variable	41	189
Maximization of flow coefficient	19	270
Maximization of non-dimensional load capacity	89	217
Maximization of mass parameter	40	191
Minimization of multi-objective function	84	200

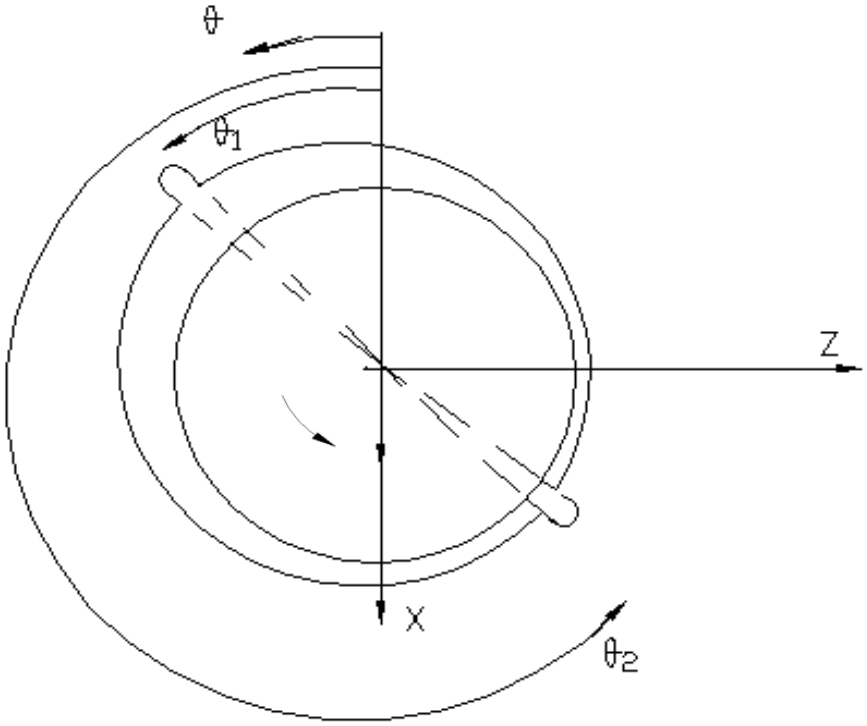

Figure 4.15: Near to the optimum configuration for minimization of friction variable

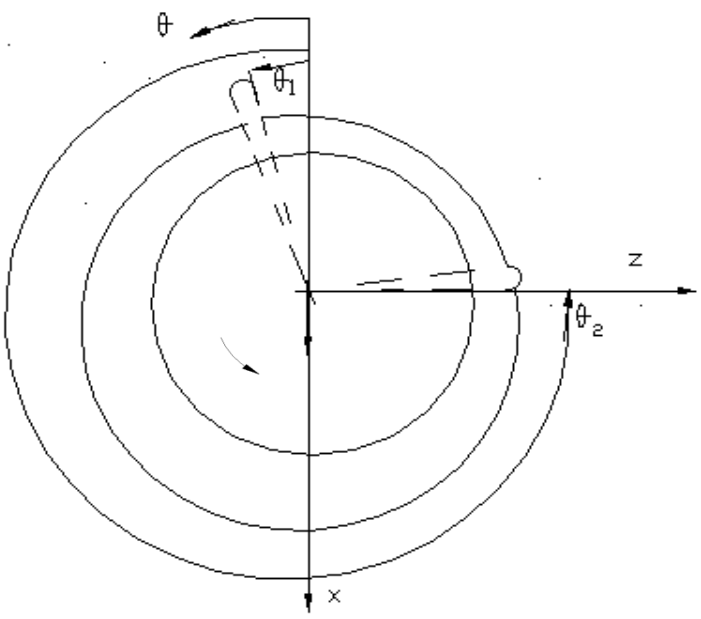

Figure 4.16: Near to the optimum configuration for maximization of flow coefficient

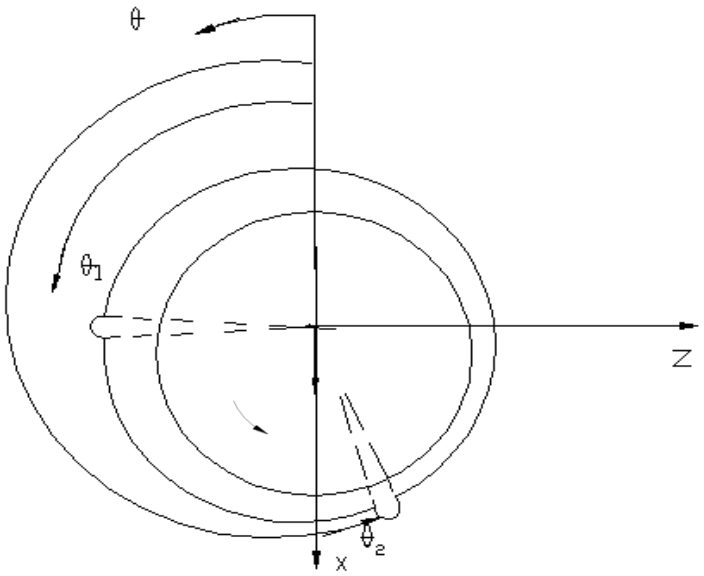

Figure 4.17: Near to the optimum configuration for maximization of non-dimensional load

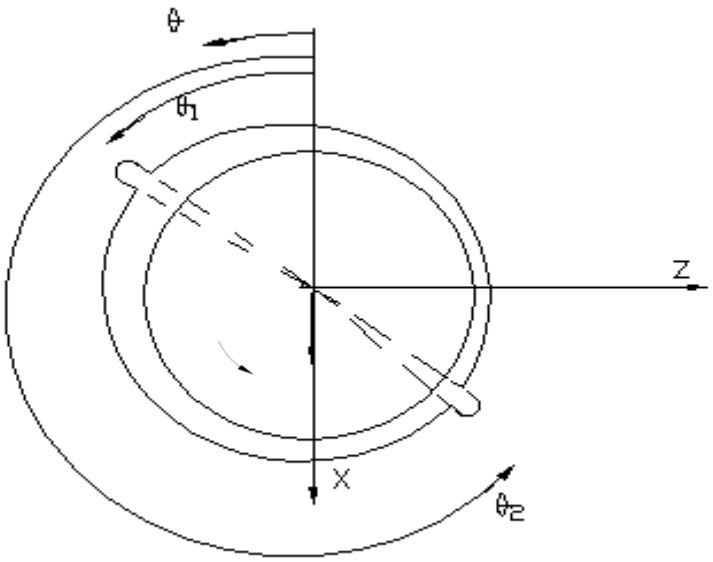

Figure 4.18: Near to the optimum configuration for maximization of mass parameter

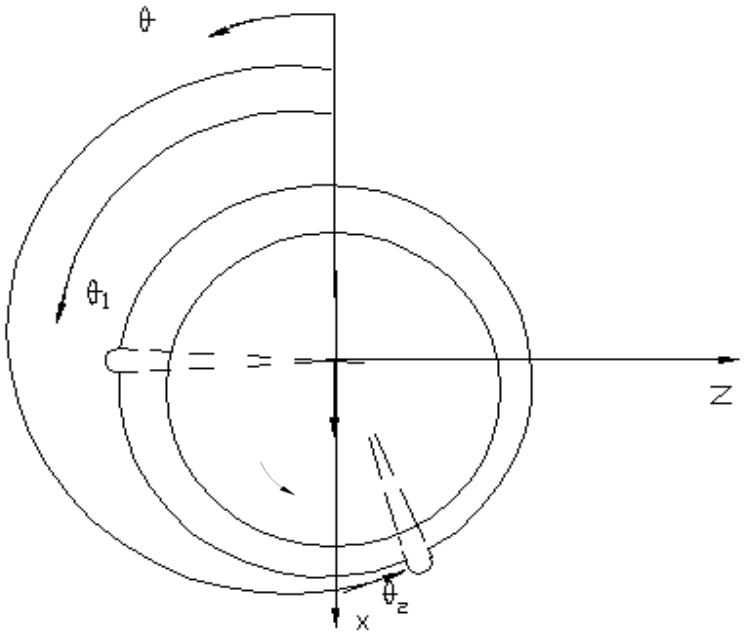

Figure 4.19: Near to the optimum configuration for of mimimization of multi-objective function

4.4 Summary:

In the present chapter, analysis (both steady state and dynamic) of two-lobe bearings is performed. The optimum groove locations for different objective functions, viz., maximization of non-dimensional load capacity, flow coefficient and mass parameter and minimization of friction variable have been obtained with the help of Genetic Algorithm (GA) toolbox of MatLab. It is observed that the optimum groove locations correspond to significant performance enhancement of two-lobe bearing. It has been found that the optimum groove locations are not only different for different objective functions but also different for different eccentricity ratios, *vis-a-vis*, loading conditions. The same observation was also made in case of two axial groove bearing. Therefore, the identification of locations of grooves for two-lobe bearing has been obtained such that the performance characteristics are near to the optimum for any loading condition (eccentricity ratio) for different objective functions.

CHAPTER 5

Analysis of three lobe bearings

5.0 Introduction

In high speed rotating machinery using hydrodynamic circular journal bearings, instabilities due to oil whip and whirl create serious problems. In such applications non-circular bearings are usually preferred because of their superior dynamic performance characteristics compared with those of circular bearings. The three-lobe bearing is a widely used noncircular bearing which in practical applications has all the lobes of equal arc length.

Multi-lobe journal bearings are often used in lightly loaded high speed applications due to their superior stability characteristics as compared to other fixed geometry designs. The stability is dependent on bearing dynamics characteristics, which is a function of bearing geometry, shaft speed, load and lubricant properties. The dynamic characteristics include the fluid film stiffness and damping coefficients and the stability margins of the journal bearing system.

As the dynamic performance is a prime consideration in the design and selection of bearings for modem high speed machinery, it appears that some optimum bearing configurations from this point of view may be derived from more detailed studies of non-circular bearing configurations as indicated by Sinhasan et.al.[31].

5.1 Estimation of Steady state and dynamic characteristics

Before starting the analysis for three bearing a comparison of comparison of non dimensional values of steady state and dynamic characteristics also made with the published results of Lund and Thomson [29] for two three lobe bearings for L/D=1 with three 20^0 axial groove and a elliptcity ratio $\delta = 0.5$ is tabulated in Table 5.1. The results are found to be in good agreement.

5.2 Analysis of steady state and dynamic characteristics

5.2.1 Groove size for better performance

To ascertain the size of the groove for better performance, a comparison of non dimensional load is made for different groove angles as shown in Table 5.2. It has been observed that the load carrying capacity is slightly higher with 10^o groove angles in comparison to 20^o and 30^o groove

angles in case of three lobe bearings (Fig. 2.4). Therefore, 10º groove angles are considered though out the analysis. The non dimensional load carrying capacity for eccentricity ratio of 0.05 is higher for 30^0 groove than that of 10^0 and 20^0 because of higher value of peak pressure development.

Table 5.1: Steady state and dynamic characteristics of three-lobe journal bearing for $\frac{L}{D} = 1.0, \delta = 0.5$ with three 20^0 axial grooves

ε	Results	S	ϕ	$\bar{K}_{XX}$	$\bar{K}_{XZ}$	$\bar{K}_{ZX}$	$\bar{K}_{ZZ}$	$\bar{C}_{XX}$	$\bar{C}_{XZ} = \bar{C}_{ZX}$	$\bar{C}_{ZZ}$
0.05	Present	1.153	65.000	10.78	14.85	-14.78	8.52	35.28	-2.33	30.28
	[29]	1.243	60.09	12.21	16.93	-16.72	9.18	38.75	-0.84	32.37
0.103	Present	0.457	68.21	6.823	4.976	-8.02	2.20	13.94	-4.373	13.684
	[29]	0.574	60.950	7.240	8.55	-7.900	4.240	20.730	-0.73	14.270
0.203	Present	0.232	62.28	5.53	4.162	-3.95	1.791	10.93	-0.968	6.696
	[29]	0.245	60.440	5.840	5.01	-3.600	2.360	12.590	0.43	6.16
0.285	Present	0.1364	58.96	5.550	3.871	-2.314	1.681	9.674	0.344	4.155
	[29]	0.138	58.220	5.540	4.220	-2.120	1.920	10.390	0.980	3.810
0.351	Present	0.0851	55.62	6.178	3.900	-1.39	1.600	9.28	1.069	2.932
	[29]	0.085	55.230	6.250	4.080	-1.260	1.710	9.640	1.350	2.970
0.389	Present	0.0620	53.02	6.982	4.068	-0.830	1.558	9.335	1.430	2.248
	[29]	0.062	52.820	7.090	4.170	-0.790	1.590	9.540	1.520	2.160
0.441	Present	0.033	45.67	10.05	4.721	0.1811	1.307	10.41	1.569	0.932
	[29]	0.034	47.190	9.700	4.650	0.110	1.420	10.030	1.670	1.230

Table 5.2: Comparison of non dimensional load values using 10^o, 20^o and 30^o groove angles

	$\bar{W}$		
ε	10^o groove	20^o groove	30^o groove
0.05	0.078	0.077	0.049
0.203	0.261	0.228	0.109
0.351	0.684	0.622	0.168
0.441	1.664	1.615	0.229

5.2.2 Bearing Performance with different Groove locations

The current practice is that the grooves are placed 120^0 apart for three-lobe bearings (Fig. 2.4). An attempt has been made in this section to find out whether the bearing performances are the same or different when groove positions are different from the current practice. In view of this many different configurations are studied and performance characteristics have been estimated. However, results showing the differences in performance characteristics of only one configuration (i.e when vertical lobe remains vertical lobe 1 separated by 140^0, other lobes separated by 110^0) have been shown here to save space (Fig 5.1). The groove angle considered is 10^o. The results are presented in Figs. 5.1 through 5.4. It has been observed that with change in groove locations, the various steady state and dynamic characteristics also change. Therefore, it is obvious that there has to be a certain configuration which corresponds to the optimum performance of three-lobe bearing.

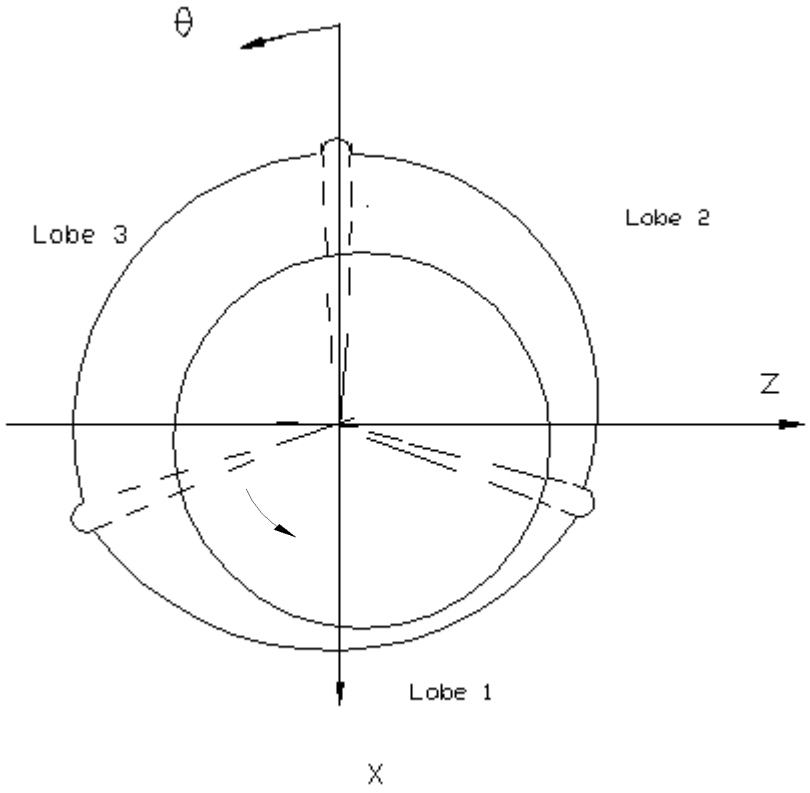

Fig 5.1: Three lobe bearing configuration where lobe 2 and lobe 3 separated by 110^0

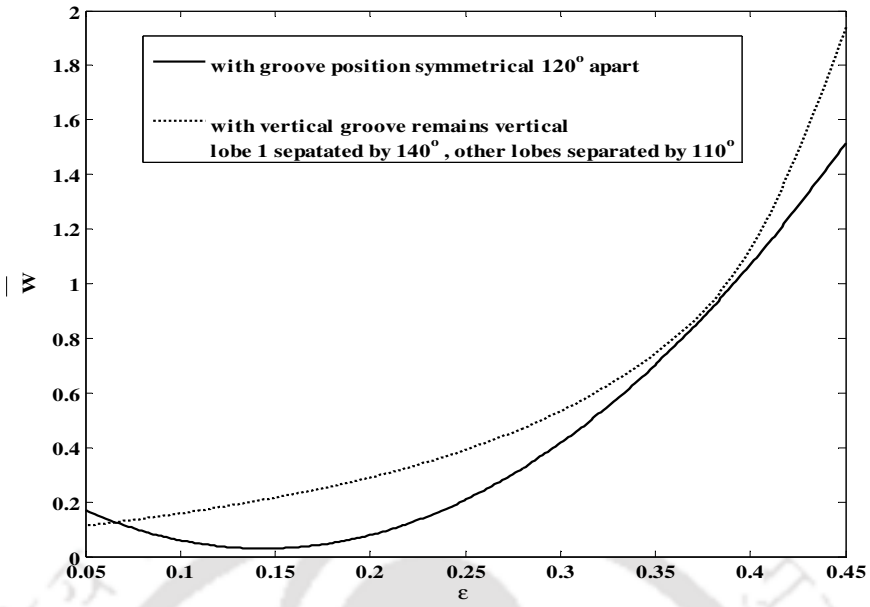

Figure 5.2: Variation of non dimensional load capacity with ε

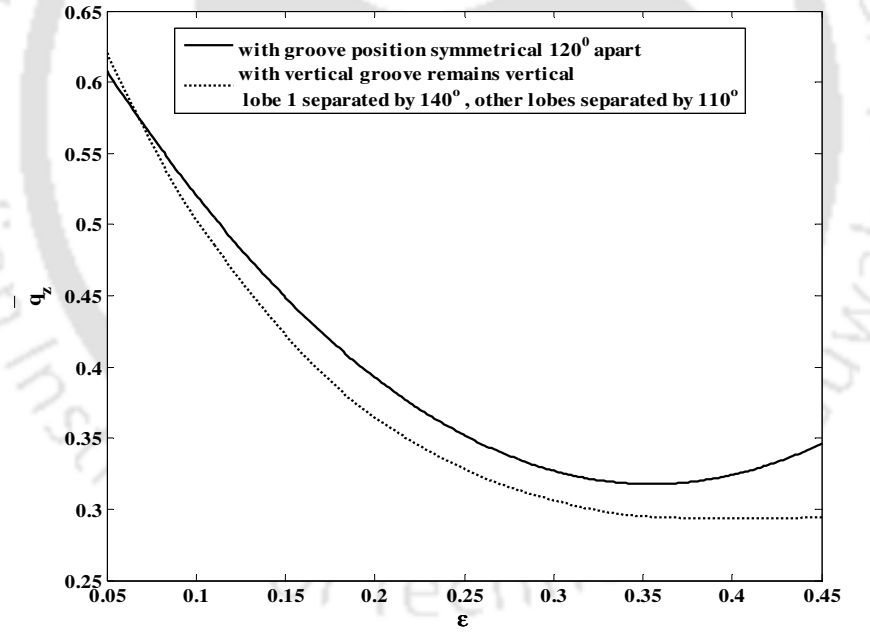

Figure 5.3: Variation of non dimensional flow coefficient with ε

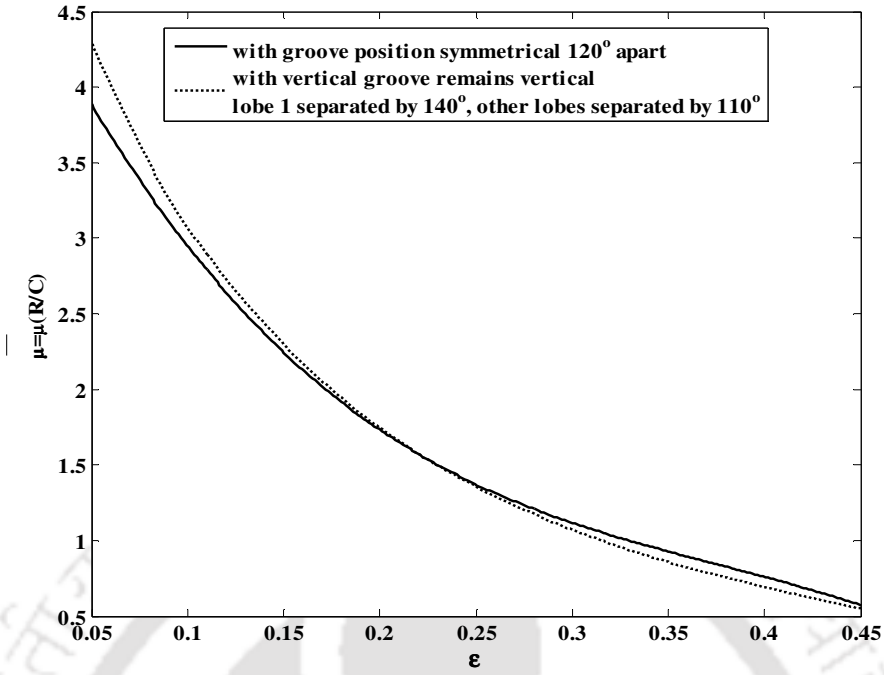

Figure 5.4: Variation of non dimensional friction variable with ε

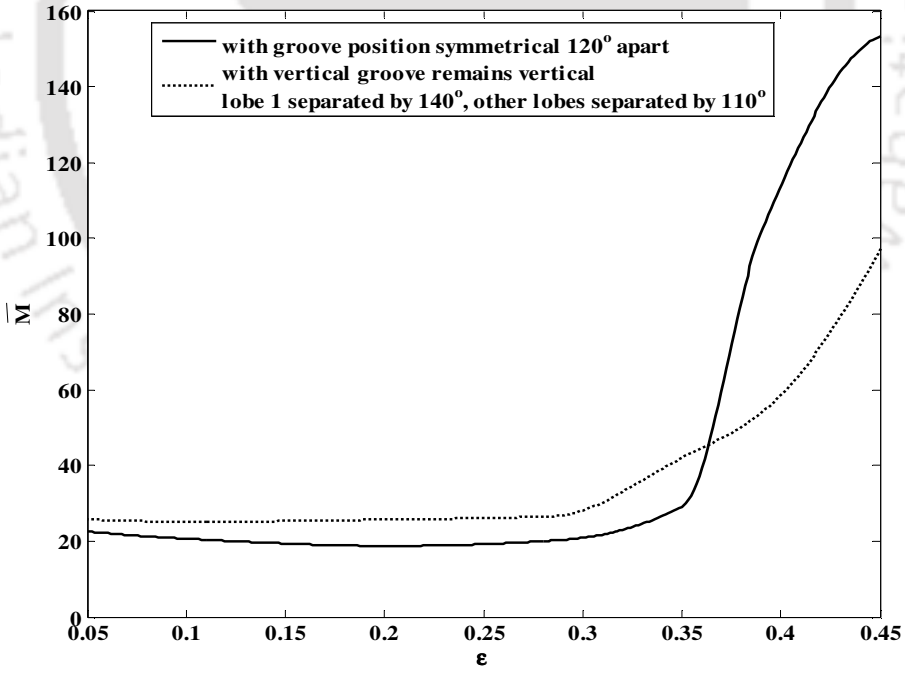

Figure 5.5: Variation of non dimensional mass parameter with ε

5.2.3 Determination of optimum location of groove

It has been shown in the previous section that the location of the groove have influence in flow ($\bar{q}_z$), frictional variable ($\bar{\mu}$), non-dimensional load capacity ($\bar{W}$) and mass parameter ($\bar{M}$). In view of this, an attempt has been made to locate the groove locations which correspond to optimum performances in terms of the four parameters mentioned above.

The objective functions and optimization technique are the same as for two-axial groove bearing and two-lobe bearing. Genetic Algorithm (GA) has been used to find the optimum solution as outlined in Chapter 2. The problem is framed with four objectives. The variables used in the problem are starting angle of first groove (θ_1), starting angle of second groove (θ_2) , starting angle of third groove (θ_3) in Case –I.

The optimum configurations have been obtained for eccentricity ratio ranging from 0.05 to 0.441 in this case. In Case –II, the eccentricity ratio (ε), starting angle of first groove (θ_1), starting angle of second groove (θ_2) and, starting angle of third groove (θ_3) are variables and act as Chromosome. The objectives are minimization of friction variable, $\bar{\mu}$ (Eqn. 2.22), maximization of non-dimensional load capacity, $\bar{W}$ (Eqn. 2.20), maximization of flow coefficient $\bar{q}_z$ (Eqn 2.21), maximization of mass parameter, $\bar{M}$ (Eqn. 2.31). Objective function framing is the same for both the cases and variable bounds are shown in Table 5.3.

Table 5.3: Variable bounds for the bearing problem

Case	Variable	Lower	Upper
I	Starting angle of first groove	10°	100°
	Starting angle of second groove	120°	190°
	Starting angle of third groove	210°	340°
II	ε	0.05	0.441
	Starting angle of first groove	10°	100°
	Starting angle of second groove	120°	190°
	Starting angle of third groove	210°	340°

Optimum groove locations for three-lobe bearings also have been obtained using Genetic Algorithm (GA) toolbox of MatLab as it was done for two axial groove in Chapter 3 and two-lobe bearings in and Chapter 4. The obtained results from GA have been compared with the results obtained using Sequential quadratic programming (SQP). The optimum value of fitness

function obtained corresponding to maximization of flow coefficient has been tabulated for both GA and SQP in Table 5.4.

It has been observed that the results obtained using both the methods are exactly the same. Similarly maximum non-dimensional load capacity, minimum friction variable, maximum mass parameter values are also found to match for both the methods. However, GA has been used in this work for the same reason as stated in Chapter 3 and Chapter 4.

Initially a single objective function has been taken up. Here in case of three-lobe bearing a population size of 50, mutation probability of 0.1 and a cross over probability of 0.8 have been selected as discussed in case of two axial groove and two lobe bearing in the previous chapters.

Table 5.4: Comparison of GA and SQP results

ε	Objective function value (Maximum flow coefficient)	
	GA results	SQP results
0.050	1.352	1.352
0.103	2.985	2.985
0.203	2.758	2.758
0.285	3.117	3.117
0.351	3.490	3.490
0.389	3.287	3.287
0.441	3.335	3.335

The optimum groove locations for minimum friction variable, non-dimensional load capacity, flow coefficient, and mass parameter at different ε are shown in Figs. 5.5 through 5.8. θ_1 , θ_2 and θ_3 are the starting locations of the first ,second and the third groove respectively in degrees.

It has been observed that the first groove location remain in the range (10^o to 96.05^0), (11.948^o to 92.55^o), (10^0 to 51.072^0) and (10^0 to 80.22^0) respectively when objective functions are friction variable, non-dimensional load capacity, flow coefficient, and mass parameter. However, the second groove location varies in the range of (120^0 to 178.93^0), (120. 929^0 to 189.24^0), (120^0 to 197.616^0), (100^0 to 208.947^0) respectively when objective functions are

friction variable, non-dimensional load capacity, flow coefficient, and mass parameter and the third groove location varies from (210^0 to 339.18^0), (227.849^0 to 338.59^0), (210^0 to 339.59^0) , (210 to 321.947^o) respectively when objective functions are friction variable, non-dimensional load capacity, flow coefficient, and mass parameter. The optimum groove locations for the multi-objective function (section 2.11) have been presented in Fig. 5.10. It has been observed that the first groove location varies in the range (20 to 33.879^0), the second groove location varies in the range (120.04^0 to 187.20^0) and the third groove location varies in the range (198^0 to 297.67^0) in this case.

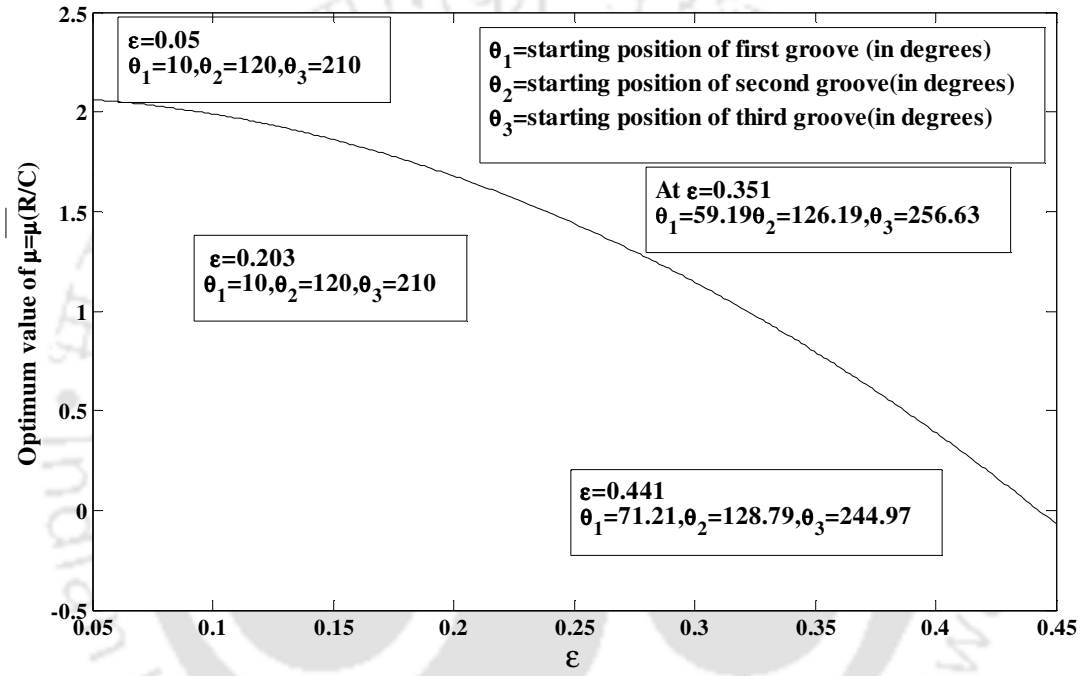

Figure 5.6: Variation of friction variable at optimum grooving location for different ε

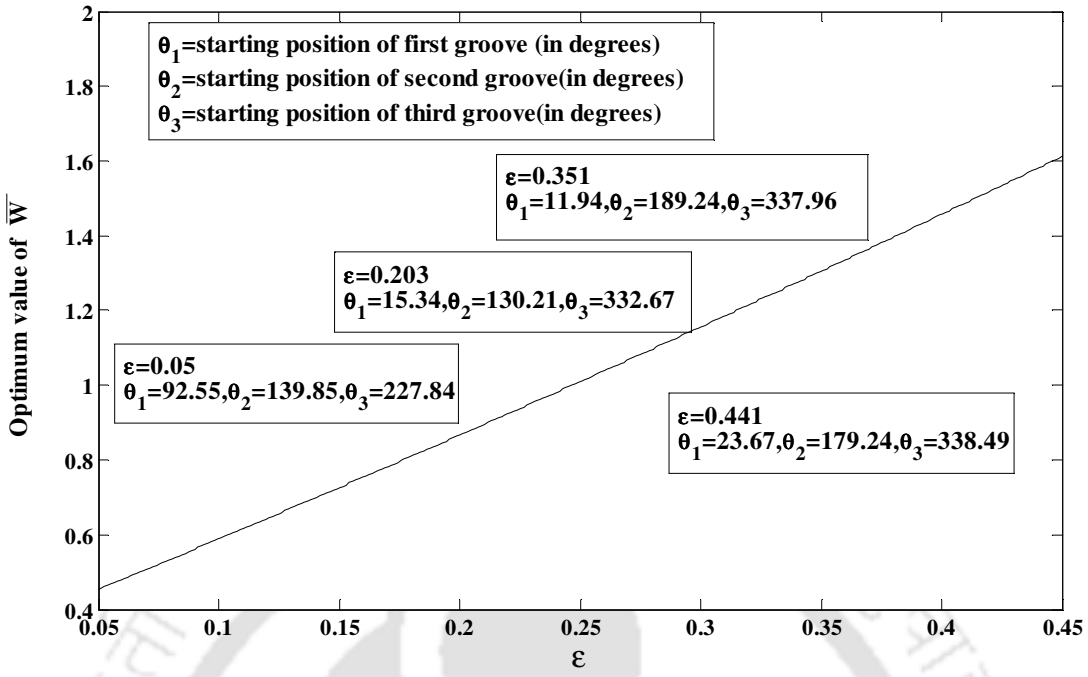

Figure 5.7: Variation of $\overline{W}$ at optimum grooving location for different ε

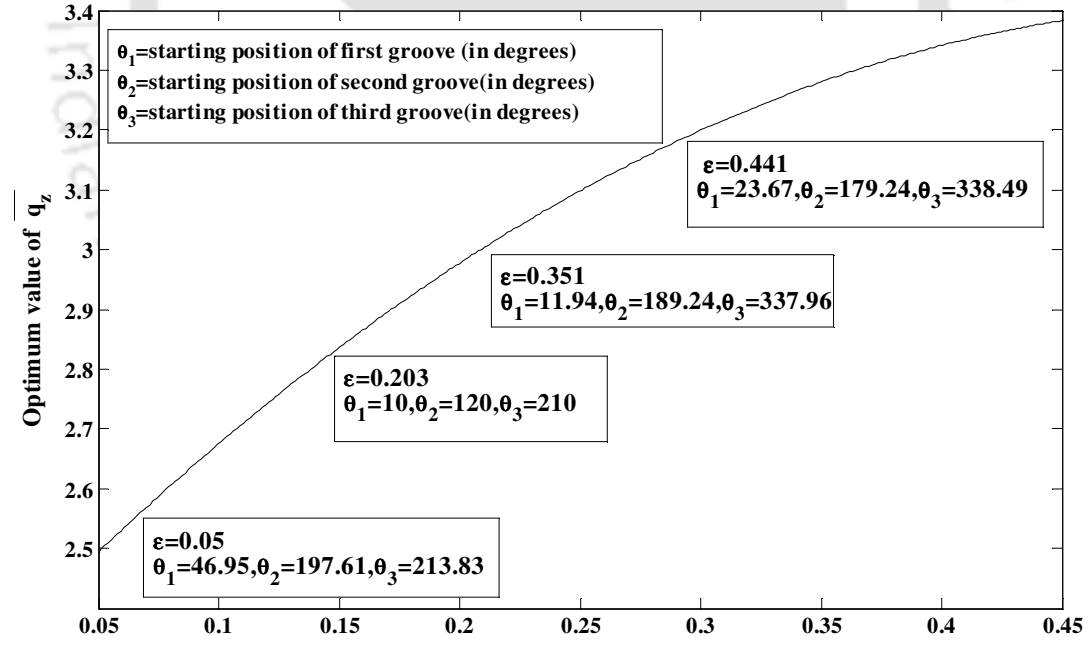

Figure 5.8: Variation of flow-coefficient at optimum grooving location for different ε

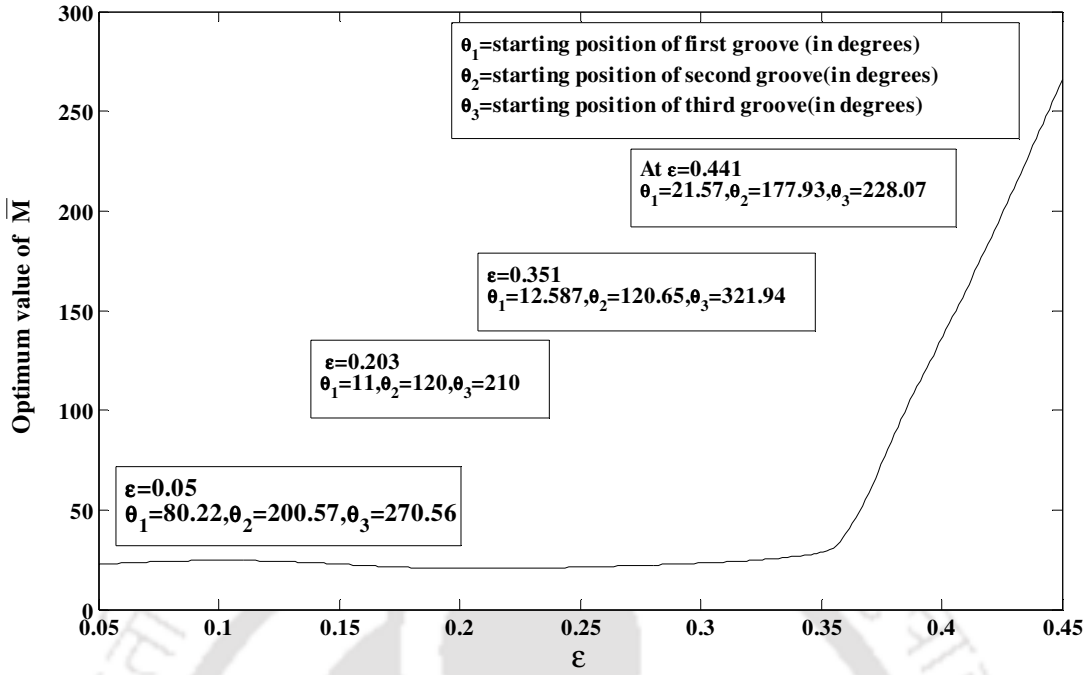

Figure 5.9: Variation of mass-parameter at optimum grooving location for different ε

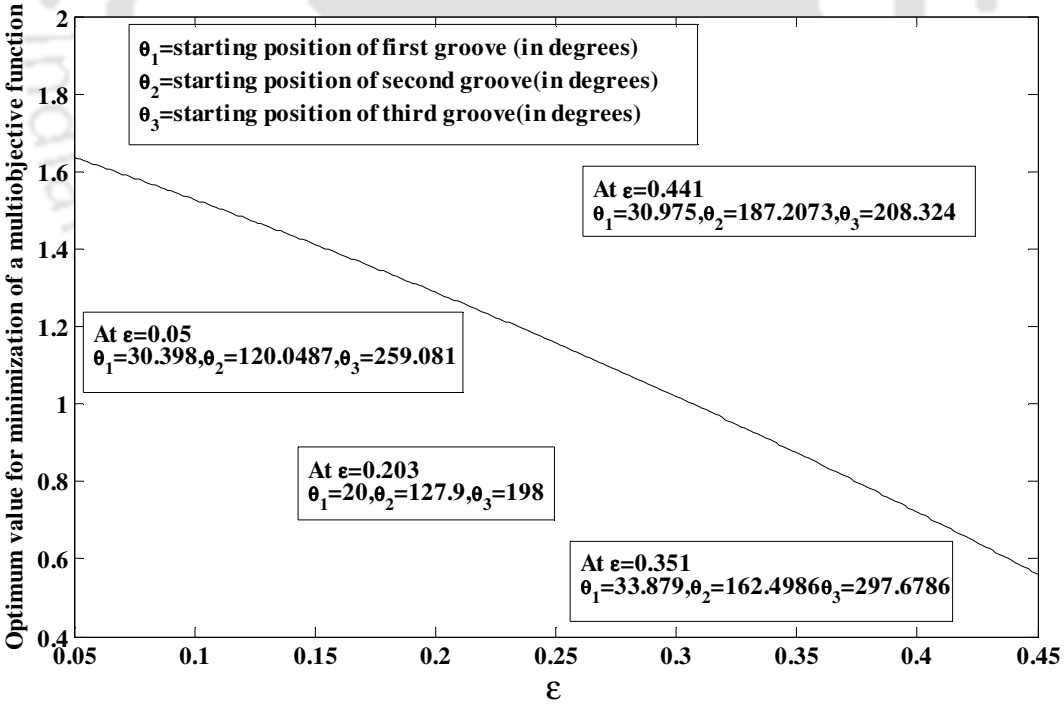

Figure 5.10: Optimum value obtained by minimization of a multi-objective function for different ε

From the results presented here, it can be inferred that the groove locations are sensitive to the type of objective function. The practice and the notion of convenience of keeping groove

locations symmetrically 120^o apart need to be thoroughly looked into as the present results show that optimum groove locations are not 120^o apart for the objective function considered in the present work. A Comparison of Optimum non-dimensional friction variable, flow coefficient, non-dimensional load capacity and mass parameter with groove location 120^0 apart has been made as shown in Tables 5.5 and 5.6. It is very much clear from the comparison that there is a significant improvement in the optimum value of friction variable, flow coefficient, non-dimensional load capacity and mass parameter value than that of three-lobe bearing with grooves location 120^0 apart.

When eccentricity ratio (ε), starting angle of first groove (θ_1), starting angle of second groove (θ_2) and starting angle of third groove (θ_3) are variables and acts as Chromosome as in Case –II, the optimum configuration for the same is presented in Table 5.7.

Table 5.5: Comparison of Optimum friction variable and flow coefficient results with groove position 120^0 apart and are symmetrically placed.

ε	Minimization of μ(R/C)	Corresponding Optimum location	Maximization of $\overline{q}_Z$	Corresponding Optimum location
	Groove locations 120^0 apart(Optimum Configuration)		Groove locations 120^0 apart (Optimum Configuration)	
0.050	4.3004(1.9813)	θ_1= 10	0.6322 (1.352)	θ_1= 46.95
		θ_2= 120		θ_2= 197.616
		θ_3= 210		θ_3= 213.83
0.103	3.015(1.979)	θ_1= 10	0.498 (2.985)	θ_1= 10
		θ_2= 120		θ_2= 120
		θ_3= 210		θ_3= 210
0.203	1.718 (1.998)	θ_1= 10	0.361 (2.758)	θ_1= 10
		θ_2= 120		θ_2= 120
		θ_3= 210		θ_3= 210
0.285	1.148(1.001)	θ_1= 96.05	0.311 (3.117)	θ_1= 28.805
		θ_2= 145.79		θ_2= 120.929
		θ_3= 333.07		θ_3= 327.66
0.351	0.853 (0.817)	θ_1= 59.19	0.295 (3.490)	θ_1= 11.948
		θ_2= 178.93		θ_2= 189.24
		θ_3= 339.18		θ_3= 337.965.
0.389	0.726 (0.251)	θ_1= 80.32	0.293 (3.287)	θ_1= 51.072
		θ_2= 126.196		θ_2= 166.027
		θ_3= 256.636		θ_3= 339.59
0.441	0.573 (0.141)	θ_1= 71.21	0.294(3.335)	θ_1= 23.675
		θ_2= 128.79		θ_2=179.2461
		θ_3= 244.97		θ_3= 338.49

Table 5.6: Comparison of optimum non dimensional load and mass parameter with non dimensional load and mass parameter with groove position 120^0 apart and are symmetrically placed.

	Maximization of $\bar{W}$	Corresponding Optimum location	Maximization of $\bar{M}$	Corresponding Optimum location Optimum
ε	Groove locations 120^0 apart(Optimum Configuration)		Groove locations 120^0 apart (Optimum Configuration)	
0.05	0.078 (0.084)	θ_1= 92.55 θ_2= 139.851 θ_3= 227.849	20.51 (21.546)	θ_1= 80.22 θ_2= 200.573 θ_3= 270.563
0.103	0.137 (1.041)	θ_1= 80.758 θ_2=133.52 θ_3=237.725	20.54 (23.432)	θ_1= 24.088 θ_2= 205.00 θ_3= 218.879
0.203	0.2612 (1.074)	θ_1= 15.345 θ_2= 130.215 θ_3= 332.677	20.76 (24.675)	θ_1= 11 θ_2= 120 θ_3= 210
0.285	0.362 (1.011)	θ_1= 28.805 θ_2= 120.929 θ_3= 327.965	20.15 (26.123)	θ_1= 14.4 θ_2= 132.76 θ_3= 208.947
0.351	0.684 (1.121)	θ_1= 12.38 θ_2= 180.24 θ_3= 335.965	26.41 (28.679)	θ_1= 12.587 θ_2= 120.65 θ_3=321.947
0.389	0.929 (1.251)	θ_1= 51.072 θ_2= 166.027 θ_3=339.59	100.00 (101.655)	θ_1= 10 θ_2= 100 θ_3= 210
0.441	1.662 (1.897)	θ_1= 23.6752 θ_2= 179.246 θ_3= 338.49	122 (239.964)	θ_1= 21.577 θ_2= 177.937 θ_3= 228.073

In genetic algorithm, in each generation the fitness values of the objective function of the individuals is determined. These values express the fitness of the solutions of the new generations, one cycle of genetic algorithm called a generation. In each generation if the solution is improved, it is stored as the best solution. This is repeated till convergence. The optimum results obtained for friction variable, flow coefficient, non-dimensional load capacity, mass parameter and for multiobjective function are shown in Figures 5.10 through 5.14.

It has been observed from the results presented in Table 5.7 that the first groove location varies in the range of (10^0 to 74.910^0) where as the second groove location varies in the range of (100^0 to 176.3843^0) and the third groove location varies in the range of (210^0 to 330.849^0). It has also been observed that the eccentricity ratio at which optimum location occurs is on the higher side for all objective functions.

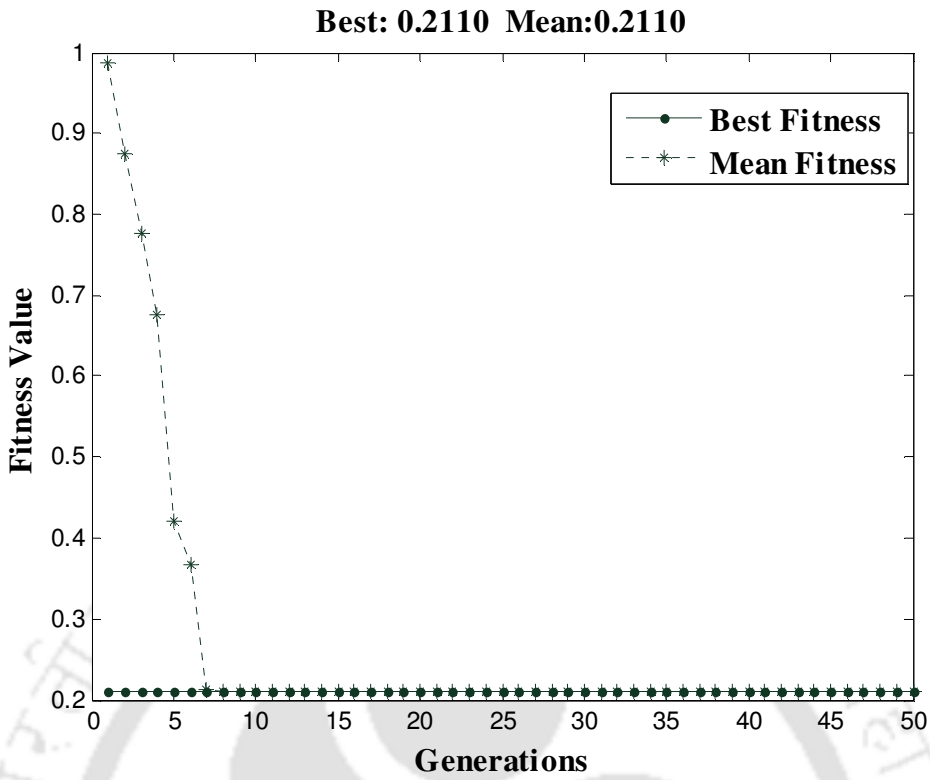

Figure 5.11:Fitness value considering friction variable as objective function

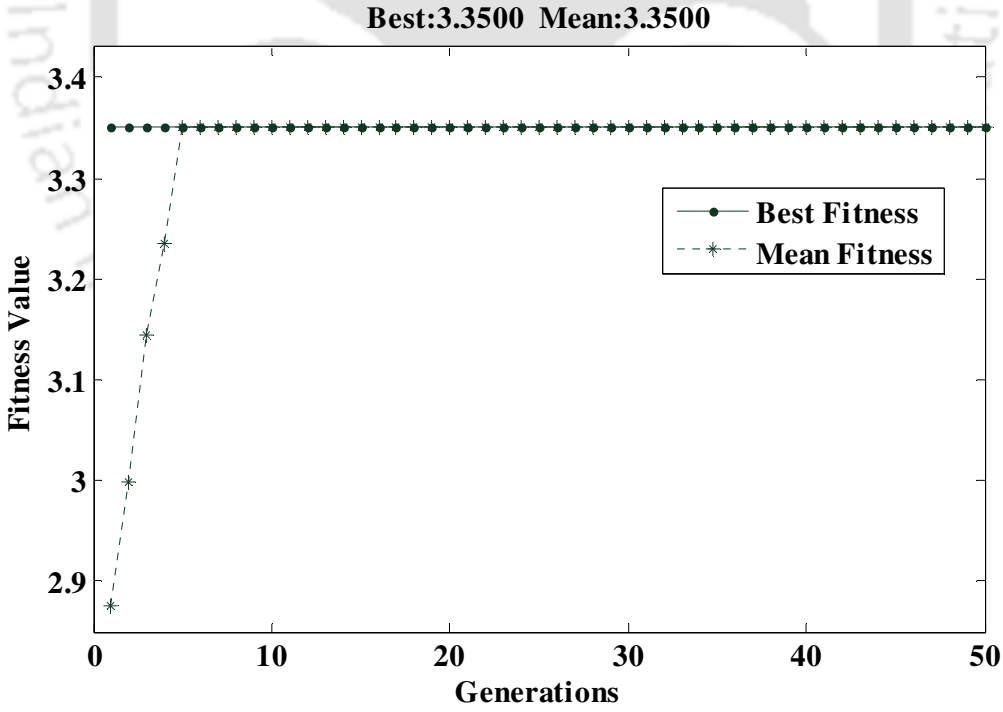

Figure 5.12: Fitness value considering flow coefficient as objective function

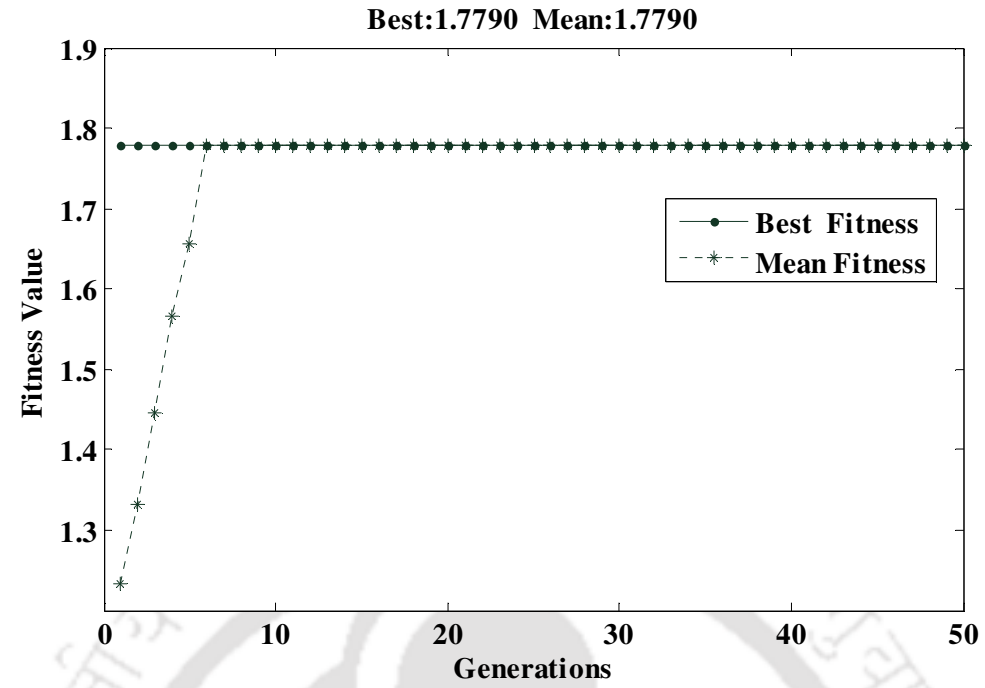

Figure 5.13: Fitness value considering load as objective function

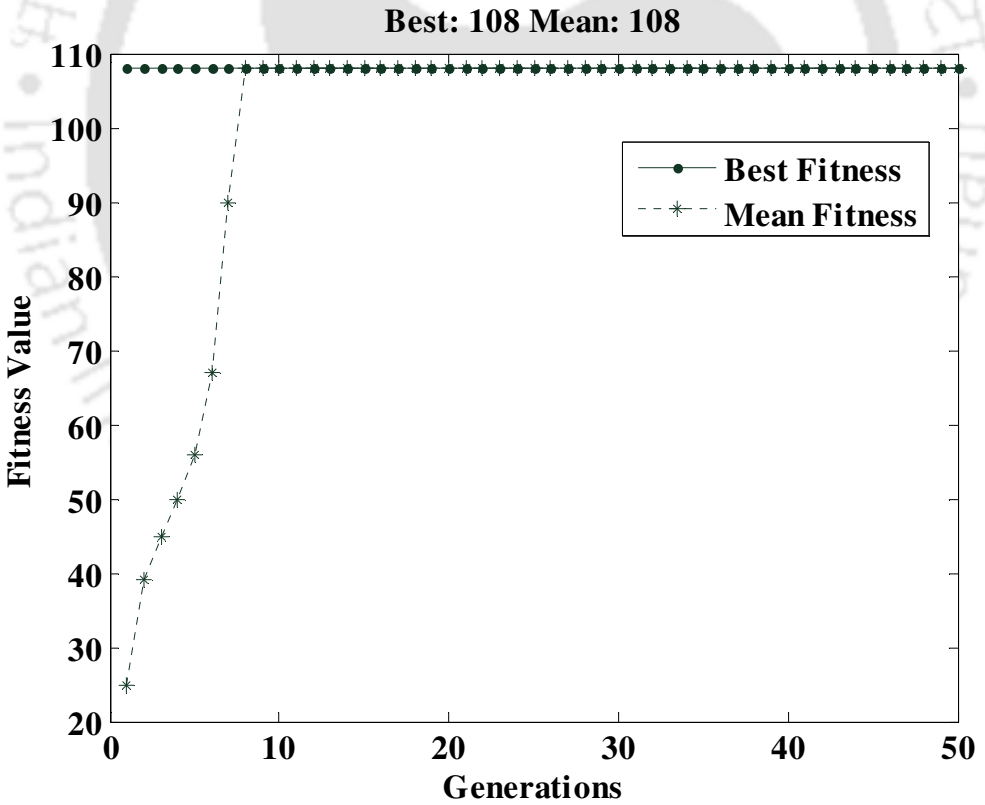

Figure 5.14: Fitness value considering mass parameter as objective function

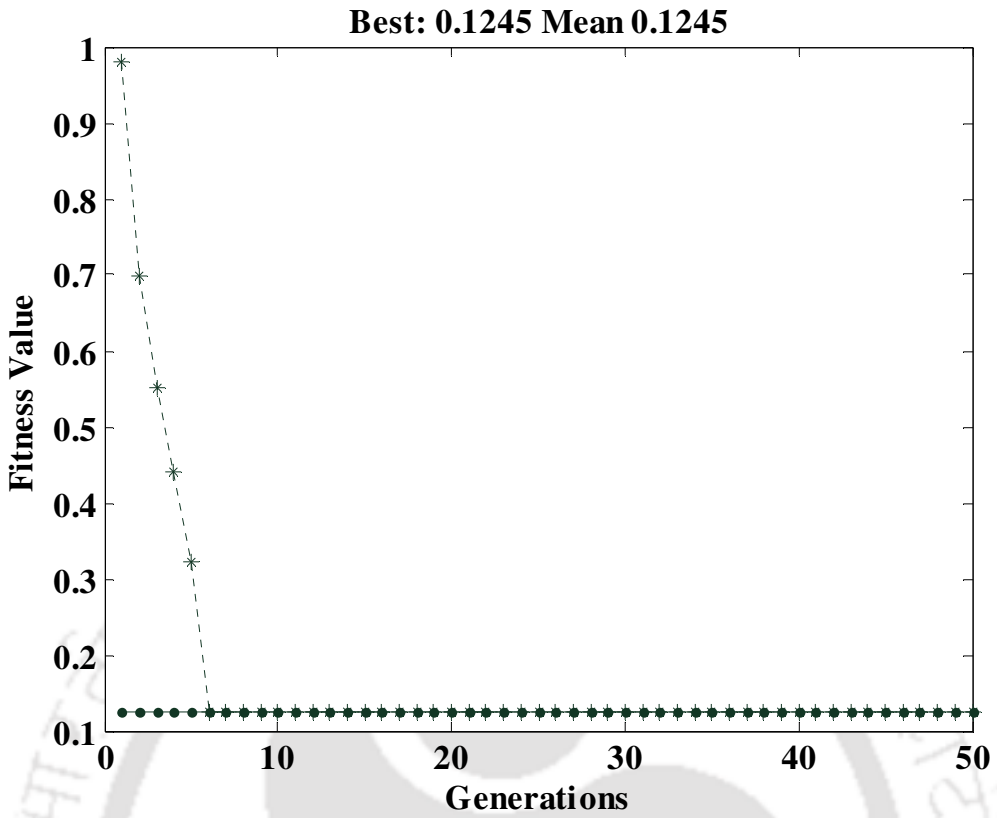

Figure 5.15: Fitness value obtained by minimization of a multi-objective function

Table 5.7: Optimum groove location with different objectives as in Case - II

Objective function	ε	θ_1	θ_2	θ_3
Minimization of friction variable	0.4266	74.910	176.3843	316.281
Maximization of flow coefficient	0.3452	79.2203	131.707	330.849
Maximization of load	0.4271	64.887	131.776	232.156
Maximization of mass parameter	0.403	10	100	210
Minimization of multiobjective function	0.343	10	120	210

5.2.4 Determination of near to the optimum location of groove

It has been observed that the optimum groove locations are different for different loading condition (eccentricity ratio) as well as for different objective functions in case of three-lobe bearing. The same was observed for two-axial groove and two-lobe bearings and therefore, 'near to the optimum configurations' were identified. Therefore, it has been decided to identify 'near to the optimum configurations' for three-lobe bearings for different objective functions following the same procedure outlined in Chapter 2. The results are presented in Table 5.8 and also in Figures 5.16 through 5.20.

Table 5.8: Near to the optimum configuration for different objectives

Objective function	θ_1	θ_2	θ_3
Minimization of friction variable	59	178	339
Maximization of flow coefficient	28	120	327
Maximization of load	15	130	332
Maximization of mass parameter	80	200	270
Minimization of multiobjective function	20	120	210

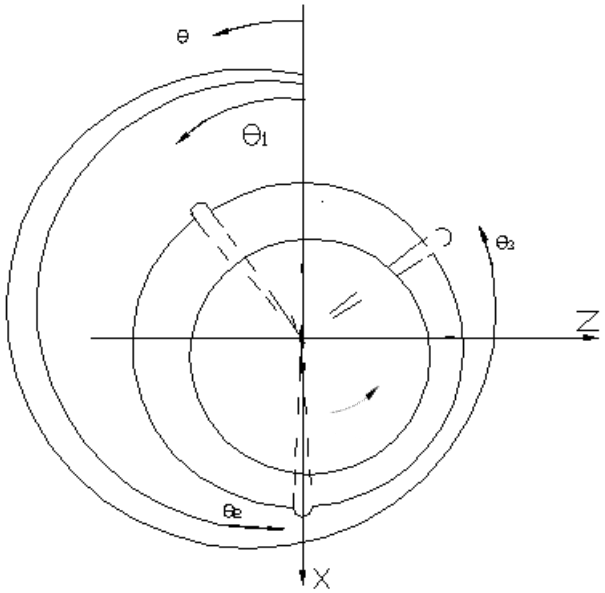

Figure 5.16:Near to the optimum configuration for minimization of friction variable

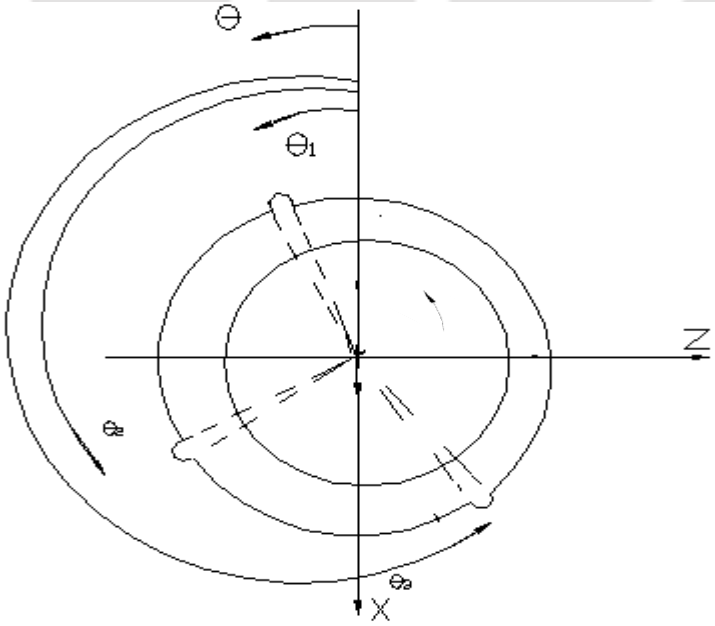

Figure 5.17:Near to the optimum configuration for maximization of flow coefficient

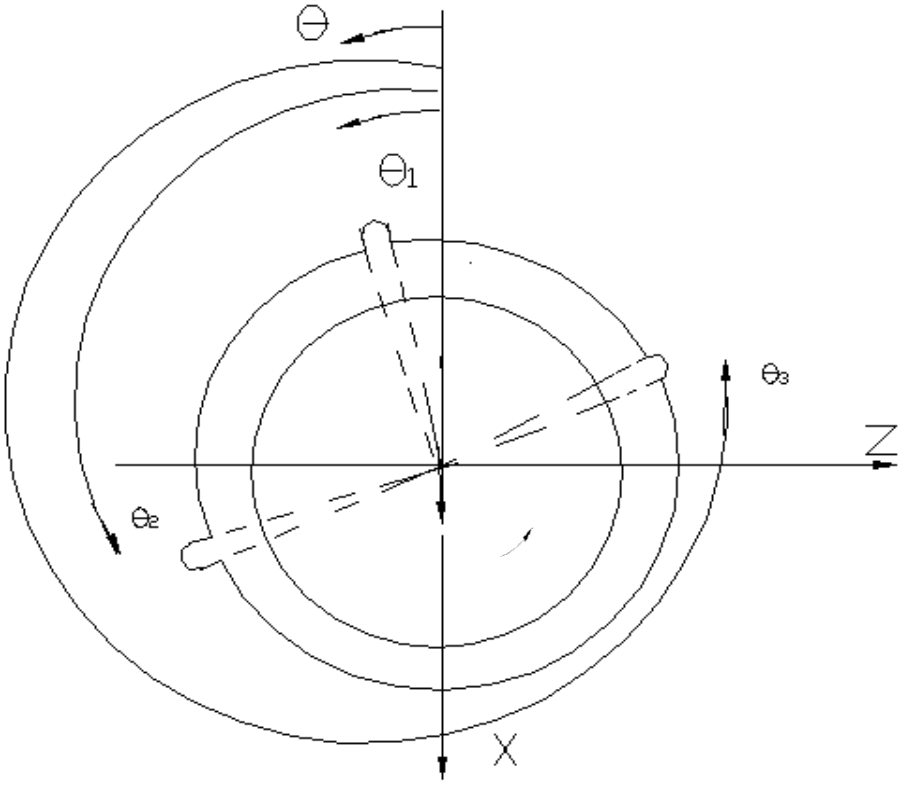

Figure 5.18:Near optimum configuration maximization of non-dimensional load capacity

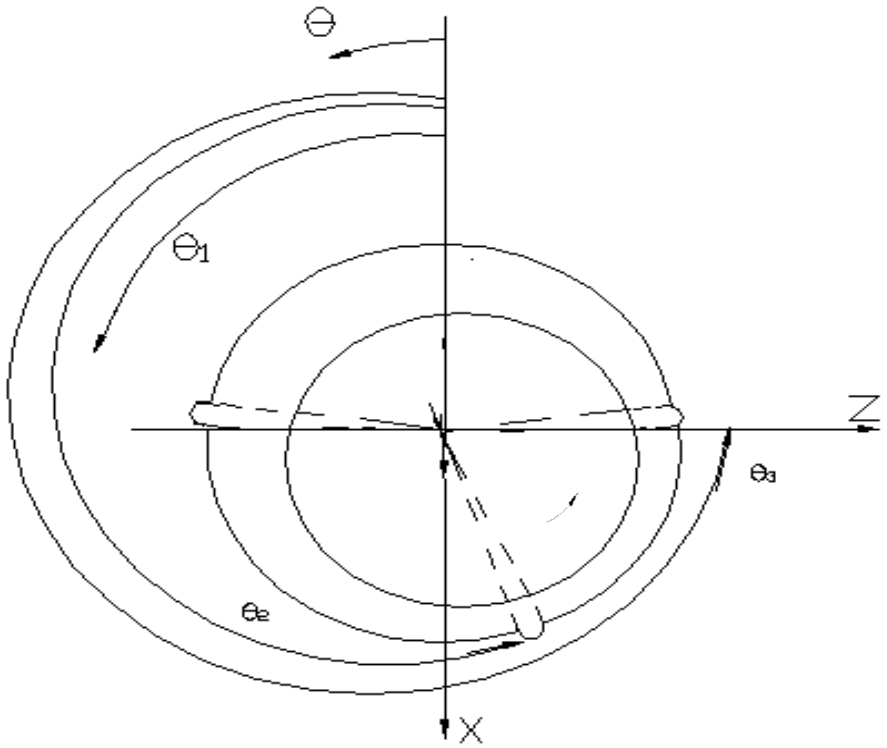

Figure 5.19:Near optimum configuration for maximization of mass parameter

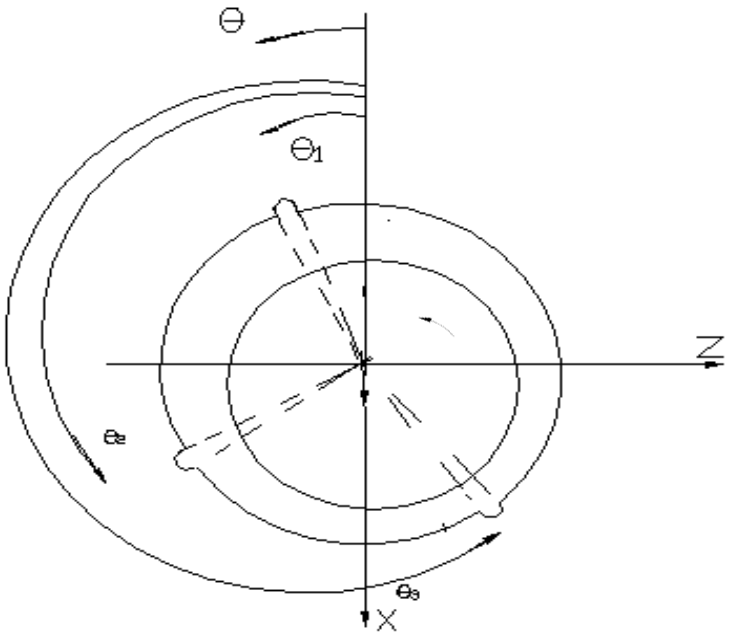

Figure 5.20: Near optimum configuration for minimization of multiobjective function

5.5 Summary:

In the present chapter, analysis (both steady state and dynamic) of three-lobe bearings is performed. The optimum groove locations for different objective functions, viz., maximization of non-dimensional load capacity, flow coefficient and mass parameter and minimization of friction variable have been obtained with the help of Genetic Algorithm (GA) toolbox of MatLab. It is observed that the optimum groove locations correspond to significant performance enhancement of three-lobe bearing. It has been found that the optimum groove locations are not only different for different objective functions but also different for different eccentricity ratios, *vis-a-vis*, loading conditions. The same observation was also made in case of two axial groove and two-lobe bearing. Therefore, the identification of locations of grooves for three-lobe bearing has been obtained such that the performance characteristics are near to the optimum for any loading condition (eccentricity ratio) for different objective functions.

CHAPTER 6

Analysis of four lobe bearings

6.0 Introduction

Excellent operating characteristics and low costs are two reasons why fluid film journal bearings are used in high speed rotating machinery in power and industrial applications. Previously, several works has been performed both experimentally and theoretically to examine the stiffness and damping characteristics of several types of bearings. One particular bearing type which receives widespread use is the multilobe bearing. The stability of ordinary journal bearings is found to increase by the use of multi-lobes [27].

As the dynamic performance is a prime consideration in the design and selection of bearings for modem high speed machinery, it appears that some optimum bearing configurations from this point of view may be derived from more detailed studies of non-circular bearing configurations as indicated by Sinhasan *et al.* [31]. No work has been reported in the literature about the optimum performance of a four-lobe bearing.

6.1 Estimation of Steady state and dynamic characteristics

Before starting the analysis of four-lobe bearing a comparison of non-dimensional values of steady state and dynamic characteristics has been made with the published results of Lund and Thomson [29] for L/D=1 with two 10^0 axial groove , $\delta = 0.5$ and presented in Table 6.1. The results are found to be in good agreement.

6.2 Analysis of steady state and dynamic characteristics

6.2.1 Groove size for better performance

To ascertain the size of the groove for better performance, a comparison of non-dimensional load capacity is made for different groove angles as shown in Table 6.2. It has been observed from the presented results that the non-dimensional load capacity is slightly higher with 10^o groove angles in comparison to 20^o and 30^o groove angles in case of four-lobe bearings. Therefore, 10^o groove angles are considered throughout the analysis.

Table 6.1: Steady state and dynamic characteristics of four-lobe journal bearing for $\frac{L}{D}$ = 1.0 with four 10^0 axial grooves, $\delta = 0.5$

ε		S	ϕ	$\bar{K}_{XX}$	$\bar{K}_{XZ}$	$\bar{K}_{ZX}$	$\bar{K}_{ZZ}$	$\bar{C}_{XX}$	$\bar{C}_{XZ} = \bar{C}_{ZX}$	$\bar{C}_{ZZ}$
0.020	Present	3.933	65.000	23.856	48.212	-46.59	24.894	99.572	1.731	97.612
	[29]	3.999	65.000	23.910	48.67	-47.220	24.94	100.520	1.730	98.870
0.050	Present	1.571	61.000	9.7940	20.21	-18.480	10.86	41.340	2.352	39.300
	[29]	1.571	61.000	9.8171	20.185	-18.47	10.875	41.271	2.361	39.285
0.103	Present	0.731	59.000	5.547	11.008	-8.652	6.385	22.278	3.036	18.986
	[29]	0.743	59.000	5.530	11.13	-8.710	6.410	22.530	3.050	19.090
0.203	Present	0.308	54.570	5.045	7.543	-3.695	4.555	15.283	3.631	8.846
	[29]	0.2231	51.230	5.900	7.043	-2.451	3.826	14.530	3.197	6.126
0.285	Present	0.162	47.800	6.548	6.548	-1.729	3.073	13.964	2.607	4.344
	[29]	0.165	47.800	6.890	6.600	-1.740	3.090	14.080	2.620	4.370
0.351	Present	0.0872	42.000	8.889	5.613	-1.003	1.996	12.838	1.727	2.358
	[29]	0.088	42.000	8.880	5.662	-1.014	2.004	12.9330	1.732	2.378
0.375	Present	0.066	40.000	9.812	5.356	-0.779	1.719	12.520	1.519	1.832
	[29]	0.068	40.000	9.780	5.410	-0.790	1.730	12.650	1.540	1.860

Table 6.2: Comparison of non dimensional load values using 10^o, 20^o and 30^o groove angles

	$\bar{W}$		
ε	10^o groove	20^o groove	30^o groove
0.05	0.0337	0.0261	0.0231
0.203	0.1717	0.1382	0.1266
0.351	0.6081	0.5253	0.3485
0.375	0.7925	0.6956	0.4338

6.2.2 Bearing Performance with different Groove locations

The current practice is that the grooves are placed 90^o apart for four lobe bearings. An attempt has been made in this section to find out if the bearing performances are the same or different when groove positions are different from the current practice. In view of this many different configurations are studied and performance characteristics have been estimated. However, results showing the differences in performance characteristics of only one configuration (i.e when lobe 3 moves 10^0 ahead of symmetrical position in the anticlockwise direction) have been shown here to save space in Figs. 6.1 through 6.4. The groove angle considered is 10^o. It has been observed that with change in groove locations, the various steady state and dynamic

characteristics also change. Therefore, it is obvious that there has to be a certain configuration which corresponds to the optimum performance of four-lobe bearing.

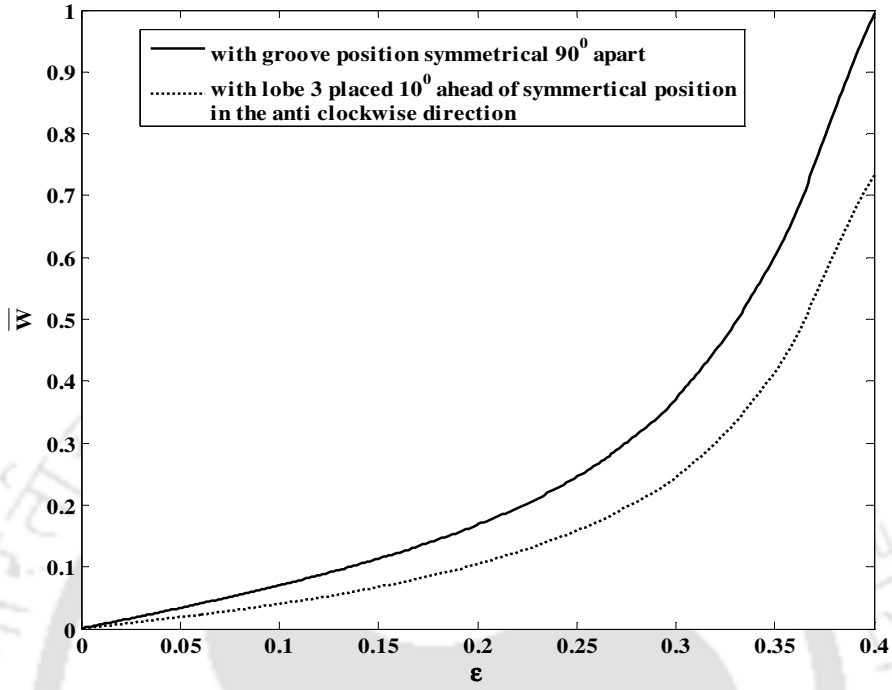

Figure 6.1: Variation of non dimensional load capacity with ε

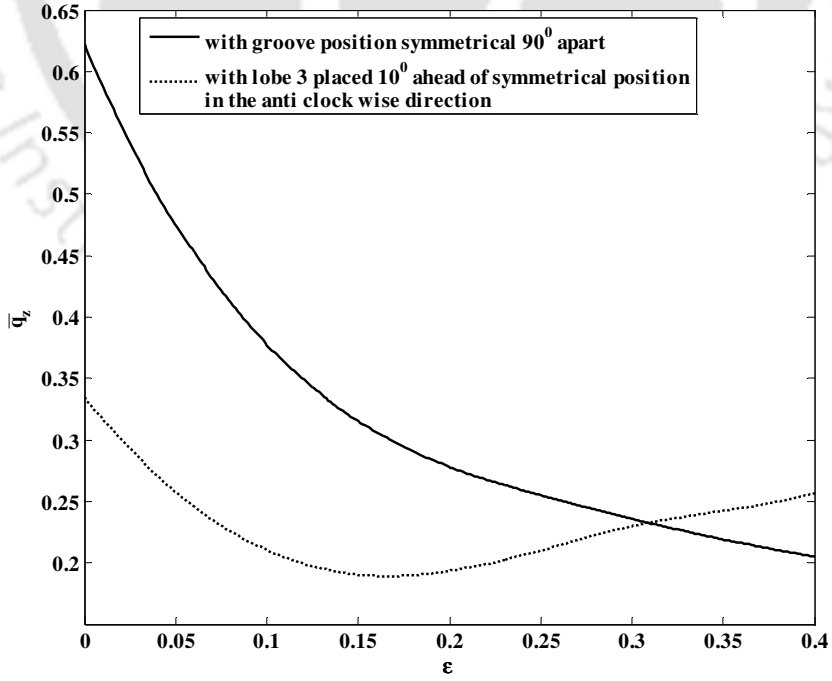

Figure 6.2: Variation of non dimensional flow coefficient with ε

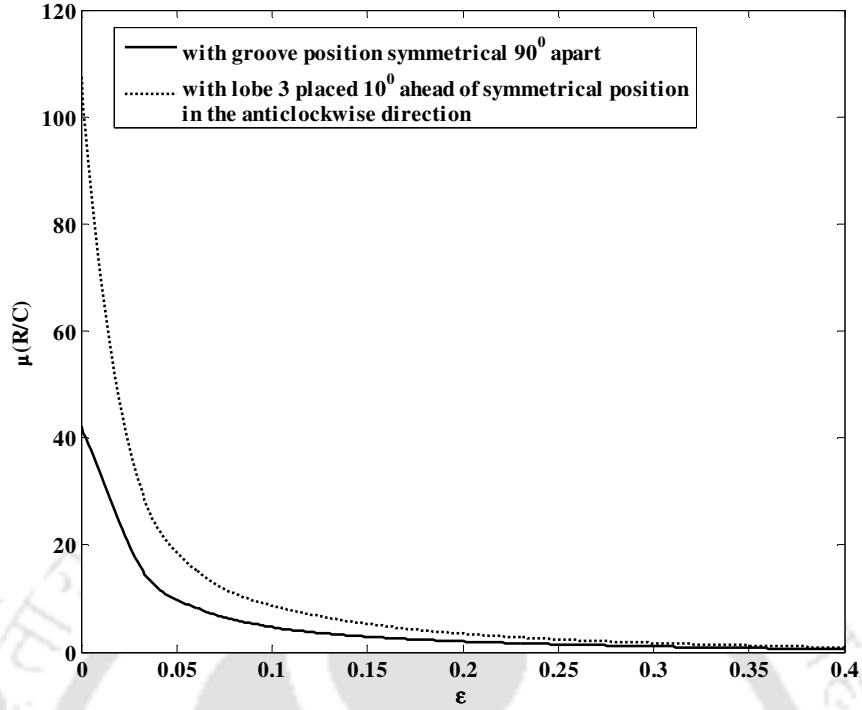

Figure 6.3: Variation of non dimensional friction variable with ε

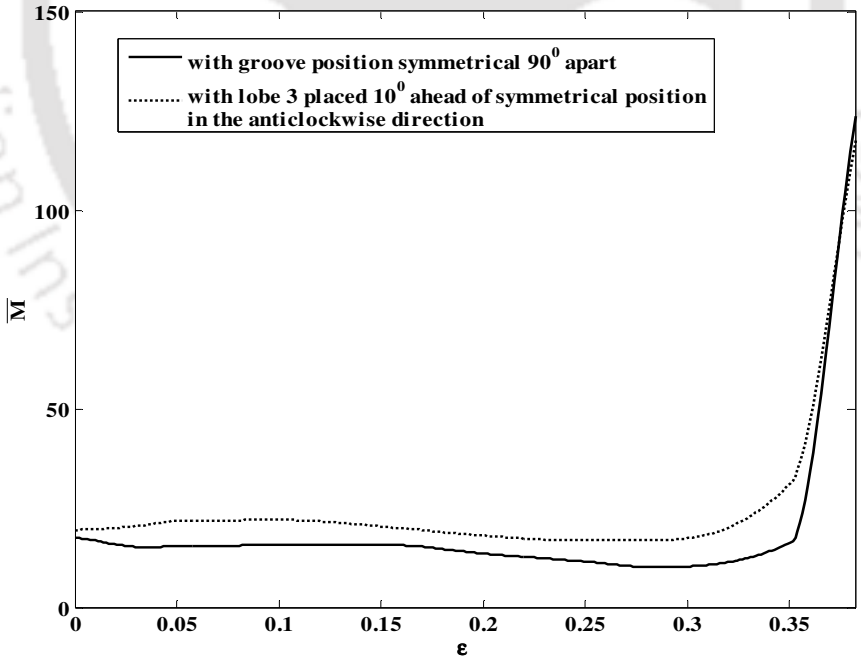

Figure 6.4: Variation of non dimensional mass parameter with ε

6.2.3 Determination of optimum location of groove

It has been shown in the previous section that the location of the groove have influence in flow ($\bar{q}_z$), frictional variable ($\bar{\mu}$), non-dimensional load capacity ($\bar{W}$) and mass parameter ($\bar{M}$). In view of this, an attempt has been made to locate the groove locations which correspond to optimum performances in terms of the four parameters mentioned above.

The objective functions and optimization technique are the same as for two-axial groove bearing. Genetic Algorithm (GA) has been used to find the optimum solution as outlined in Chapter 2. The problem is framed with four objectives. The variables used in the problem are starting angle of first groove (θ_1), starting angle of second groove (θ_2), starting angle of third groove (θ_3) and starting angle of fourth groove (θ_4) in Case –I. The optimum configurations have been obtained for eccentricity ratio ranging from 0.05 to 0.375 in this case. In Case –II, the eccentricity ratio (ε), starting angle of first groove (θ_1), starting angle of second groove (θ_2), starting angle of third groove (θ_3) and starting angle of fourth groove (θ_4) are variables and act as Chromosome. The objectives are minimization of friction variable, $\bar{\mu}$ (Eqn. 2.22), maximization of non-dimensional load capacity, $\bar{W}$ (Eqn. 2.20), maximization of flow coefficient $\bar{q}_z$ (Eqn 2.21), maximization of mass parameter, $\bar{M}$ (Eqn. 2.31). Objective function framing is the same for both the cases and variable bounds are shown in Table 6.3.

Table 6.3: Variable bounds for the bearing problem

Case	Variable	Lower	Upper
I	Starting angle of first groove(θ_1)	10°	65°
	Starting angle of second groove (θ_2)	95°	160°
	Starting angle of third groove(θ_3)	190°	250°
	Starting angle of fourth groove(θ_4)	280°	340°
II	ε	0.05	0.375
	Starting angle of first groove(θ_1)	10°	65°
	Starting angle of second groove (θ_2)	95°	160°
	Starting angle of third groove(θ_3)	190°	250°
	Starting angle of fourth groove(θ_4)	280°	340°

Optimum groove locations for four-lobe bearings have been obtained using Genetic Algorithm (GA) toolbox of MatLab as it was done for two axial groove bearings in Chapter 3, Chapter 4 and Chapter 5. The obtained results from GA have been compared with the results

obtained using Sequential quadratic programming (SQP). The optimum value of fitness function obtained corresponding to maximization of flow coefficient has been tabulated for both GA and SQP in Table 6.4.

Table 6.4: Comparison of GA and SQP results

ε	Objective function value (Maximum flow coefficient)	
	GA results	SQP results
0.02	0.889	0.889
0.05	1.364	1.364
0.103	1.830	1.830
0.203	3.202	3.202
0.285	7.635	7.635
0.350	19.151	19.151
0.375	36.560	36.560

It has been observed that the results obtained using both the methods are exactly the same. Similarly maximum non-dimensional load capacity, minimum friction variable, maximum mass parameter values are also found to match for both the methods. However, GA has been used in this work for the same reason as stated in Chapter 3.

Initially a single objective function has been taken up. Here in case of four lobe bearing also a population size of 50, mutation probability of 0.1 and a cross over probability of 0.8 have been selected as discussed in case of two groove bearing in previous chapter. The optimum groove locations for minimum friction variable, non dimensional load capacity, non dimensional flow coefficient , mass parameter and combined objective function at different ε are shown in Figs. 6.5 through 6.9. θ_1 , θ_2, θ_3 and θ_4 are starting positions of first , second , third and fourth groove respectively in degrees.

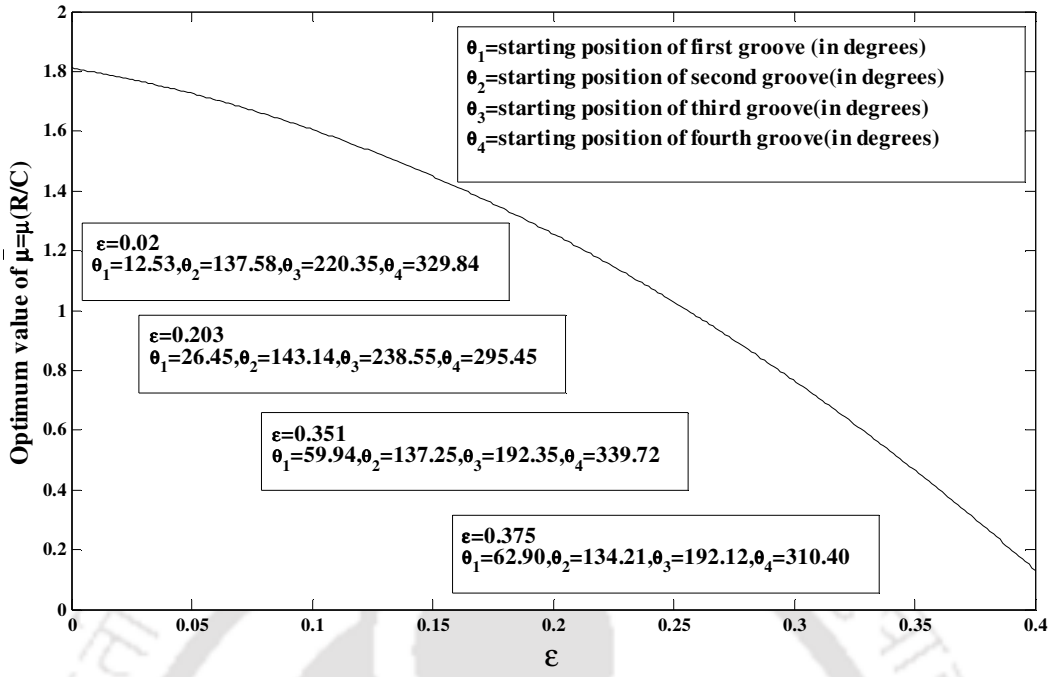

Figure 6.5: Variation of friction variable at optimum grooving location for different ε

It has been observed that the first groove location remain in the range (12.53^0 to 62.908^0), (11.42^0 to 64.455^0), (15.887^0 to 47.135^0) and (10^0 to 13.986^0) respectively when objective functions are friction variable, non-dimensional load capacity, flow coefficient, and mass parameter. However, the second groove location varies in the range of (134.214^0 to 143.142^0), (110.038^0 to 149.598^0), (147.479^0 to 160.247^0), (100.76^0 to 150.76^0) respectively when objective functions are friction variable, non-dimensional load capacity, flow coefficient, and mass parameter, the third groove location varies from (192.125^0 to 238.552^0), (198.071^0 to 281.432^0), (190.019^0 to 220.645^0) , (201.87^0 to 250^0) and the fourth groove location varies from (295.45^0 to 339.72^0), (294.148^0 to 337.64^0), (301.302^0 to 337.64^0) , (287.91^0 to 338.87^0).

The optimum groove locations for the multi-objective function (section 2.11) have been presented in Fig. 6.9. It has been observed that the first groove location varies in the range (10 to 62.01^0) , the second groove location varies in the range (96.89^o to 150.60^o) , the third groove location varies in varies in the range (200.09^0 to 240.10^0) and fourth groove location varies in varies in the range (280^0 to 334.50^0) in this case.

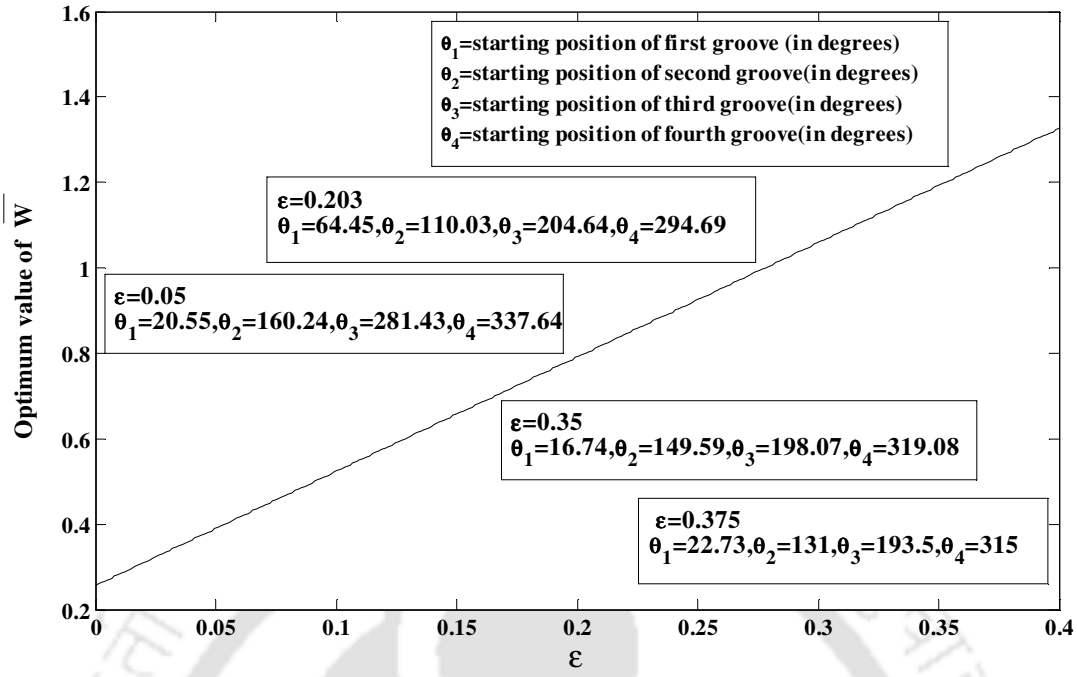

Figure 6.6: Variation of $\overline{W}$ at optimum grooving location for different ε

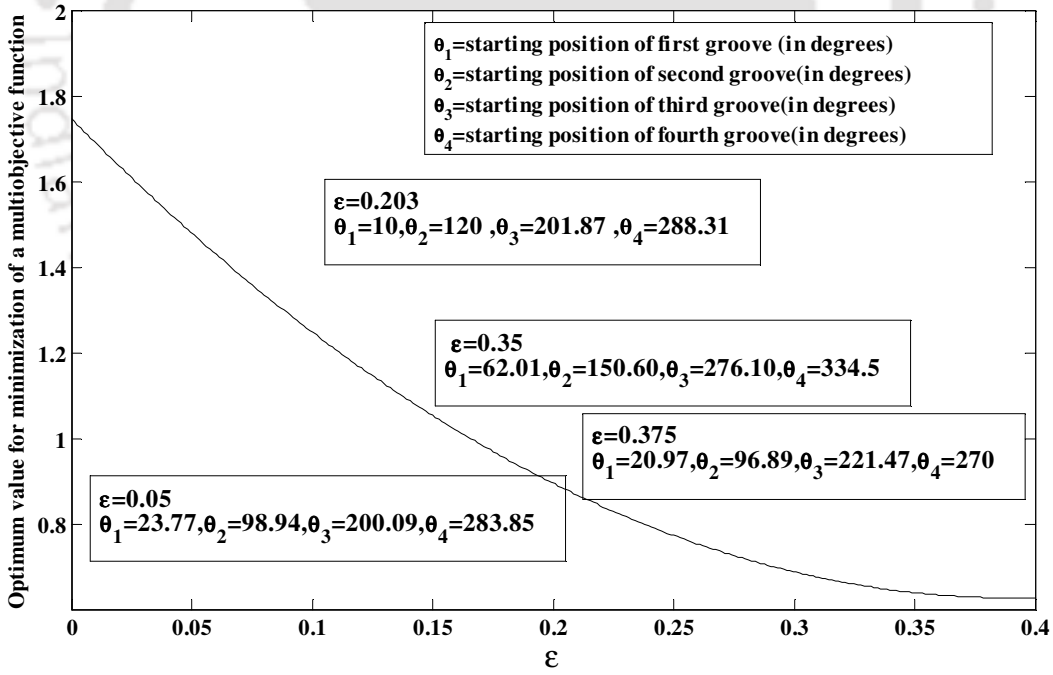

Figure 6.7: Variation of flow coefficient at optimum grooving location for different ε

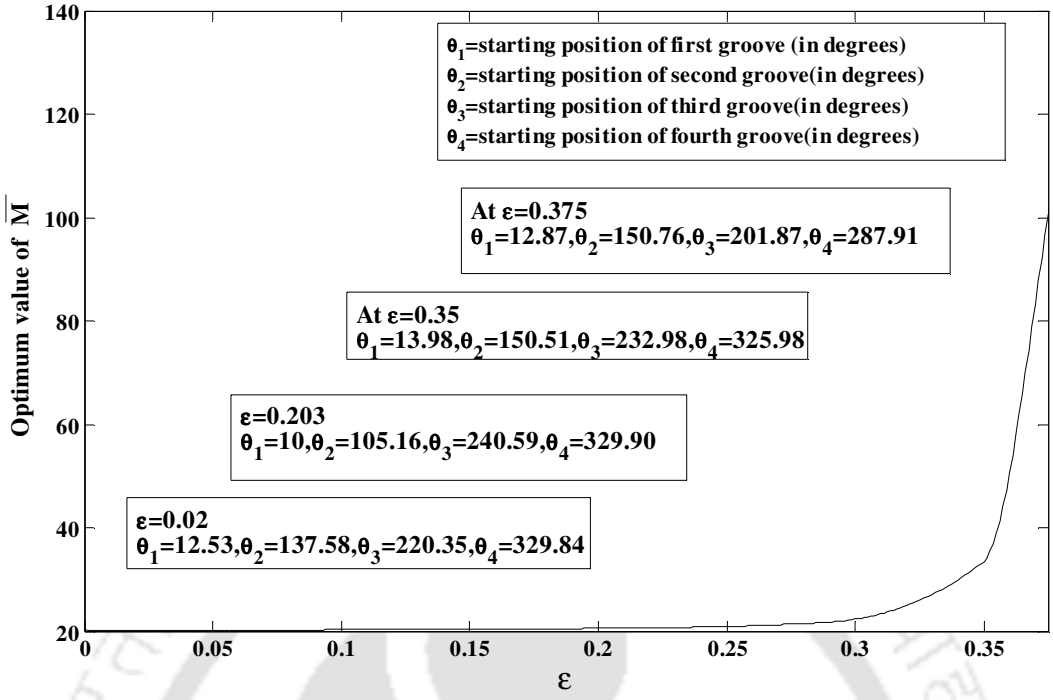

Figure 6.8: Variation of non dimensional mass parameter at optimum groove location for different ε

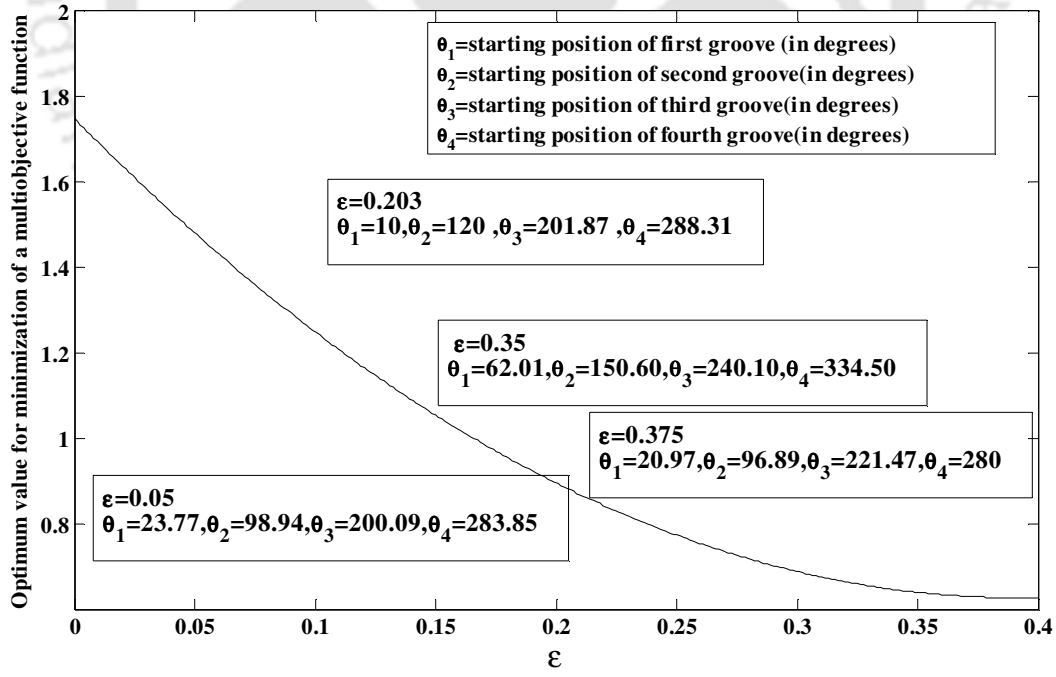

Figure 6.9: Optimum value obtained by minimization of a multi-objective function

From the results presented here, it can be inferred that the groove locations are sensitive to the type of objective function. The practice and the notion of convenience of keeping groove locations 90^o apart need to be thoroughly looked into as the present results show that optimum groove locations are not 90^o apart for the objective function considered in the present work. A Comparison of Optimum non-dimensional friction variable, flow coefficient, non-dimensional load capacity and mass parameter with groove location 90^0 apart has been made as shown in Tables 6.5 and 6.6. It is very much clear from the comparison that there is a significant improvement in the optimum value of friction variable, flow coefficient, non-dimensional load capacity and mass parameter value than that of four-lobe bearing with grooves location 90^0 apart.

In genetic algorithm, in each generation the fitness values of the objective function of the individuals is determined. These values express the fitness of the solutions of the new generations, one cycle of genetic algorithm called a generation. In each generation if the solution is improved, it is stored as the best solution. This is repeated till convergence.

When eccentricity ratio (ε), starting angle of first groove (θ_1), starting angle of second groove (θ_2), starting angle of third groove (θ_3) and starting angle of fourth groove (θ_4) are variables and acts as Chromosome as in Case –II, the optimum configuration for the same is presented in Table 6.7. The optimum results obtained for friction variable, flow coefficient, non-dimensional load capacity and mass parameter and for minimization of a multi-objective function are shown in Figures 6.10 through 6.14.

It has been observed from the results presented in Table 6.7 that the first groove location varies in the range (15^o to 57.68^o), the second groove location varies in varies in the range (100^0 to 150.77^0), the third groove location varies in varies in the range (210^0 to 245.89^0) and the fourth groove location varies in varies in the range (280.46^0 to 337.67^0). It has also been seen that optimum eccentricity ratios are different for different objective functions and it occurs at higher values for each objectives.

Table 6.5: Comparison of optimum friction variable and flow coefficient with friction variable and flow coefficient with groove position 90^0 apart and are symmetrically placed.

ε	Minimization of μ(R/C)	Corresponding Optimum location	Maximization of $\overline{q}_z$	Corresponding Optimum location
	Groove locations 90^0 apart(Optimum Configuration)		Groove locations 90^0 apart (Optimum Configuration)	
0.02	24.22 (1.981)	θ_1= 12.53	0.556(0.889)	θ_1= 29.27
		θ_2= 137.58		θ_2= 155.177
		θ_3= 220.35		θ_3= 220.645
		θ_4= 329.84		θ_4= 301.302
0.05	9.701 (1.46)	θ_1= 23.776	0.474(1.364)	θ_1= 23.776
		θ_2= 98.943		θ_2= 160.247
		θ_3= 200.09		θ_3= 281.432
		θ_4= 243.85		θ_4= 337.64
0.103	4.500 (1.98)	θ_1= 25.655	0.373(1.830)	θ_1= 15.887
		θ_2= 139.409		θ_2=155.925
		θ_3= 233.305		θ_3=212.85
		θ_4= 317.857		θ_4=312.358
0.203	1.925 (1.68)	θ_1= 26.457	0.276(3.202)	θ_1= 47.135
		θ_2= 143.142		θ_2= 157.459
		θ_3= 238.552		θ_3= 220.645
		θ_4= 295.45		θ_4= 324.673
0.285	1.141 (1.001)	θ_1= 67.23	0.241(7.635)	θ_1= 44.006
		θ_2= 94.804		θ_2= 159.341
		θ_3= 244.085		θ_3=195.331
		θ_4= 337.77		θ_4=325.40
0.35	0.767 (0.707)	θ_1= 59.945	0.218(19.151)	θ_1= 41.523
		θ_2= 137.25		θ_2= 147.479
		θ_3= 192.351		θ_3= 192.72
		θ_4= 339.72		θ_4= 307.75
0.375	0.667(0.231)	θ_1= 62.908	0.211(36.56)	θ_1=35.156
		θ_2= 134.214		θ_2=147.88
		θ_3= 192.125		θ_3=190.019
		θ_4= 310.407		θ_4= 316.621

6.2.4 Determination of near to the optimum location of groove

It has been observed that the optimum groove locations are different for different loading condition (eccentricity ratio) as well as for different objective functions in case of two and three-lobe bearing. The same was observed for two-axial groove bearings and therefore, 'near to the

optimum configurations' were identified. Therefore, it has been decided to identify 'near to the optimum configurations' for four-lobe bearings for different objective functions following the same procedure outlined in Chapter 2. The results are presented in Table 6.8 and also in Figures 6.15 through 6.19.

Table 6.6: Comparison of optimum non dimensional load and mass parameter with non dimensional load and mass parameter with groove position 90^0 apart and are symmetrically placed.

ε	Maximization of $\overline{W}$	Corresponding Optimum	Maximization of $\bar{M}$	Corresponding Optimum location
	Groove locations 90^0 apart (Optimum Configuration)		Groove locations 90^0 apart (Optimum Configuration)	
0.02	0.013 (0.016)	θ_1= 20.55	18.50 (20.010)	θ_1= 12.539
		θ_2= 160.24		θ_2= 137.581
		θ_3= 281.432		θ_3= 220.357
		θ_4= 337.64		θ_4= 329.848
0.05	0.033 (0.146)	θ_1= 67.115	18.46 (20.014)	θ_1= 10.220
		θ_2= 114.2		θ_2= 115.16
		θ_3= 197.91		θ_3= 220.59
		θ_4= 302.93		θ_4= 310.43
0.103	0.072 (1.041)	θ_1= 64.455	19.58 (20.301)	θ_1= 12.014
		θ_2= 110.038		θ_2= 108.16
		θ_3= 204.646		θ_3= 243.59
		θ_4= 294.692		θ_4= 320.9
0.203	0.171 (1.074)	θ_1= 54.961	19.94 (20.543)	θ_1= 10
		θ_2= 95.392		θ_2= 105.16
		θ_3= 206.232		θ_3= 240.59
		θ_4= 326.905		θ_4= 329.9
0.285	0.325 (1.081)	θ_1= 26.105	16.858 (21.554)	θ_1= 13.014
		θ_2= 109.894		θ_2= 100.76
		θ_3= 245.202		θ_3=250
		θ_4= 291.439		θ_4= 338.87
0.350	0.608(1.097)	θ_1= 16.747	31.78 (33.50)	θ_1= 13.986
		θ_2= 149.598		θ_2= 150.51
		θ_3= 198.071		θ_3= 232.98
		θ_4= 319.081		θ_4= 325.98
0.375	0.792(1.114)	θ_1= 11.42	95.49 (101.06)	θ_1= 12.876
		θ_2= 152.77		θ_2= 150.76
		θ_3= 213.61		θ_3= 201.87
		θ_4= 294.148		θ_4= 287.91

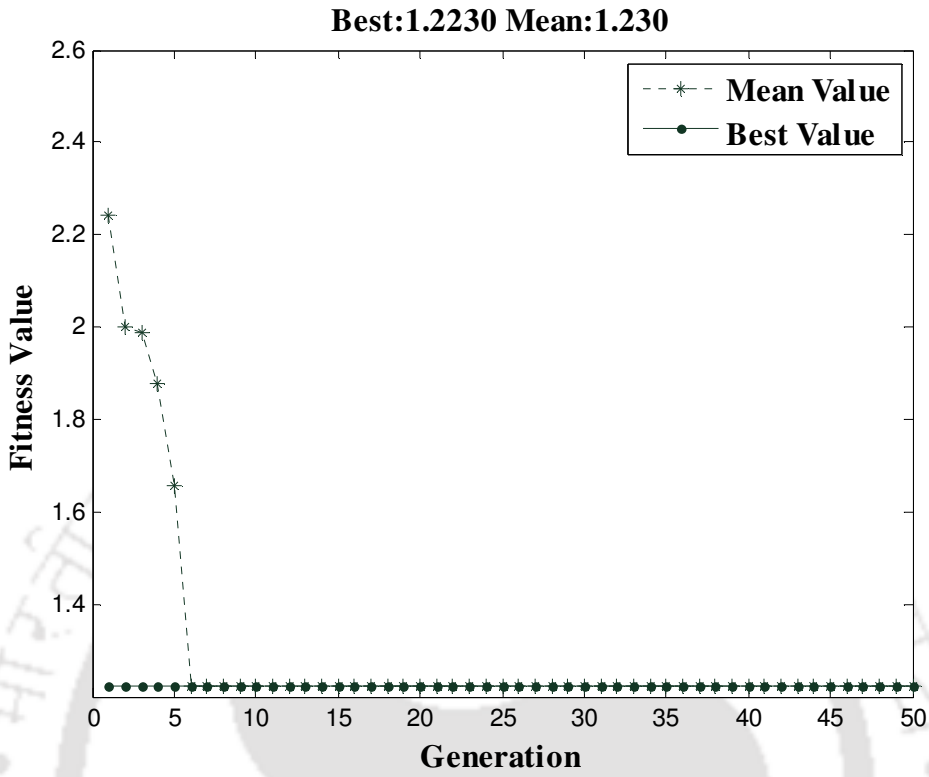

Figure 6.10:Fitness value considering friction variable as objective function

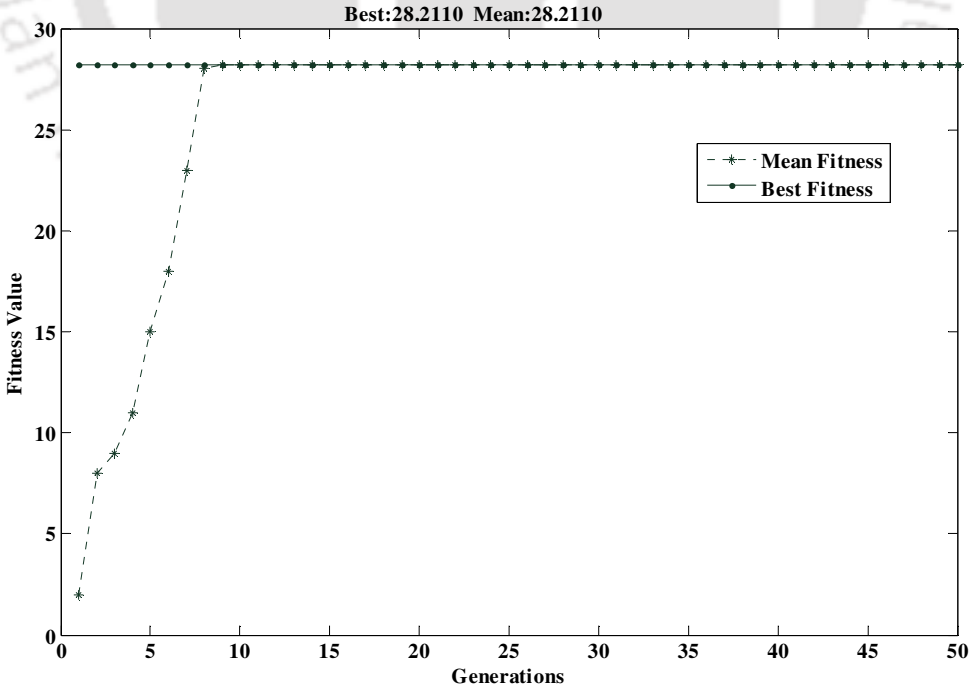

Figure 6.11: Fitness value considering flow coefficient as objective function

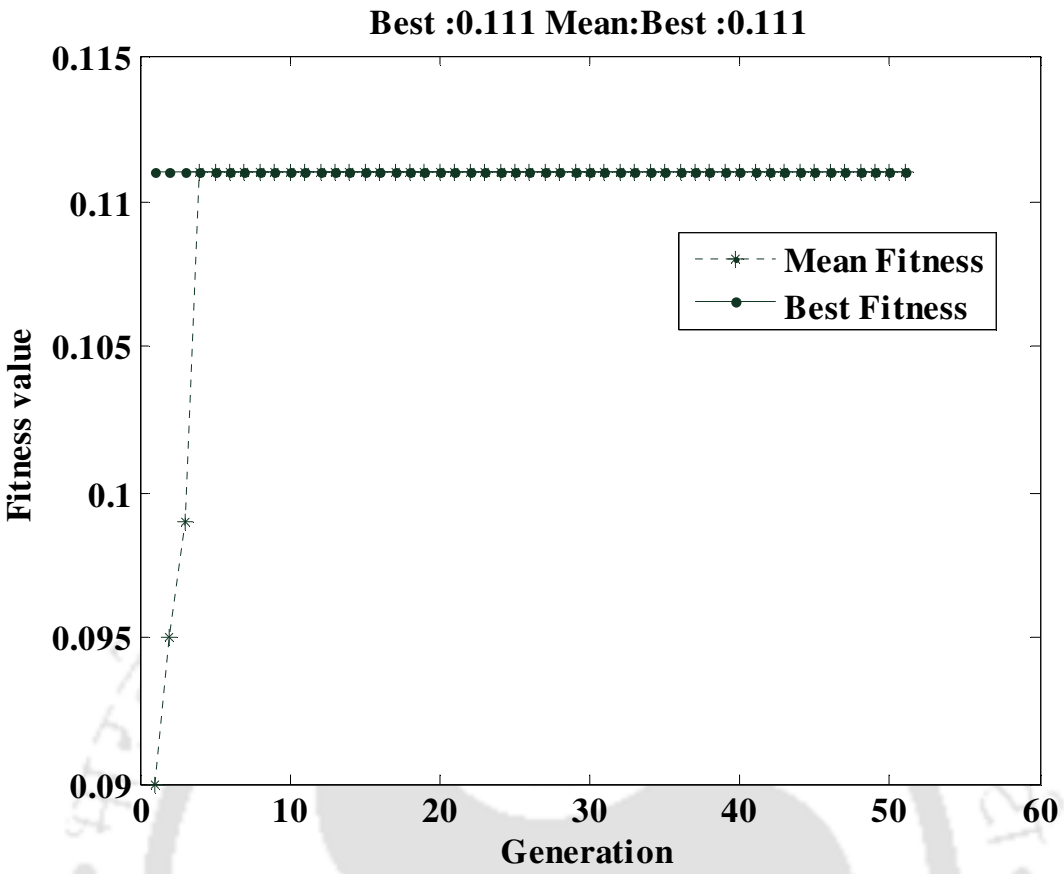

Figure 6.12: Fitness value considering load as objective function

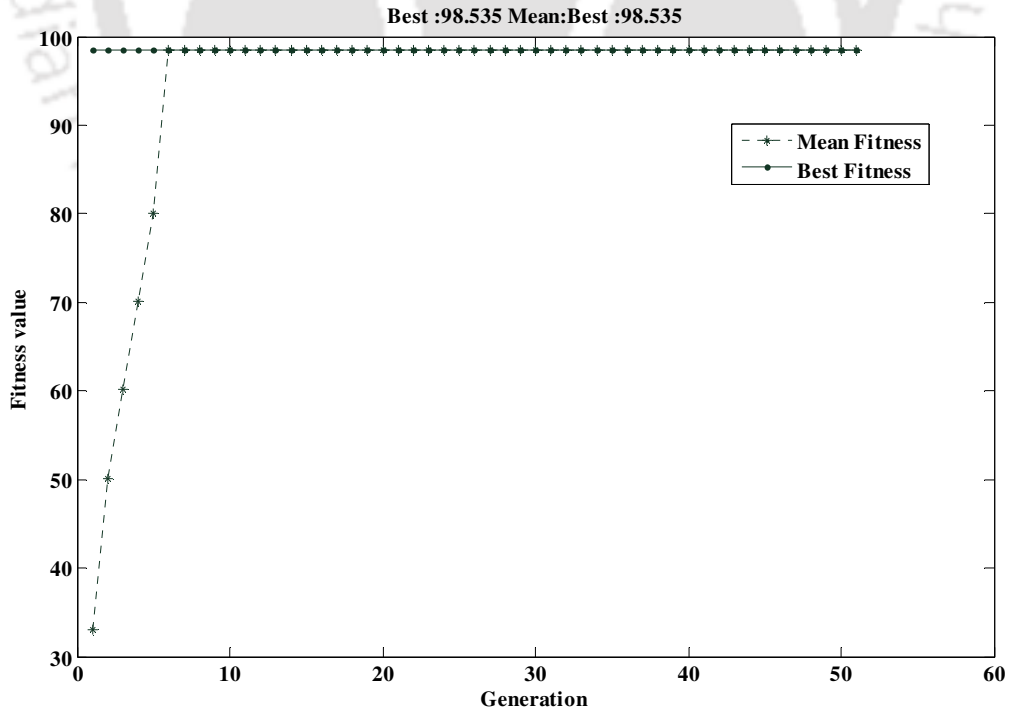

Figure 6.13: Fitness value considering mass parameter as objective function

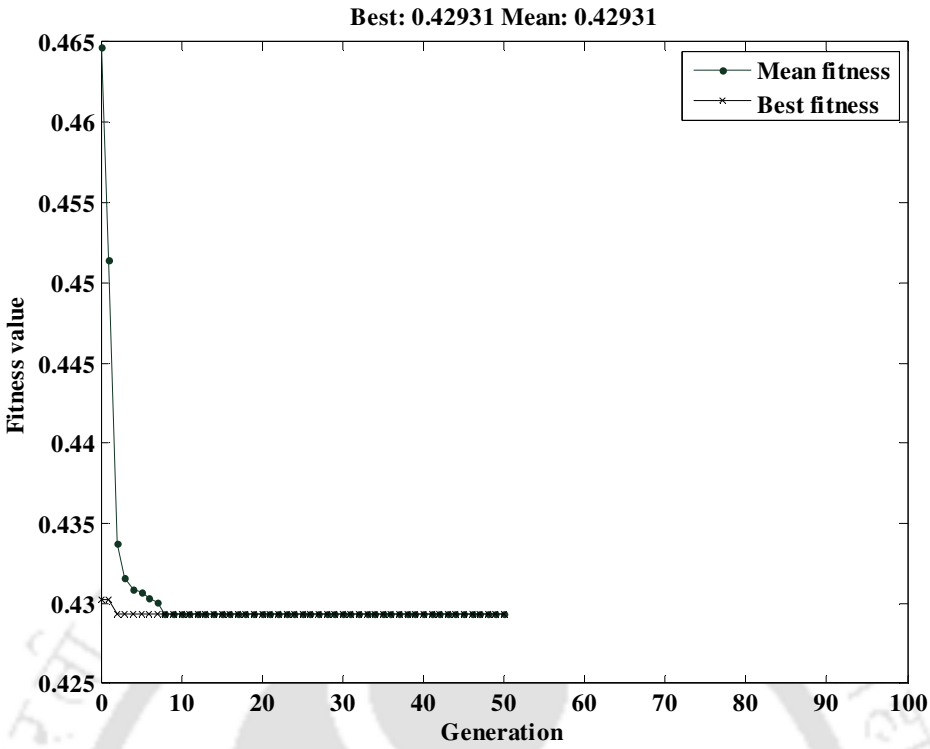

Figure 6.14: Fitness value obtained by minimization of a multi-objective function

Table 6.7: Optimum groove location with different objectives as in Case - II

Objective function	ε	θ_1	θ_2	θ_3	θ_4
Minimization of friction variable	0.325	30.98	143.832	205.065	314.129
Maximization of flow coefficient	0.375	34.204	145.733	210.46	336.71
Maximization of load	0.353	57.68	101.539	201.247	280.469
Maximization of mass parameter	0.375	15.876	150.77	245.898	337.677
Optimization of all the combined objectives	0.350	15	100	210	320.098

Table 6.8: Near to the optimum configuration for different objectives

Objective function	θ_1	θ_2	θ_3	θ_4
Minimization of friction variable	26	143	239	295
Maximization of flow coefficient	15	155	213	312
Maximization of load	64	110	205	295
Maximization of mass parameter	10	115	220	310
Minimization of multi-objective function	10	120	210	288

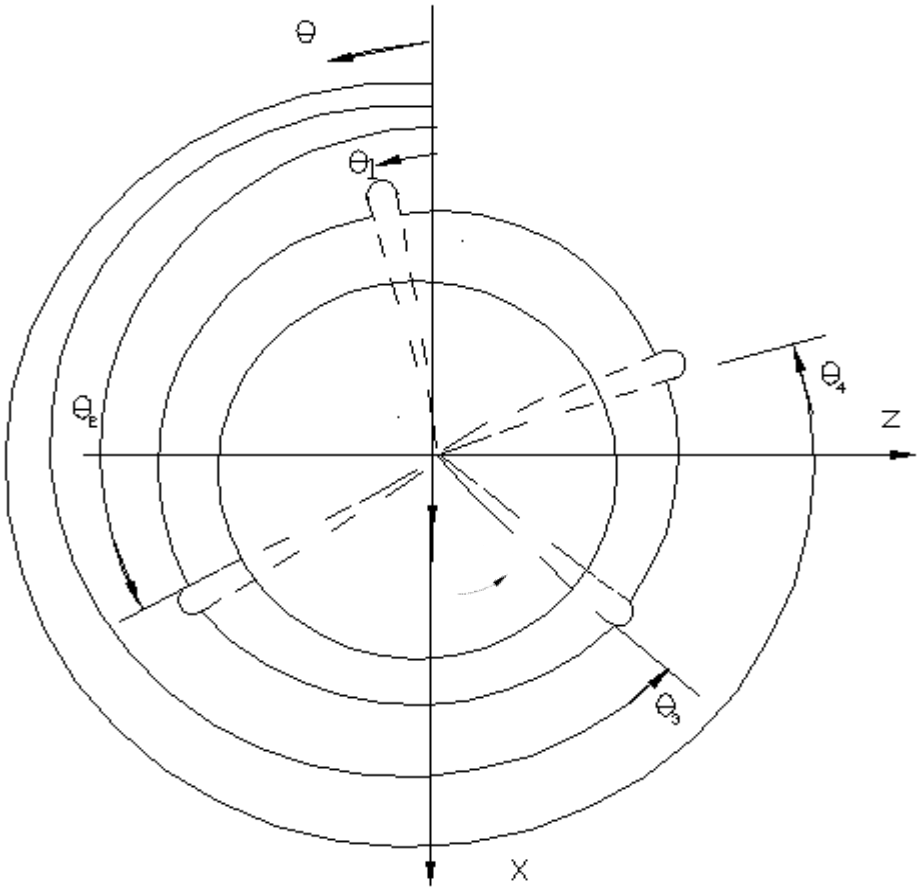

Figure 6.15: Near to the optimum configuration for minimization of friction variable

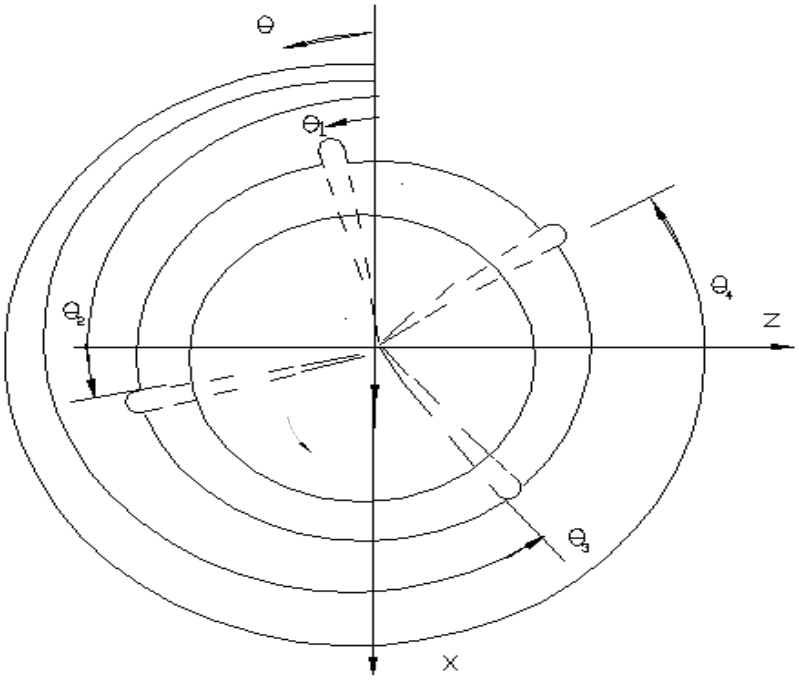

Figure 6.16: Near to the optimum configuration for maximization of flow coefficient

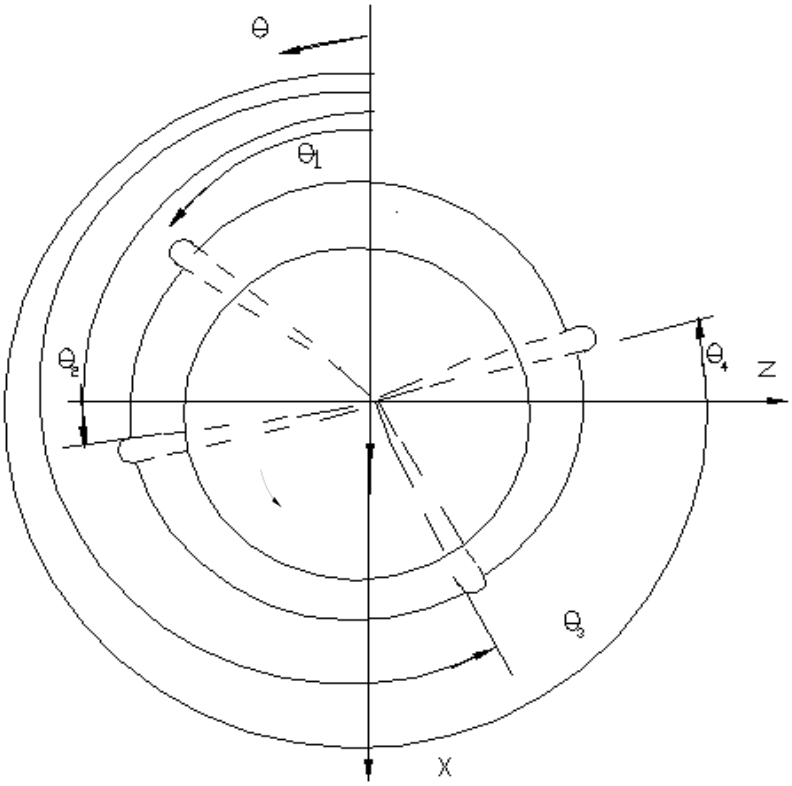

Figure 6.17: Near to the optimum configuration for maximization of non dimensional load

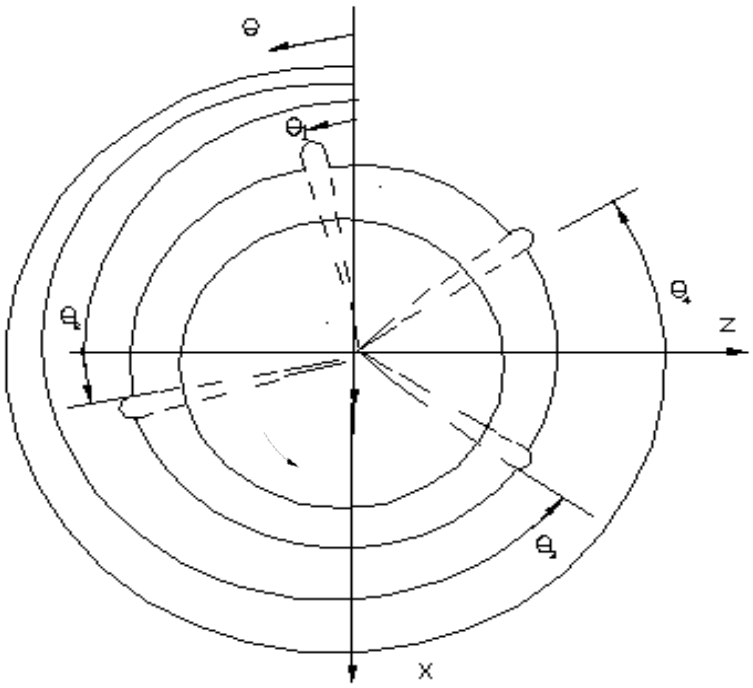

Figure 6.18: Near to the optimum configuration for maximization mass parameter

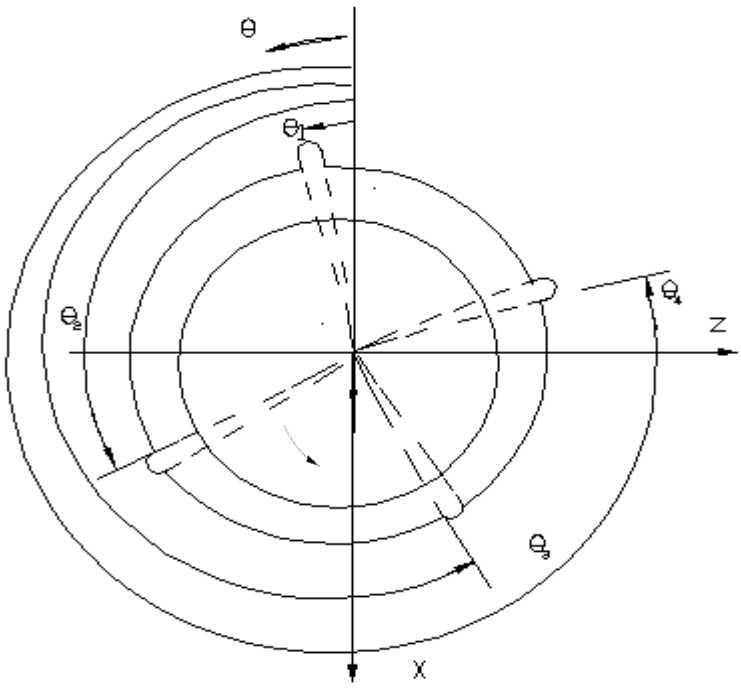

Figure 6.19: Near to the optimum configuration for minimization of multi-objective function

6.3 Summary:

In the present chapter, analysis (both steady state and dynamic) of four-lobe bearings is performed. The optimum groove locations for different objective functions, viz., maximization of non-dimensional load capacity, flow coefficient and mass parameter and minimization of friction variable have been obtained with the help of Genetic Algorithm (GA) toolbox of MatLab. It is observed that the optimum groove locations correspond to significant performance enhancement of four-lobe bearing. It has been found that the optimum groove locations are not only different for different objective functions but also different for different eccentricity ratios, *vis-a-vis*, loading conditions. The same observation was also made in case of two axial groove two-lobe bearing and three-lobe bearing. Therefore, the identification of locations of grooves for four-lobe bearing has been obtained such that the performance characteristics are near to the optimum for any loading condition (eccentricity ratio) for different objective functions.

CHAPTER 7

Concluding Remarks

7.0 Introduction

The thesis deals with the analysis and study on the effect of different groove locations on various design parameters like friction variable, flow rate, load carrying capacity and mass parameter and to optimize the groove locations of two groove , two lobe, three lobe and four lobe bearings with single and multi objective functions. Based on the literature review presented in Chapter 1, the scope of the present work has been drawn. It is noteworthy that the most of the investigations carried out earlier were on some particular configuration of bearings only. It was indicated by Malik et.al. [31] that some optimum bearing configurations may be derived from more detailed studies of non-circular bearing configurations. However, there was no attempt made to find out the optimum groove locations for better performance of the bearings.

The basic equations and the mathematical formulation in the hydrodynamic theory of lubrication is discussed in Chapter 2. Some preliminary theory of genetic algorithm is discussed in the same chapter. The analysis of two groove bearing and optimization of the groove locations of two groove bearings with single and multi objective functions have been presented in Chapter 3. Determination of groove locations for near to optimum performance characteristics for two-groove bearing is also included in the same Chapter. Following chapters, *i.e.*, Chapter 4, Chapter 5 and Chapter 6, deal the same issues for two-lobe, three-lobe and four-lobe bearings respectively.

A comparison of optimum results obtained for friction variable, flow coefficient, non-dimensional load capacity and mass parameter for two lobe, three-lobe and four-lobe bearings at different eccentricity ratios are shown in Table 7.1 and also in Figs. 7.1 through 7.12

Table 7.1 : Comparison of optimum performance parameter for two lobe, three-lobe and four-lobe bearings at different eccentricity ratios

ε	μ(R/C) (Two lobe) {Three lobe} [Four lobe]	$\overline{q}_z$ (Two lobe) {Three lobe} [Four lobe]	$\overline{W}$ (Two lobe) {Three lobe} [Four lobe]	$\overline{M}$ (Two lobe) {Three lobe} [Four lobe]
0.050	(0.031) {1.9813} [1.710]	(7.0472) {1.352} [1.364]	(0.167) {0.084} [0.146]	(19.400) {22.55} [20.014]
0.100	(0.036) { 1.975} [1.681]	(7.9675) {2.976} [1.803]	(0.205) {0.691} [0.597]	(20.400) {22.62} [20.22]
0.150	(0.032) {1.966} [1.449]	(6.4145) {2.989} [1.993]	(0.252) {0.719} (0.698]	(20.543) {23.01} [20.41]
0.200	(0.039) {1.933} [1. 631]	(5.9923) {2.750} [3.158]	(0.273) {0.871} [0.798]	(20.700) {23.35} [20.53]
0.239	(0.039) {1.416} [1.08]	(5.569) {2.656} [4.081]	(0.329) {0.981} [0.896]	(20.998) {23.71} [20.80]
0.250	(0.032) {1.334} [1.028]	(5.686) {2.686} [4.406]	(0.334) {1.008} [0.921]	(21.098) {23.83} [20.93]
0.260	(0.039) {1.269} [0.981]	(6.3981) {2.729} [4.791]	(0.368) {1.039} [0.950]	(21.630) {23.93} [21.08]
0.304	(0.038) {0.961} [0.744]	(6.853) {2.899} [9.095]	(0.556) {1.165} [1.072]	(22.450) {24.09} [22.77]
0.350	(0.039) {0.817} [0.78]	(12.506) {3.497} [19.151]	(0.7190) {1.309} [1.097]	(26.345) {28.62} [33.47]
0.381	(0.039) {0.244} [0.297]	(18.010) {3.121} [30.15]	(0.9151) {1.402} [1.237]	(28.425) {96.74} [101.1]
0.451	(0.005) {0.139} [0.198]	(49.101) {3.601} [47.63]	(2.370) {1.631} [1.326]	(81.260) {265.9} [201.2]

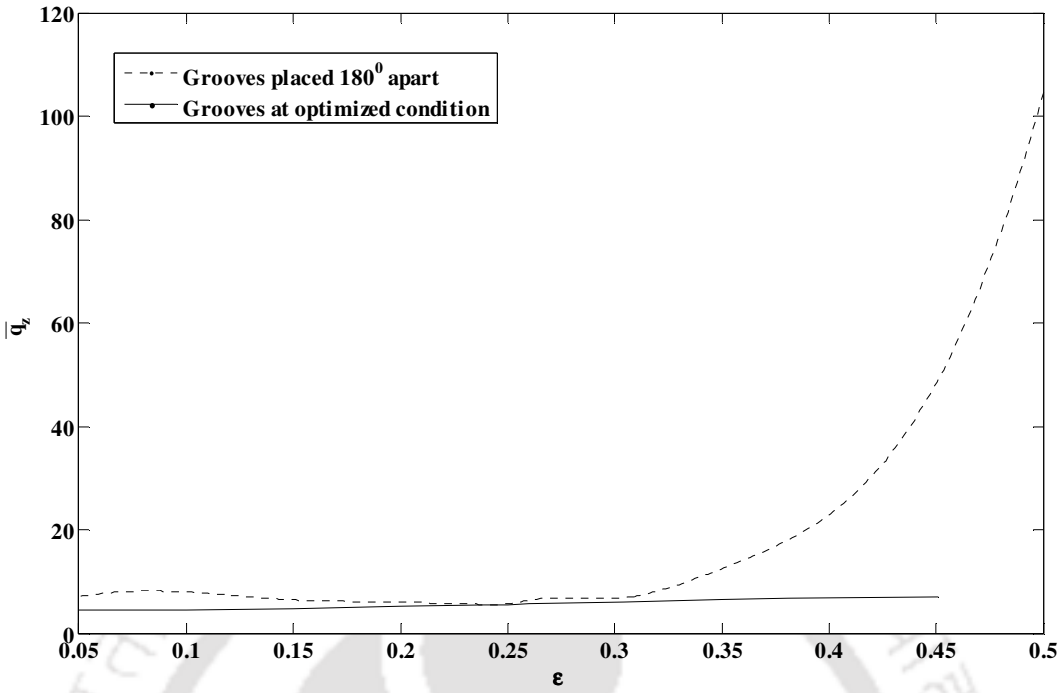

Figure 7.1. Comparison of flow coefficient for two bearing configurations

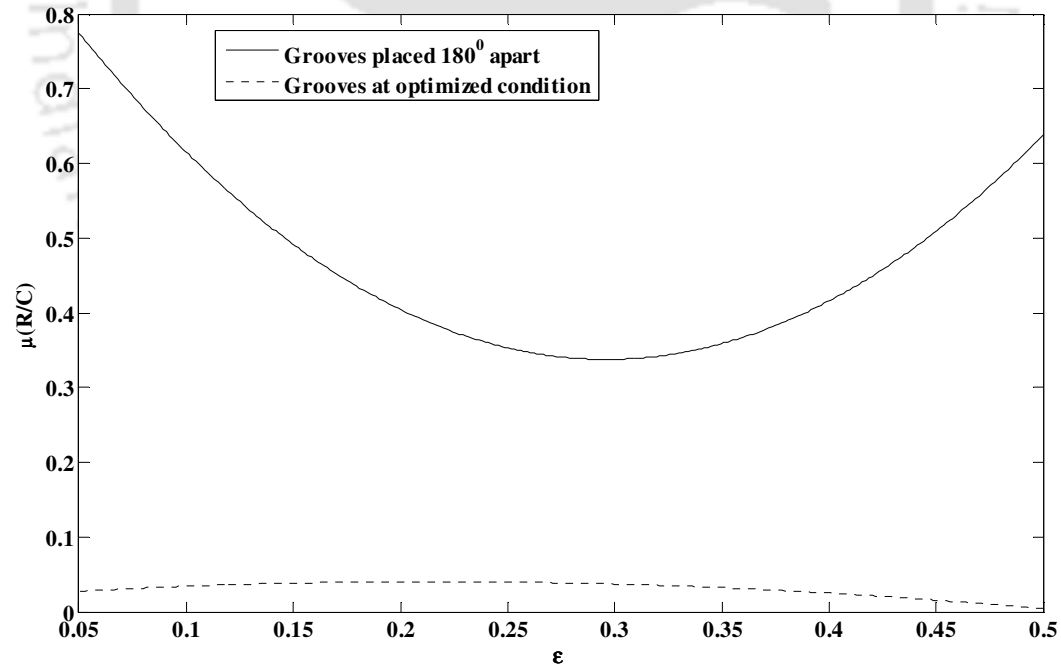

Figure 7.2. Comparison of friction coefficient for two bearing configurations

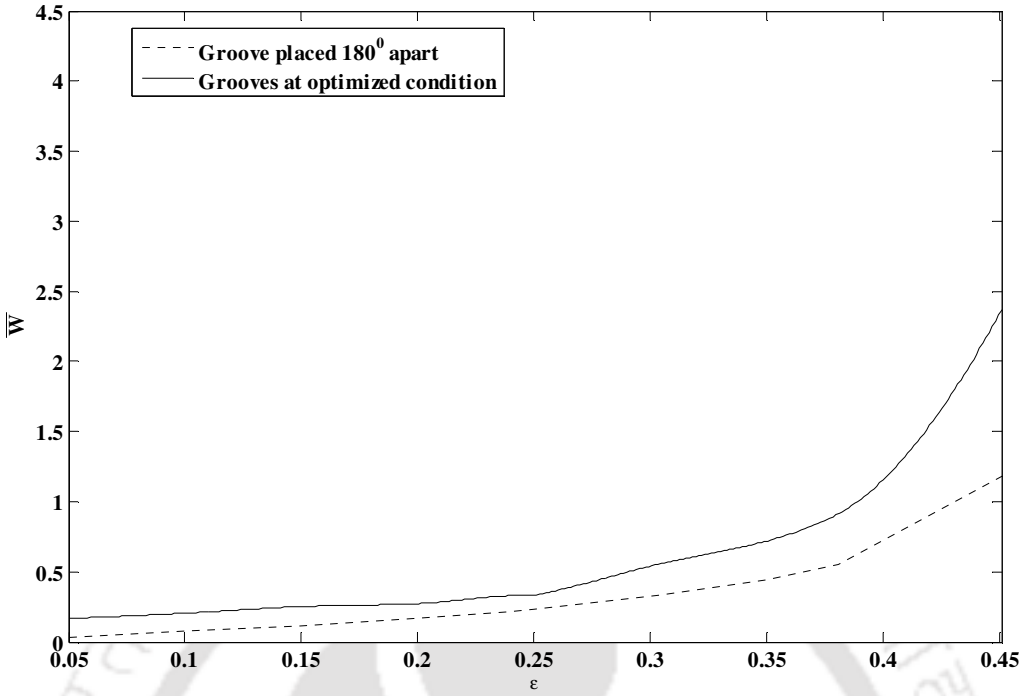

Figure 7.3. Comparison of non dimensional load capacity for two bearing configurations

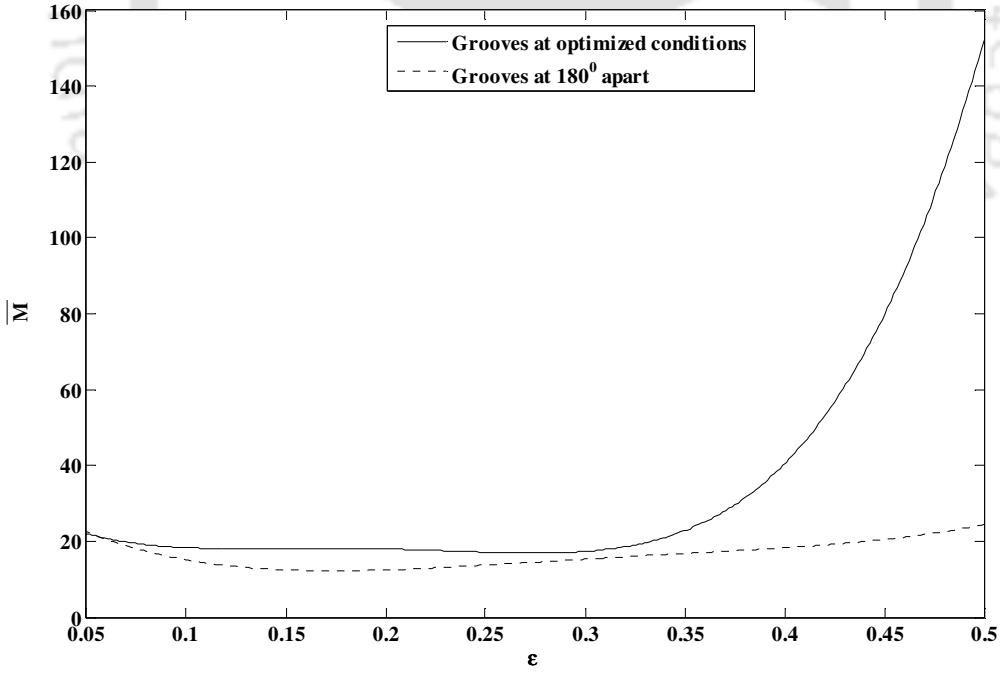

Figure 7.4. Comparison of mass parameter for two bearing configurations

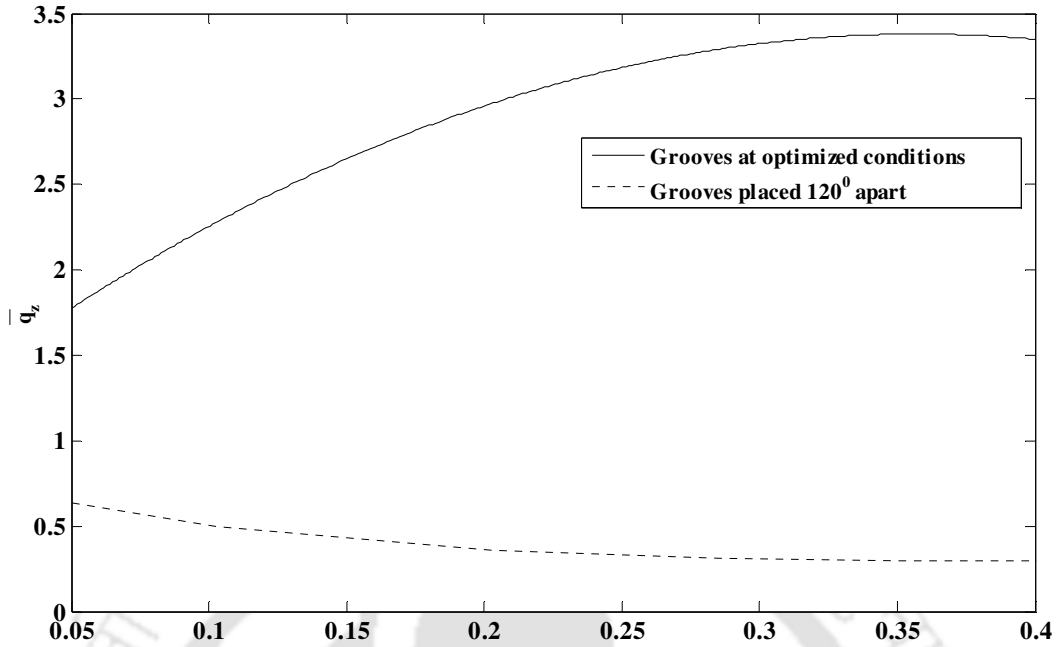

Figure 7.5. Comparison of flow coefficient for three lobe bearing configurations

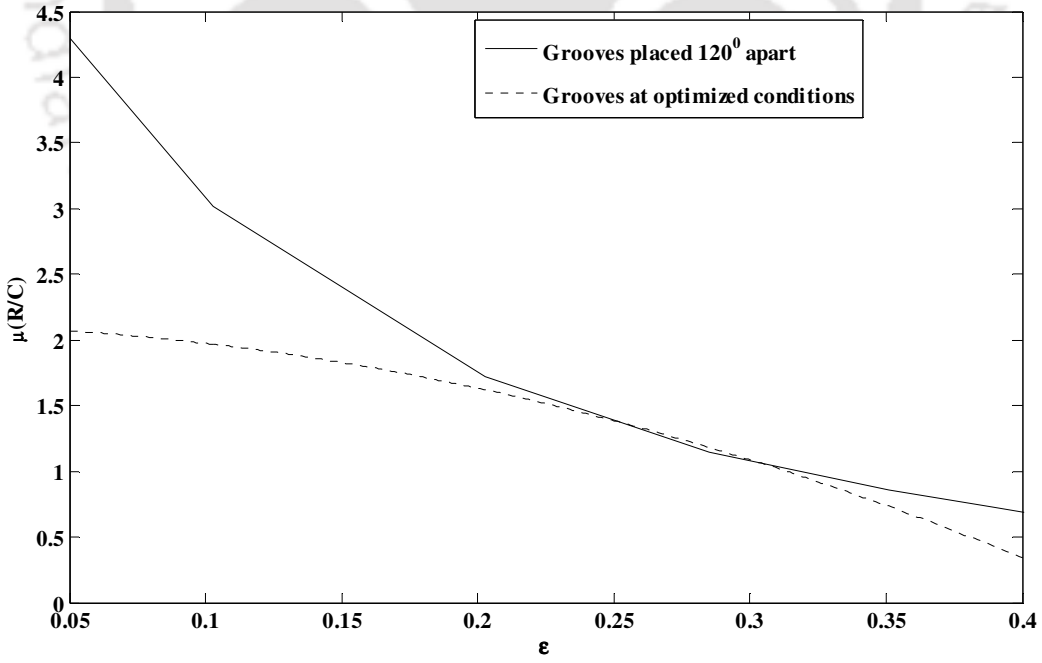

Figure 7.6. Comparison of friction coefficient for three lobe bearing configurations

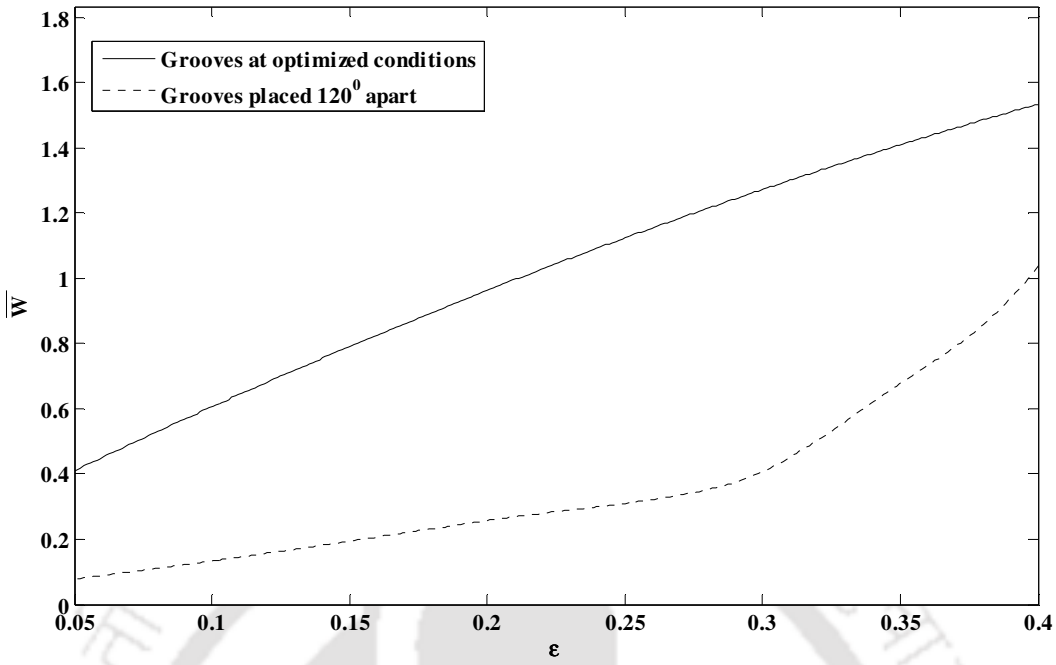

Figure 7.7. Comparison of non dimensional load capacity for three lobe bearing configurations

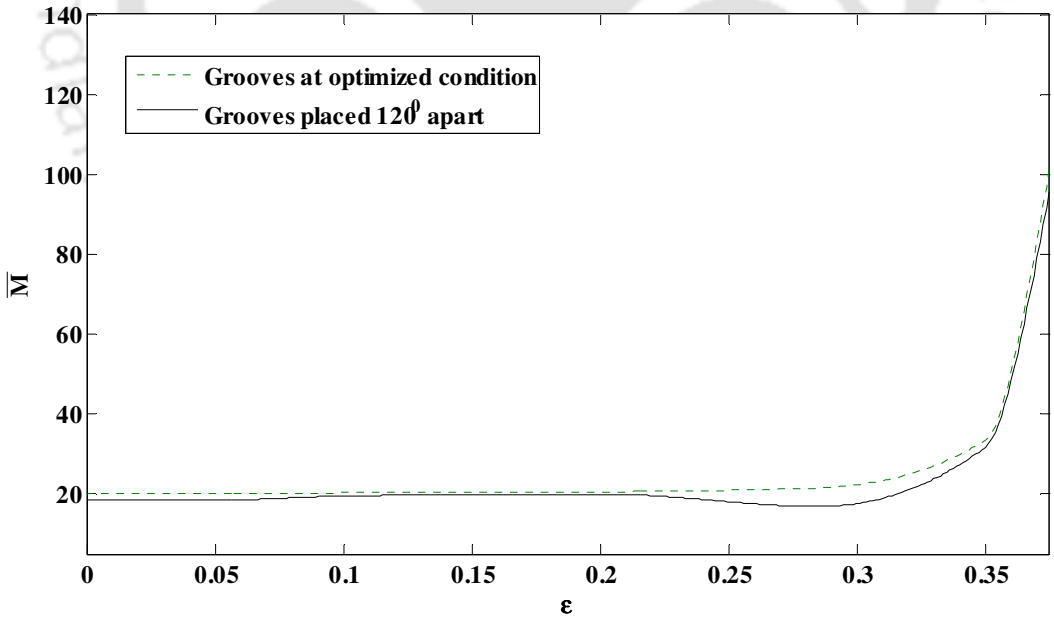

Figure 7.8. Comparison of mass parameter for three lobe bearing configurations

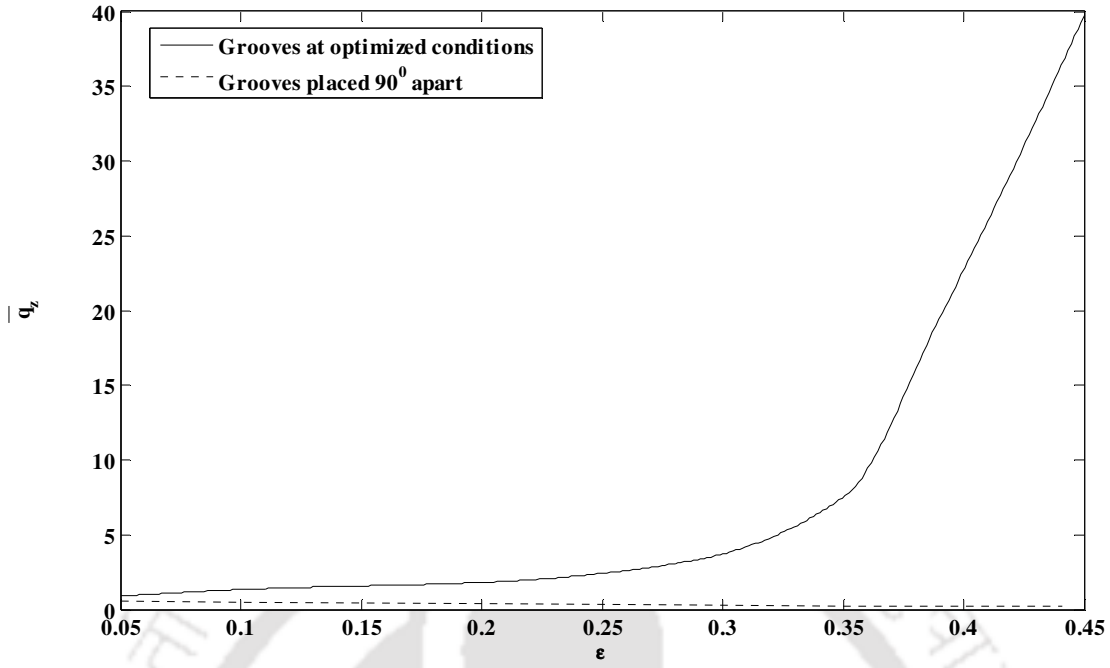

Figure 7.9 Comparison of flow coefficient for four lobe bearing configurations

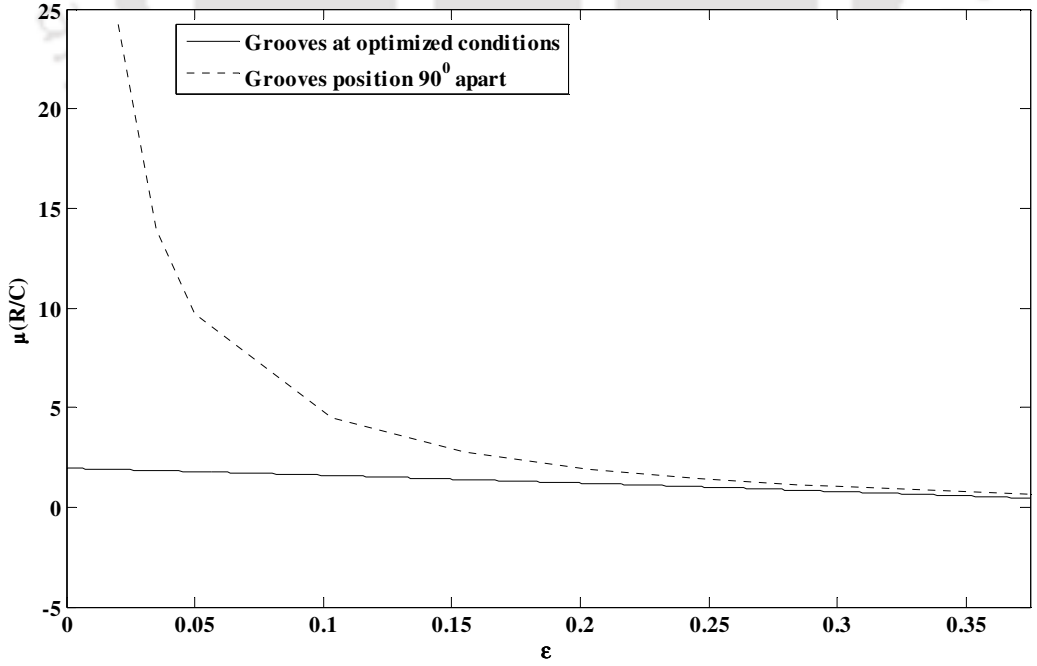

Figure 7.10. Comparison of friction coefficient for four lobe bearing configurations

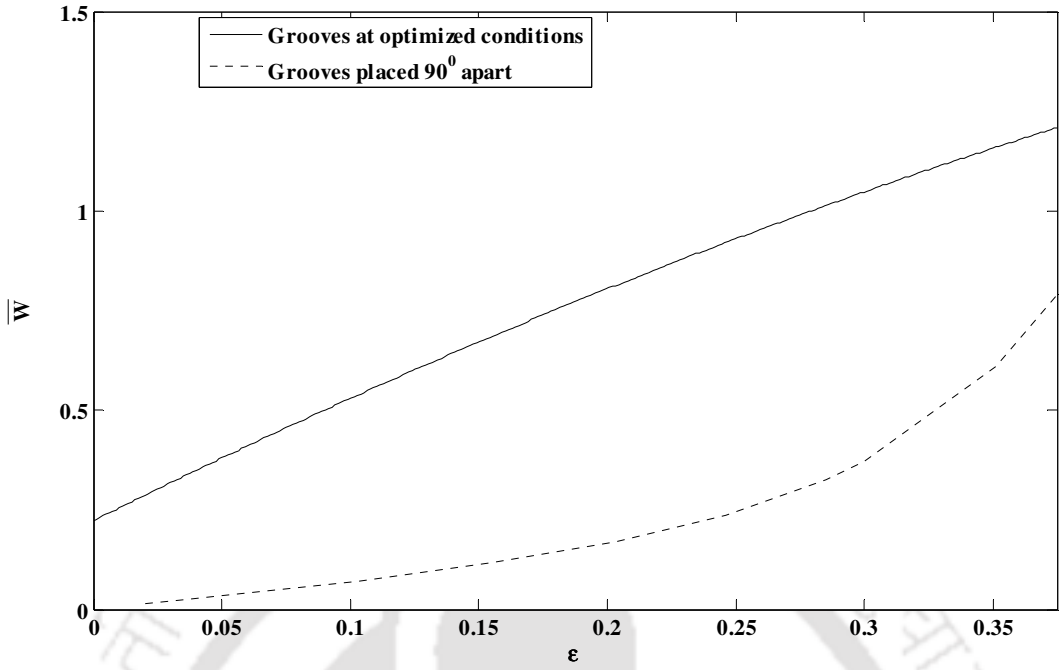

Figure 7.11. Comparison of non dimensional load capacity for four lobe bearing configurations

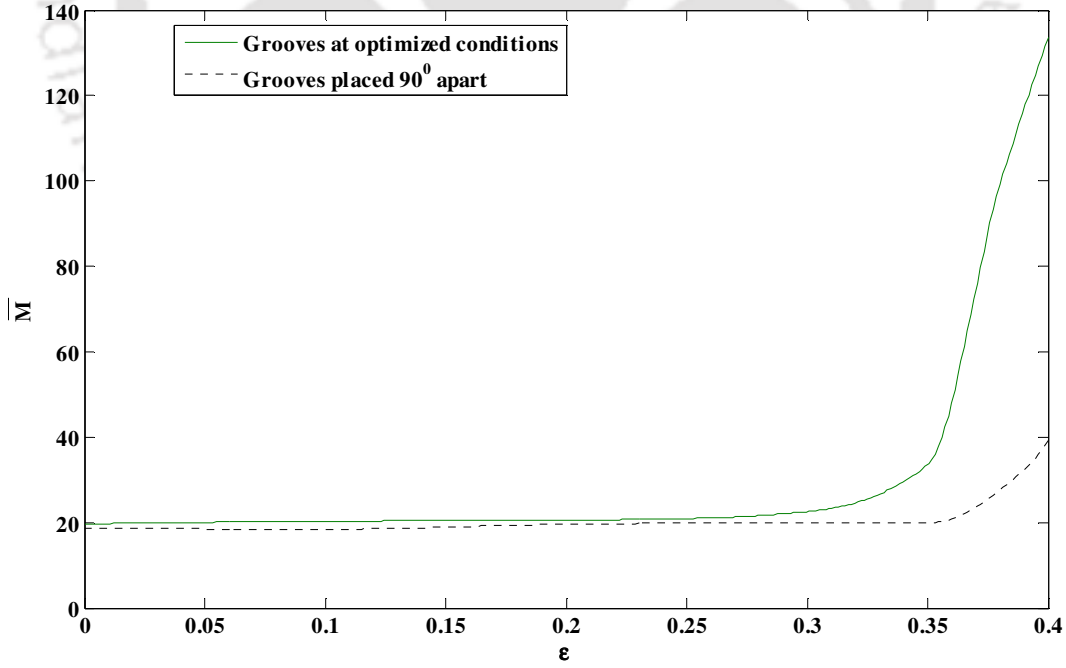

Figure 7.12. Comparison of mass parameter for four lobe bearing configurations

7.1 Concluding Remarks

Following inferences are made from the presented results in this thesis:

- In case of two groove and two lobe bearings the second groove locations are sensitive to the type of objective function whereas the first groove is more or less same for any objective function.

- In case of three-lobe bearings the second and third groove locations are sensitive to the type of objective function whereas the first groove is more or less the same.

- In case of four-lobe bearing the second, third groove and fourth groove locations are sensitive to the type of objective function whereas the first groove locations are more or less the same.

- In case of two groove and two-lobe journal bearing the optimum performance characteristics correspond to locations of both the grooves above the horizontal axis.
- In case of two groove bearing when the eccentricity ratio (ε), starting angle of first groove (θ_1), starting angle of second groove (θ_2) are variables and act as Chromosome, it has been observed that the eccentricity ratio at which optimum location occurs is on the higher side for all objective functions except for the combined objective.

- The optimum values of two groove bearings improve when compared with groove position in the horizontal direction 180^0 apart. At optimum position there is an improvement in the performance characteristics, e.g., friction variable, flow coefficient, non-dimensional load capacity and mass parameter values.

- The magnitude of flow coefficient is much higher at optimum groove position for two-lobe bearing in comparison to two groove bearing, three-lobe and four-lobe bearings.

- The magnitude of non dimensional friction variable is much lower for two lobe bearing in comparison to three-lobe and four-lobe bearings.

- Optimum value of mass parameter found to be the highest for four lobe bearing.

It has been pointed out in the concerning chapters that the optimum configurations are not only different for different objective functions, but also different for different loading condition, vis-a-vis, eccentricity ratio. The operators will be confused as to which bearing

configuration should be used when there is a variation of load during operation. Many a time the bearings are selected for better frictional property or flow property or stability. Therefore, near-to-optimum configurations ensuring better, if not the best, performance of the bearings are suggested for all the four types of bearings. This will definitely help the designers as well as the operators in deciding the bearing configuration with focus to the particular bearing performance parameter from among non-dimensional load, flow coefficient, friction variable, mass parameter or combination of all the four parameters based upon the priority to performance parameter.

The optimal configurations for all four bearings are found to have unequal bearing arcs of different lobe and the first groove is more or less located at the load line. The physics behind this can only be ascertained when further studies of film thickness profile and pressure profile are carried out in detail.

7.2 Scope for Future Works

- In this analysis the parameters like speed, oil feed flow rate, pressure & temperature were not considered. The other equally important factors like temperature rise of lubricant, oil feed flow and power loss may be incorporated in future for more realistic parametric study.
- Geometry of the groove can be incorporated in the list of Chromosomes to find out the optimum groove geometry and optimum location. Also different groove size can be considered in the analysis.
- Experimental investigation is very much necessary to show the validity of the presented theoretical predictions. From the practical point of view, it is easier to machine a two axial groove or a two lobe bearing when the grooves are situated in a horizontal plane. However, to enhance the performance of the bearings, some manufacturing considerations would be required to position the grooves in locations other than the currently practised ones. This issue may be of interest for the bearing manufacturers and R&D inputs in this regard may be required to achieve it.
- Other optimization techniques like NSGA-II, Particle Swarm Optimization can be applied to the same problem.

7.3 Summary

An attempt has been made in this thesis to study and analyze four commonly used bearing configurations, viz, two axial groove bearings, two-lobe bearing, three-lobe bearings and four-lobe bearings. The whole analysis is carried out in non dimensional form. An attempt has been made to find out the optimum groove locations of the bearing configurations depending on maximization of flow coefficient, non-dimensional load, mass-parameter and minimization of friction variable using Genetic Algorithm. Also a comparison of various performance characteristics of two-lobe, three-lobe and four-lobe bearings have been made with the current practice of groove locations of these bearings. It is hoped that the study presented here would be useful to correlate optimum design configuration. In view of the above, it may be concluded that the results generated using the above methodology for identifying the locations of grooves such that the performance characteristics are near to the optimum for any loading condition (eccentricity ratio) for any particular objective function would be much beneficial to manufacturers and designers.

References

[1] Raimondi A. and Boyd J., " A solution for the finite journal bearing and its application to analysis and design, Parts I, II, and III," 1958, Transactions of ASLE, 1(1), pp.159-209.

[2] Pinkus O and Sternlicht B., "Theory of hydrodynamic lubrication," 1961,McGraw-Hill, New York

[3] Dowson D., Taylor C. M., and Miranda A. A. S., "The prediction of liquid film journal bearing performance with a consideration of lubricant film reformation: Part 1: Theoretical results," 1985, Proceedings of the Institution of Mechanical Engineers, Part C: Journal of Mechanical Engineering Science, 199, pp. 95-102.

[4] Salamone D.J., "Journal bearing design types and their applications to turbomachinery," 1985, Proceedings of thirteenth Turbo machinery Symposium, pp.179-188

[5] Gethin D.T and Deihi M.K.I.EI., "Effect of loading direction on the performance of a twin-axial groove cylindrical bore bearing," 1987,Tribology International,20(4), pp.179-185.

[6] Chandrawat H. N. and Sinhasan R., "A comparison between two numerical techniques for hydrodynamic journal bearing problems,"1987,Wear,119, pp.77 – 87.

[7] Reynolds O., "On the theory of lubrication and its application to Mr. Beauchamps Tower's Experiments, including an experimental determination of the viscosity of olive oil," 1889,Phil. Trans. Roy. Soc. (London) A 177, pp.157–234.

[8] Claro J. C. P., Miranda A.A S., "The performance of journal bearings with a single axial groove," 1990, IMechE Seminar: Developments in Plain Bearings for 90's, pp.19-25.

[9] Vijayraghavan D., and Keith T.G., "Effect of type and location of oil groove on the performance of journal bearings," 1992, Tribology Transactions,35(1), pp. 98-106.

[10]Hirani H., Athre K., Biswas S.,"Dynamic Analysis of Engine Bearings,"1999, International Journal of Rotating Machinery, 5(4), pp.283-293.

[11] Cho M.R, Shin H. J, Han D.C., "A study on the circumferential groove effects on the minimum oil film thickness in engine bearings," 2000, KSME International Journal,14(7), pp.737- 743.

[12] Jang G.H.,"Stability analysis of a hydrodynamic journal bearing with rotating herringbone grooves," 2003, Journal of Tribology,125, pp. 291-300

[13] Costa L., Miranda A. S., Fillon M., and Claro J. C. P., 2003, "An Analysis of Oil Supply Conditions on The Thermohydrodynamic Performance of A Single-Groove Journal Bearing", Proc. Inst. Mech. Engrs., Vol. 217, Part J: J. Engg. Tribol., pp. 133-144.

[14] Brito F.P., Miranda A.S., Bouyer J. and Fillon M. "Experimental investigation of the influence of the supply temperature and supply pressure on the performance of a two axial groove hydrodynamic journal bearing" ASME Journal of Tribology, Vol 129 (2007), pp 98-105

[15] Naimi S., Chouchane M, Ligier J.L.,"Steady state analysis of a hydrodynamic short bearing supplied with a circumferential groove," 2010, Mecanique 338, pp. 338–349

[16] Pinkus O., "Analysis of elliptical bearing," 1956, Transaction of ASME, Journal of basic Engineering,78, pp. 965-973.

[17] Pinkus O.,"Power loss in elliptical and three lobe bearings,"1956, Transaction of ASME, 78, pp. 894- 904.

[18] Pinkus O., "Experimental investigation of resonant whip," 1956, Transaction of ASME, J.Appl. Mech.,78, pp. 975–983.

[19] Singh D.V., Sinhasan R. and Kumar A., "A variational solution of two lobe bearing," 1977, Mechanism and Machine Theory,22, pp. 323-330

[20] Kumar A., Sinhasan R., Singh D.V., "Performance characteristics of two lobe hydrodynamic journal bearing," 1980, Journal of Lubrication technology,102, pp.425-429.

[21] Kumar A., Sinhasan R. and Singh D.V., "A comparative study of some two lobe journal bearing configuration," 1983, Transactions of ASLE, 26(1), pp. 118-124

[22] Soni S.C., Sinhasan R. and Singh D.V., "Performance characteristics of non circular bearings in laminar and turbulent flow regimes," 1981, Transactions of ASLE, 24(1), pp. 29-41

[23] Soni S.C., Sinhasan R. and Singh D.V., "Non-linear analysis of two lobe bearings in turbulent flow regimes,", 1985,Wear,103, pp.11-27.

[24] Sinhasan R., Goyal K.C, "Transient response of two lobe journal bearing with non Newtonian lubricant," 1995, Tribology International , 28(4), pp. 233-239

[25] Rao T.V.V.L.N, Biswas S. and Athre K., "A methodology for dynamic co-efficient and non-linear response of the multi lobe journal bearings," 2001,STLE Tribology Transactions, 44(1), pp. 111-117.

[26] Sharana B, Satish J., Sharma C., and Jain S.C., "Performance of an orifice compensated two lobe hole entry hybrid journal bearing," 2008, Advances in Tribology,(2008), pp. 1-10.

[27] Pinkus O., "Analysis and characteristics of three lobe bearing,"1959, Transaction of ASME, Journal of Basic Engineering,81, pp.74-50.

[28] Falkenhagen G.L., Gunter E.J. and Schuller F.T., "Stability and transient motion of a vertical three lobe bearing system," 1972, Journal of Engineering for Industry, pp. 665-677.

[29] Lund W., and Thomson K. K., "A Calculation Method and Data for the Dynamic Coefficients of Oil Lubricated Journal Bearings", 1978, Proceedings of the ASME Design and Engineering Conference, Minneapolis, pp. 1-28.

[30] Malik M., Sinhasan R. and Chandra M., "Design data for three-lobe bearings," 1981, Transactions of ASLE, 24(3), pp.345-353.

[31] Sinhasan R., Malik M. and Chandra M., "A comparative study of some three lobe bearing configurations." 1981,Wear,72, pp. 277-286

[32] Malik M., Chandra M. and Sinhasan R., "Performance characteristics of tilted three lobe journal bearing configuration," 1981, Tribology International, pp. 345-349

[33] Mehta N.P. and Rattan S.S., "Performance of three lobe pressure dam bearing," 1993, Tribology International, 26(6) pp.435-442.

[34] Taylor D.V., Kostrzewsky G.J., Flack R. D., Barrett L.E ., "Measured performance of highly preloaded three-lobe Journal bearing-Part I: Static Characteristics,"1995, Tribology Transaction, 38(3), pp. 507-516.

[35] Arumugam P., Swarnamani S., Prabhu B.S., "Effect of journal misalignment on the performance of three lobe bearing," 1997, Wear, 206, pp.122-129

[36] Carmen M.M.K, Barret L.E. and Flack R.D., "Influence of fluid nonlinearity on the experimental determination of dynamic stiffness and damping coefficients for three-lobe journal bearings," 1997, STLE Tribology Transaction, 40(1), pp.49-56

[37] Pettinato B and Flack R.D.,"Test results for a highly preloaded there lobe journal Bearing-Effect of load orientation on static and dynamic characteristics," 2001, Journal of the Society of Tribologists and Lubrication Engineers, pp. 23-30.

[38] Mehta N.P., Rattan S.S. and Verma R., "Stability Analysis of Three lobe hydrodynamic journal bearing: Couple stress fluid effects," 2010, International Journal of Engineering Science and Technology, 2(10), pp. 5736-5745.

[39] Batra N. K., Bhushan G., Mehta N. P., "Effect of turbulence on the performance of an inverted three-lobe pressure dam bearing," August 2011, International Journal of Scientific & Engineering Research 2(8), pp. 1-5.

[40] Bhushan G., "Effect of load orientation on the stability of a three-lobe bearing supporting rigid and flexible rotors," 2011, World Academy of Science, Engineering and Technology, 57, pp.195-198.

[41] Flack R.D., Leader M.E., Allaire P.E., "An experimental and theoretical investigation of pressure in four lobe bearings," 1980, Wear, 61, pp. 233-242.

[42] Leader M.E., Flack R.D. and Lewis D.W., "An experimental determination of instability of a flexible rotor in four-lobe bearing", 1980, Wear, 58, pp.35-47.

[43] Bhushan G, Rattan S.S. and Mehta N.P., "Stability analysis of four lobe pressure-dam bearings." 2002, Tribology Letters, 13, pp. 1-7.

[44] Bhushan, G. Rattan S.S. and Mehta N.P., "Effect of pressure dams and relief tracks on the performance of four lobe bearing," 2005,IE(I) Journal –MC, pp. 194-198.

[45] Bhusan G., Rattan S.S, Mehta N.P., "Effect of L/D ratio on the performance of a four lobe pressure dam bearing," 2007, International Journal of Mathematical, Physical and Engineering Science, 1(4), pp. 203-207.

[46] Mehta N.P., Rattan S.S., and Bhushan G., "Static and dynamic characteristics of four lobe pressure dam bearings," 2003,Tribology Letters, 15(4), pp. 415-420.

[47] Pai R. and Majumdar B. C., "Stability of submerged four-lobe oil journal bearings under dynamic load," 1992, Wear, 154, pp.95-108.

[48] Chetti B., "Static and Dynamic analysis of hydrodynamic four-lobe journal bearing with couple stress Lubricants," 2011, Jordan Journal of Mechanical and Industrial Engineering 5(1), pp. 23-28.

[49] Seireg A.and Ezzat H., "Optimum design of hydrodynamic journal bearings," 1969, J. of Lubrication Tech., 91(3), pp. 516-521.

[50] Bosma R., Moes H.,"Design Charts for Optimum Bearing Configurations:2-The pivoted-Pad thrust bearing,"1970, J. of Lubrication Tech. 92(4), pp.572-577.

[51] Rowe W.R, Donoghue J.P.O, and Cameron A., "Optimization of externally pressurized bearings for minimum power and low temperature rise," 1970, Transaction of ASME ,Journal of Tribology, pp. 153-157.

[52] Dowson D. and Ashton J.N., "Optimum computerized design of hydrodynamic journal bearings," 1976, Int. Journal of Mechanical Science, 18, pp. 215-222

[53] Rowe W., and Koshal.D., "A New Basis for the Optimization of Hybrid Journal Bearings," 1980,Wear,64, pp. 115 – 131.

[54] Mcallister G.T., Rodhe S.M., "Optimum Design of one-dimensional journal bearings," 1983, Journal of optimization Theory and applications, 41(4), pp. 559-617

[55] Kumar V., "Optimization of tolerance for minimum manufacturing cost of satisfactory journal bearings," 1983, Wear, 86, pp. 21 - 27

[56] Herbinyt M. EI, Salem F, Hefnawy N. El., "Optimum design of hydrostatic journal bearings Part I: Maximum load capacity,"1984, Tribology international,17(3), pp. 155-161.

[57] Schittkowski K., "NLQPL: A FORTRAN-Subroutine Solving Constrained Nonlinear Programming Problems," 1985,Annals of Operations Research, Vol. 5, pp 485-500.

[58] Matsumoto K., and Hashimoto, H., "Improvement of operating characteristics of high-speed hydrodynamic journal bearings by optimum design: Part I-Formulation of methodology and its Application to elliptical bearing design," 2001, Transaction of ASME , J. Tribology, 123(2),pp. 305-313.

[59] Yang B.S, Lee Y.H , Choi B.K , Kim H.J., " Optimum design of short journal bearings by artificial life algorithm," 2001,Tribology International,34, pp. 427–435

[60] Boedo S and Eshkabilov S.L .," Optimal shape design of steadily loaded journal bearing using Genetic Algorithms," 2003,Tribology Transactions 46,1, pp. 134–143.

[61] Hirani H., "Multiobjective optimization of a journal bearing using the Pareto optimality concept" 2004, Proc. Instn Mech. Engrs, Part J: J. Engineering Tribology, Vol. 218 (4), pp. 323-336.

[62] Marler R.T. and Arora J.S., "Survey of multi-objective optimization methods for engineering," 2004, Struct Multidisc Optim,26, pp.369–395.

[63] McCall J., "Genetic algorithms for modelling and optimization," 2005, Journal of Computational and Applied Mathematics, 184(2005), pp. 205–222.

[64] Song J.D., Yang B.S , Choi B.G., Kim H.J ., "Optimum design of short journal bearings by enhanced artificial life optimization algorithm," 2005 ,Tribology International,38,pp. 403-412.

[65] Hirani H., "Multiobjective optimization of journal bearing using mass conserving and Genetic Algorithms," Proc. IMechE, 2005. Vol. 219 (3) Part J: J. Engineering Tribology pp. 235-248.

[66] Hirani H and Suh N.P., "Journal bearing design using multiobjective genetic algorithm and axiomatic design approaches" 2005, Tribology International,38, pp. 481–491.

[67] Chetan S., Ketan T. and George P. M., "Optimum Design of a journal bearing– a review," 2011,National Conference on Recent Trends in Engineering & Technology,13-14 May Gujarat,India.

[68] Mathew Tom V**,** Beasley D, David R. Bull, and Martin R.R., "An overview of genetic algorithms: Part 2, research topics," 1993, University Computing, 15(4), pp.170-181.

[69] Bean J. C., "Genetic algorithms and random keys for sequencing and optimization", Spring 1994, ORSA Journal on Computing vol. 6, pp.154-160.

[70] Fonseca C. M, Fleming P. J**., "**An overview of evolutionary algorithms in multiobjective optimization," 1995, Spring 3(1), pp.1-26.

[71] Tamaki, H. Kita, H.;Kobayashi, S., "Multi-objective optimization by genetic algorithms: a review," 1996., Proceedings of IEEE International Conference on May 20-22.

[72] Veldhuizen D.V.V., and Lamont G.B.,"Multiobjective evolutionary algorithms: analyzing the state-of-the-art" 2000, Evolutionary Computation, 8(2), pp. 125-147

[73] Marler R.T. and Arora J.S.,"Survey of multi-objective optimization methods for engineering," 2004, Struct Multidisc Optim, 26, pp. 369–395.

[74] Kao Y.T., and Zahara E., "A hybrid genetic algorithm and particle swarm optimization for multimodal functions," 2008, J. Applied Soft Computing 8, pp. 849– 857.

[75] Majumdar B. C., 2011-2012, Introduction to Tribology of Bearings, S.Chand ,New Delhi, India.

List of Publications

International Journal

- [1] L. Roy and S. K. Kakoty, "Optimum Groove Location of Hydrodynamic Journal Bearing Using Genetic Algorithm", Advances in Tribology, Volume 2013 (2013), pp. 1-13.
- [2] L. Roy and S. K. Kakoty,"Optimum Groove Location of Three-lobe and four lobe bearing Using Genetic Algorithm," Proceedings of the IMechE, Part J: Journal of Engineering Tribology, 2015, Vol. 229(1) 47–63

International Conference

- L. Roy and S. K. Kakoty, "Stability and flow optimized bearing configuration of two groove bearing," ISTAM, 58th Congress of the Indian Society of Theoretical and Applied Mechanics (ISTAM), 18-21 December, 2013,pp 79
- L. Roy and S. K. Kakoty, "Application of Genetic Algorithm in Optimization of Hydrodynamic bearings," Proceedings of Fourth International Conference on Soft Computing for Problem Solving Advances in Intelligent Systems and Computing Volume 335, 2015, pp 207-217,Springer India 2015.

Vitae

Born and brought up in Guwahati, Assam Mr. Lintu Roy is the middle son of Mr. HariPada Roy and Mrs. Molina Roy. After schooling from Guwahati, he graduated in Mechanical Engineering from National Institute of Technology, Silchar (erstwhile Regional Engineering College, Silchar) in 1994(December) . He joined as Lecturer in Mechanical Engineering Department, National Institute of Technology, Silchar in 2000. He took his Master of Engineering (M.E) degree in Mechanical Systems Design from Indian institute of Technology, Kharagpur in 2005. Then he joined Department of Mechanical Engineering of Indian Institute of Technology Guwahati as a part time Research Scholar in 2008 and worked under the supervision of Prof. S K Kakoty.